

**Identification, regulation and physiological role of enzymes
involved in triacylglycerol and phosphatidylcholine synthesis
on lipid droplets**

DISSERTATION

zur Erlangung des akademischen Grades

Doctor rerum naturalium

(Dr. rer. nat)

vorgelegt

der Fakultät Mathematik und Naturwissenschaften

der Technischen Universität Dresden

von

Dipl.-Biologin Christine Mössinger

geboren am 12.06.1980 in Marburg, Deutschland

Gutachter:	Prof. Dr. Bernard Hoflack	Technische Universität Dresden
	Prof. Dr. Christoph Thiele	MPI-CBG Dresden und LIMES Universität Bonn

Eingereicht am: 06.11.2009

Tag der Verteidigung: 03.03.2010

Declaration according to §5.5 of the doctorate regulations

I herewith declare that I have produced this paper without the prohibited assistance of third parties and without making use of aids other than those specified; notions taken over directly or indirectly from other sources have been identified as such. This paper has not previously been presented in identical or similar form to any other German or foreign examination board.

This thesis work was conducted from 01.05.2006 to 06.11.2009 under the supervision of Prof. Dr. Christoph Thiele at the Max Planck Institute of Molecular Cell Biology and Genetics in Dresden, Germany.

I declare that I have not undertaken any previous unsuccessful doctorate proceedings.

I declare that I recognize the doctorate regulations of the Fakultät für Mathematik und Naturwissenschaften of the Technische Universität Dresden.

Dresden, 06.11.2009, Christine Mössinger

Contents

1. Summary	1
2. Introduction	3
2.1. Lipids and life	3
2.2. Lipid droplets (LDs)	3
2.2.1. Structure of LDs	4
2.2.2. Function of LDs	5
2.2.3. Biogenesis of LDs	5
2.2.4. Mobilization of stored lipids	6
2.2.5. Storage of lipids	8
2.2.5.1. Acyl-CoA synthetases ligases (ACSLs)	9
2.3. TAG biosynthesis	10
2.3.1. Diacylglycerol acyltransferases (DGATs)	10
2.4. PC biosynthesis	11
2.4.1. Lyso-phosphatidylcholine acyltransferases (LPCATs)	12
2.5. Dynamics of lipids	13
2.6. Lipids and diseases	15
3. Aim of the thesis	17
4. Results	19
4.1. LDs locally synthesize their lipid components	19
4.1.1. DGAT2 catalyzes the formation of TAG on LDs	19
4.1.1.1. Localization of DGAT2 in COS7 cells	20
4.1.1.2. The activity of DGAT2 on LDs	20
4.1.2. LPCAT1 and LPCAT2 catalyze the formation of PC on LDs	21
4.1.2.1. Localization of LPCAT1 and LPCAT2	22
4.1.2.2. The activity of LPCAT1 and LPCAT2 on LDs	25
4.2. Physiological role of LPCAT activities	28
4.2.1. LPCAT1 and LPCAT2 participate in the synthesis of the LD surface	29
4.2.2. LPCAT1 and LPCAT2 influence the morphology of LDs	31
4.2.3. LPCAT1 is important for lipoprotein particle secretion	39
4.3. Monotopic topology is a common feature of LD membrane proteins	41
4.3.1. Topology of LPCAT1 and LPCAT2	42
4.3.2. Topology of DGAT2	43
4.4. Regulation of DGAT2 localization and activity	45
4.4.1. DGAT2 interacts with ACSL1	49
4.4.1.1. Identification of DGAT2 interaction partner	49
4.4.1.2. DGAT2 and ACSL1 partially localize to the same compartments	51
4.4.1.3. Validation of the interaction between DGAT2 and ACSL1	51
4.4.2. Physiological role of the DGAT2-ACSL1 interaction	54

5. Discussion	61
5.1. LDs grow by local synthesis of TAG and PC	61
5.2. Physiological significance of local TAG and PC synthesis	63
5.2.1. Size regulation of LDs	63
5.2.2. LD size influences the lipid metabolism	64
5.3. Formation and regulation of subcellular lipid pools	66
5.3.1. Interaction of DGAT2 and ACSL1	67
5.4. Impact of DGAT2, LPCAT1 and LPCAT2 on lipid metabolic diseases	69
6. Materials and Methods	71
6.1. Materials	71
6.1.1. Cell lines, cell culture media, bacteria strains and <i>Drosophila melanogaster</i> strains	71
6.1.2. Chemicals	71
6.1.3. Plasmids, ESTs, DNA primer, siRNAs, enzymes	72
6.1.4. Lipids and radioactive substances	73
6.1.5. Antibodies	73
6.2. Methods	74
6.2.1. Methods of molecular biology	74
6.2.1.1. Cloning	74
6.2.2. Methods of cell biology	74
6.2.2.1. Bacteria culture	74
6.2.2.2. Cell culture	75
6.2.2.3. Fly culture	75
6.2.2.4. Isolation of larval fat bodies from <i>Drosophila melanogaster</i> .	75
6.2.2.5. Transfection	75
6.2.2.6. Imaging	76
6.2.2.7. Lipid droplet isolation and density gradients	76
6.2.2.8. ApolipoproteinB, lipid and hepatitis C virus secretion . . .	77
6.2.3. Biochemical methods	79
6.2.3.1. SDS-polyacrylamide gel electrophoresis, Coomassie staining and western blot	79
6.2.3.2. Protein topology	79
6.2.3.3. Radioactive labeling, extraction and identification of cellular lipids	80
6.2.3.4. Protein and lipid mass spectrometry	81
6.2.3.5. Enzyme activity assays	82
6.2.3.6. Identification of protein-protein interaction	83
Appendices	86
A. Supplementary figures	87
B. Supplementary tables	105
C. Abbreviations	109
D. Bibliography	111
E. Publications and Awards	121
F. Acknowledgments	123

List of Figures

2.1. Structure of LDs	5
2.2. Models of LD biogenesis	6
2.3. Lipolysis	7
2.4. Pathways of TAG and PC synthesis	11
2.5. Overview of the dynamics of LDs and their connection to different cellular processes	14
2.6. Simplified receptor-mediated human lipoprotein metabolism	15
4.1. Cellular localization of DGAT2	20
4.2. DGAT2 localizes to LDs	21
4.3. DGAT2 enables LDs to locally synthesize TAG	21
4.4. Expression of LPCAT1 and LPCAT2 in HuH7, A431 and COS7 cells	22
4.5. Localization of LPCAT1 in A431 cells	23
4.6. Localization of LPCAT2 in A431 cells	24
4.7. Localization of LPCAT1 and LPCAT2 in COS7 cells	25
4.8. LPCAT1 and LPCAT2 localize to LDs	26
4.9. LDs possess LPCAT activity	27
4.10. LDs locally synthesize PC by the Lands cycle	28
4.11. Isolated LDs have a unique surface lipid profile	30
4.12. Silencing of LPCAT1 and LPCAT2 by siRNA reduces the amount of the respective proteins in A431 cells	31
4.13. Silencing of LPCAT1 and LPCAT2 by siRNA increases the size of LDs in A431 cells	32
4.14. Silencing of LPCAT1 and LPCAT2 by siRNA increases the mean size of LDs in A431 cells significantly	33
4.15. Silencing of LPCAT1 in HuH7 cells reduces cellular LPCAT1 protein and activity	34
4.16. Silencing of LPCAT1 by siRNA increases the size of LDs in HuH7 cells . . .	35
4.17. Silencing of LPCAT1 by siRNA increases the mean size of LDs in HuH7 cells significantly	36
4.18. Changes in LD size distribution in HuH7 cells upon LPCAT1 knock-down . .	36
4.19. Knock-down of LPCAT1 in HuH7 cells has no influence on TAG synthesis rate	37
4.20. Silencing of LPCAT1 in HuH7 cells does not influence the amount of stored neutral lipids	37
4.21. Knockout of the LPCAT1/2 <i>Drosophila melanogaster</i> homologue CG32699 leads to enlarged LDs in the fat body of L3 larvae	38
4.22. LPCAT1 is important for lipoprotein particle secretion in HuH7 hepatoma cells	40
4.23. LD-localizing membrane proteins contain a long hydrophobic stretch	42
4.24. LPCAT1 and LPCAT2 insert into LDs and membranes in a monotopic conformation	44
4.25. LPCAT1 and LPCAT2 insert into membranes in a monotopic conformation .	45
4.26. Topology of DGAT2	46
4.27. DGAT2 is a monotopic membrane protein	47
4.28. DGAT2 behaves like a single-span membrane protein	47

4.29. Domain structure and conservation of DGAT2	48
4.30. Identification of ACSL1 as interaction partner of DGAT2	50
4.31. Cellular localization of DGAT2 and ACSL1	52
4.32. DGAT2 and ACSL1 partially localize to the same compartments	53
4.33. DGAT2 interacts with ACSL1 in COS7 cells	54
4.34. DGAT2 associates with an ACSL activity in COS7 cells	55
4.35. The ratio between DGAT2 and ACSL1 influences the packaging of stored TAG	57
4.36. ACSL1 and DGAT2 influence the size of LDs	58
4.37. The ratio between DGAT2 and ACSL1 influences the size distribution of LDs	59
5.1. A model to integrate triglyceride and phospholipid metabolism	66
A.1. DGAT2 localization under oleate-fed conditions	87
A.2. Coomassie gel of purified LD proteins for mass spectrometric analysis	87
A.3. Characterization of antibodies against LPCAT1 and LPCAT2	88
A.4. Purity of LD fractions used for lipid mass spectrometry	88
A.5. Silencing of LPCAT1 and LPCAT2 in A431 cells does not influence TAG synthesis	89
A.6. Silencing of LPCAT1 and LPCAT2 in A431 cells does not influence the amount of stored TAG	89
A.7. Inhibition of PC de novo synthesis channels fatty acids towards TAG synthesis	90
A.8. Silencing of LPCAT1 and LPCAT2 in choline-depleted A431 cells increases LD size	91
A.9. Silencing of LPCAT1 and LPCAT2 in choline-depleted A431 cells does not influence TAG synthesis	92
A.10. Silencing of LPCAT1 and LPCAT2 in choline-depleted A431 cells does not influence the amount of stored TAG	92
A.11. L3 larvae of crosses between the three different CG32699 <i>Drosophila melanogaster</i> knockout strains show enlarged LDs in the fat body	93
A.12. ApoB secreted by HuH7 cells is associated with lipoprotein particles	94
A.13. Secreted radioactively labeled lipids from HuH7 cells	94
A.14. Hydrophobicity plots of human LPCAT1 and LPCAT2	95
A.15. Topology of LPCAT1	96
A.16. Topology of LPCAT2	97
A.17. Coomassie gels for identification of DGAT2 interaction partner	98
A.18. Cellular localization of DGAT2 and ACSL1 under delipidated conditions . .	99
A.19. Cellular localization of DGAT2 and ACSL1 under oleate conditions	100
A.20. Interaction with ACSL1 does not increase DGAT2 activity in COS7 cells . .	101
A.21. Interaction of ACSL1 and DGAT2 does not change lipid synthesis in COS7 cells	102
A.22. Interaction with ACSL1 does not influence stability of DGAT2 in COS7 cells	103

List of Tables

6.1. Plasmids	72
6.2. Primary antibodies	73
B.1. Mass spectrometric analysis of LD proteins from A431 cells	105
B.2. Quantification of LD size changes upon silencing of LPCAT1 and LPCAT2 by siRNA in A431 cells	106
B.3. Quantification of LD size changes upon silencing of LPCAT1 by siRNA in HuH7 cells	106
B.4. Potential interaction partner of DGAT2	107

1. Summary

Metabolic energy is most efficiently stored as triacylglycerol (TAG). This neutral lipid accumulates mainly within adipose tissues, but it can be stored and used in all types of cells. Within cells it is packed in organelles called lipid droplets (LDs). They consist of a core of neutral lipids like TAG and cholesterol esters, which is surrounded by a phospholipid monolayer that mainly consists of phosphatidylcholine (PC). Attached to or inserted into this monolayer are various proteins, mainly LD specific structural proteins or lipid metabolic enzymes. Though excess uptake of nutrition leads to lipid accumulation in all kinds of body tissues, which is accompanied by the augmentation of LDs and results in cellular dysfunction and the development of metabolic diseases, relatively little is known about the biogenesis and growth of LDs.

This thesis focuses on diacylglycerol acyltransferase 2 (DGAT2), an enzyme of the TAG biosynthetic pathway, and on lyso-phosphatidylcholine acyltransferases 1 and 2 (LPCAT1 and LPCAT2), both enzymes of one of the PC biosynthetic pathways called Lands cycle. The data presented in this thesis show that these enzymes can localize to LDs and that they actively synthesize TAG and PC at the surface of LDs. While the LPCATs reside on LDs independent from the nutrition status of the cell, DGAT2 accumulates on LDs upon excess availability of oleic acid.

DGAT2, LPCAT1 and LPCAT2 differ in their structure from other iso-enzymes that catalyze the same reactions. This thesis shows that they exhibit a monotopic conformation and that they contain a hydrophobic stretch that presumably forms a hairpin. This topology enables them to localize to both a phospholipid bilayer like the membrane of the endoplasmic reticulum and to a phospholipid monolayer like the surface of LDs. The different biophysical properties of the structures of iso-enzymes might be responsible for their subcellular localization and the formation of distinct TAG or PC pools that are destined for different purposes. This would explain, why the iso-enzymes are often not able to replace each other.

Knock-down and overexpression experiments performed in this thesis show that the activity of LPCAT1, LPCAT2 and DGAT2 influence the packaging of lipids within LDs. Knock-down

of LPCAT1 and LPCAT2 leads to an increase in LD size without concomitant increase in the amount of TAG. Combined with the finding that the profile of the PC species of the LD surface reflects the substrate preferences of LPCAT1 and LPCAT2, the results suggest that these enzymes are responsible for the formation of the LD surface. Therefore, the increase in LD size upon LPCAT1 and LPCAT2 knock-down results from an adjustment of the surface-to-volume ratio in response to reduced availability of surface lipids. The connection between LPCATs and LD size was corroborated in the model organism *Drosophila melanogaster*. Three different knockout fly strains of the *Drosophila* homologue of LPCAT1 and LPCAT2, *CG32699*, exhibit enlarged LDs in the fat body of the L3 larvae. Furthermore, the data presented suggest that the morphology of LDs is important for the secretion of stored lipids. The reduction of LPCAT1 in liver cells leads to a reduction in lipoprotein particle release. This was shown by measuring the amount of released apolipoproteinB with two different methods, by measuring the release of lipids and by quantification of the amount of released hepatitis C virus, which is known to rely on LD interaction for replication and on lipoprotein particles for cellular release.

DGAT2 is recruited to LDs upon excess availability of oleic acid and its overexpression leads to the formation of many, but relatively small LDs. Here, it is shown that DGAT2 interacts with acyl-CoA synthetase ligase 1 (ACSL1), an enzyme that catalyzes the activation of free fatty acids with Coenzyme A. This interaction does not influence the stability of DGAT2 nor does it seem to affect lipid synthesis. Nevertheless, it shows an influence on lipid packaging in LDs. While overexpression of DGAT2 results in the appearance of smaller LDs, overexpression of ACSL1 leads to an increase in LD size. Coexpression of ACSL1 and DGAT2 reverses the phenotypes obtained by single overexpression and normalizes the mean LD diameter to values observed at normal conditions.

In conclusion, this thesis shows that LDs are able to synthesize the components of their core and their surface, which underlines their independent function in metabolism. Additionally, the results show that LDs can grow by local synthesis and that the responsible enzymes exhibit a monotopic membrane topology, which might be crucial for LD localization. Furthermore, the obtained data suggest that the localization and the ratio between different enzyme activities influence the packaging of lipids and affects lipid secretion and therefore impact the whole body lipid metabolism.

2. Introduction

This chapter gives an overview about the role of lipids and their metabolism in cells. It describes how major lipids are synthesized, stored and mobilized, and what the consequences are, if these processes are disturbed. Additionally, more detailed information is provided about lipid metabolic enzymes, which are subject of further investigation within this thesis.

2.1. Lipids and life

Lipids are important components of cells. They separate the cell from its surroundings by formation of a cell membrane. Additionally, they create different compartments within the cell by the formation of organelle membranes. Besides their structural role, they participate in protein modification, signaling and hormonal regulation and they provide energy for cellular processes. There are diverse lipids, which differ in their physical and chemical properties and participate in many processes within organisms. While phospholipids are amphipathic molecules that are optimized for the separation of lipid and water phases, neutral lipids like triacylglycerides (TAG) are optimized as energy containing molecules. The characteristics of TAG allow a dense packing of these molecules [1]. They accumulate in lipid droplets (LDs). Most neutral lipids in the body are stored in adipose tissues, which are specialized to store TAG and to release them upon energy requisition. Besides their function in lipid storage, adipose tissues participate in hormonal regulation and organ protection.

2.2. Lipid droplets (LDs)

LDs are the cellular location of neutral lipid storage. Every eukaryotic cell analyzed so far is able to form LDs [2]. Some cells exhibit LDs under normal physiological conditions, while others must be induced to LD formation by the addition of lipids. LDs have a uniform ultrastructure, but they differ in size between different cell types. Adipocytes exhibit few

large droplets [3, 4], whereas muscle cells have multiple small droplets [5, 6]. Some cells have many droplets of equal size, others have droplets of a broad range of size. In some cell types LDs aggregate in big clusters, often close to the nucleus, whereas in others they are very dispersed and located to the cell periphery.

2.2.1. Structure of LDs

LDs consist of a core of neutral lipids like TAG and cholesterol esters (CE), which is surrounded by a monolayer of phospholipids (figure 2.1). This monolayer is characteristic for LDs and consists mainly of phosphatidylcholine (PC) [7, 8]. Several proteomic analyses of purified LDs from different cell types revealed that different proteins are attached to LDs, which can be classified into structural components, lipid metabolic enzymes and proteins belonging to other processes like ubiquitination, signaling and membrane traffic [9–16].

The most abundant structural proteins of LDs belong to the PAT-family, named after its members **p**erilipin, **a**dipophilin (ADRP) and **t**ail-interacting protein 47 (TIP47), which share a characteristic PAT1 homology region. Perilipin [17] is highly expressed in adipose tissue, while ADRP [18, 19] and TIP47 [20–22] are found on LDs of many cell types. The additional family members OXPAT/MLDP [23] and S3-12 [24] are found mainly in oxidative tissues and white adipose tissue, respectively. In adipocytes, smaller LDs harbor mainly TIP47 and S3-12, whereas ADRP and perilipin are found predominantly on large droplets. During adipocyte differentiation, the PAT family members S3-12 and TIP47 are replaced by ADRP and perilipin [25]. Besides their structural function, PAT family proteins seem to be involved in LD biogenesis and regulation of lipolysis (see section 2.2.3 and 2.2.4). Additionally, LDs harbor many proteins involved in lipid metabolism, for example acyl-CoA synthetase ligase (ACSL) family member 1, 3 and 4, NAD(P)H steroid dehydrogenase-like protein (NSDHL) or lipases such as hormone-sensitive lipase (HSL) and adipose triglyceride lipase (ATGL). The set of proteins localizing to LDs depends on the cell type and can change upon hormonal or nutritional stimulation.

Similarly, the lipid components of LDs vary between cell types. Besides TAG, the core of LDs harbors diacylglycerol (DAG), CE and other esters like retinol esters in different proportions [26–28]. The phospholipid monolayer consists mainly of PC, but contains also phosphatidylethanolamine (PE), phosphatidylinositol (PI), lyso-phosphatidylcholine (LPC), lyso-phosphatidylethanolamine (LPE) and free cholesterol [8, 29].

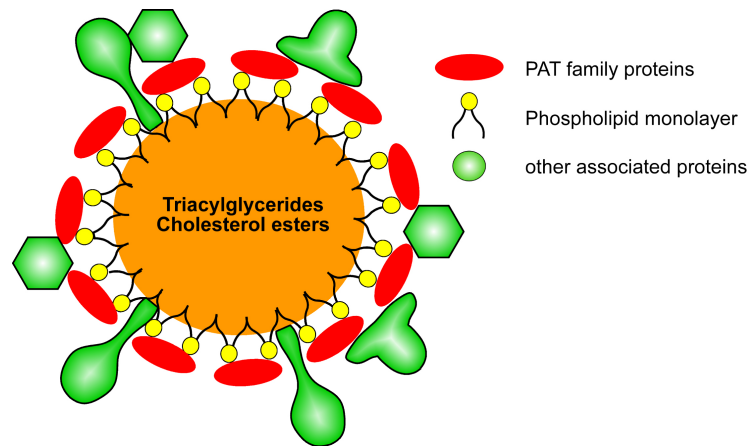


Figure 2.1.: Structure of lipid droplets

2.2.2. Function of LDs

Besides their role in storage of energetic molecules and precursors for membranes, steroid hormones and signaling molecules, LDs are suggested to function in detoxification. Some cellular lipids, for example LPC or free fatty acids (FFAs), are toxic for the cell, if they accumulate, and LDs might serve to sequester them [30]. It has been suggested that they have a similar function for proteins. LDs can sequester proteins for future use or for degradation [31], for example histones accumulate on LDs in *Drosophila* embryos [32]. The localization of many proteins involved in ubiquitination to LDs further suggests a role in protein degradation. Additionally, LDs seem to play a role in infection and inflammation. It was reported that LDs are formed in leukocytes following bacterial infection [33, 34]. The increase of LD number correlated with an increased generation of eicosanoids. Furthermore, LDs function in hepatitis C virus assembly [35–37] and replication of *Chlamydia trachomatis* [38].

2.2.3. Biogenesis of LDs

Though LDs were studied intensively for several years, their origin is still unclear. Whether they originate from other organelles or represent self-replicating organelles is a matter of debate. Most theories suggest the ER as site for LD formation (figure 2.2). Electron microscopic images show LDs in close contact to ER membranes and ADRP-rich egg-cup like domains that might represent the location for LD assembly [39]. In the monolayer budding theory, neutral lipids accumulate between the leaflets of the ER membrane. This lipid accumulation bulges out into the cytosol and is finally released by budding. Thus the phospholipid monolayer would be derived from the cytoplasmic leaflet of the ER. In the bicelle formation or hatching theory, the lipid accumulation between the ER leaflets is released by disruption of the membrane next to the accumulation. Thus the phospholipid

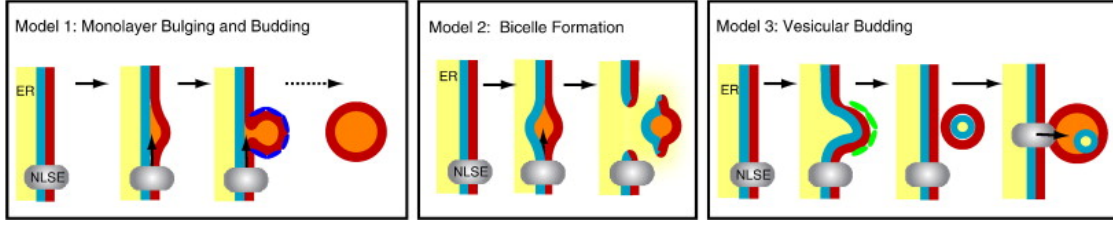


Figure 2.2.: Models of lipid-droplet biogenesis

Model 1: LD biogenesis by ER budding. Neutral lipids (orange) are synthesized by neutral lipid-synthesizing enzymes (NLSE) and bulge from the outer leaflet of the ER membrane (red). The nascent droplet may be coated by proteins (dark blue) that facilitate the budding process. Model 2: Bilayer excision. Newly synthesized neutral lipids accumulate between the inner (blue) and outer (red) leaflets of the ER membrane and cause bulging. This entire lipid lens is then excised from the ER, leaving a transient hole in the membrane. ER contents (yellow) might leak through this hole into the cytosol. Model 3: Vesicular budding. A vesicle containing both leaflets of the ER membrane (red and blue) and a lumen (yellow) is formed by the vesicular budding machinery (green) at the ER membrane. The vesicle is subsequently tethered to the ER, where NLSEs (grey) fill the intramembranous space with neutral lipids (orange). The luminal space (yellow) is compressed, and its contents may leak into the cytosol. This process may trap luminal proteins within a compartment of the LD. This figure is taken from [40].

monolayer of the LD would be derived from both leaflets of the ER membrane. The opening of the ER compartment generated during LD release has been suggested to participate in ER-associated degradation of proteins and the release of viruses from the ER lumen. In the vesicular budding theory, vesicles are formed and stay tethered to the ER. The intramembrane space of these vesicles is then filled with neutral lipids, which displace the vesicular lumen until it remains as an aqueous inclusion within the LD or is released into the cytosol ([40] and references therein).

2.2.4. Mobilization of stored lipids

The best-studied process concerning LDs is the release of stored TAG. Besides a cellular basal level, lipolysis is stimulated by multiple signaling pathways. In the classical hormonal pathway, catecholamines activate the β -adrenergic receptor. This leads to the activation of protein kinase A via the G-protein coupled activation of adenylate cyclase and increased levels of cAMP [41]. Protein kinase A phosphorylates perilipin A and hormone-sensitive lipase (HSL) [42, 43] (figure 2.3). The phosphorylation leads to the release of *comparative gene identification-58* (CGI-58) from the LD [44]. CGI-58 can interact with adipose triacylglyceride lipase (ATGL) and seems to activate the enzyme [45]. ATGL is reported to hydrolyse TAG into DAG and fatty acid (FA) [46]. DAG is hydrolyzed by HSL to monoacylglycerol (MAG) and FA [42]. During hormonal stimulation of lipolysis, HSL translocates from the cytosol to LDs and binds to phosphorylated perilipin A [47, 48]. The last step in TAG lipolysis is catalyzed by monoacylglycerol lipase (MGL), which hydrolyses MAG to glycerol and FA [49].

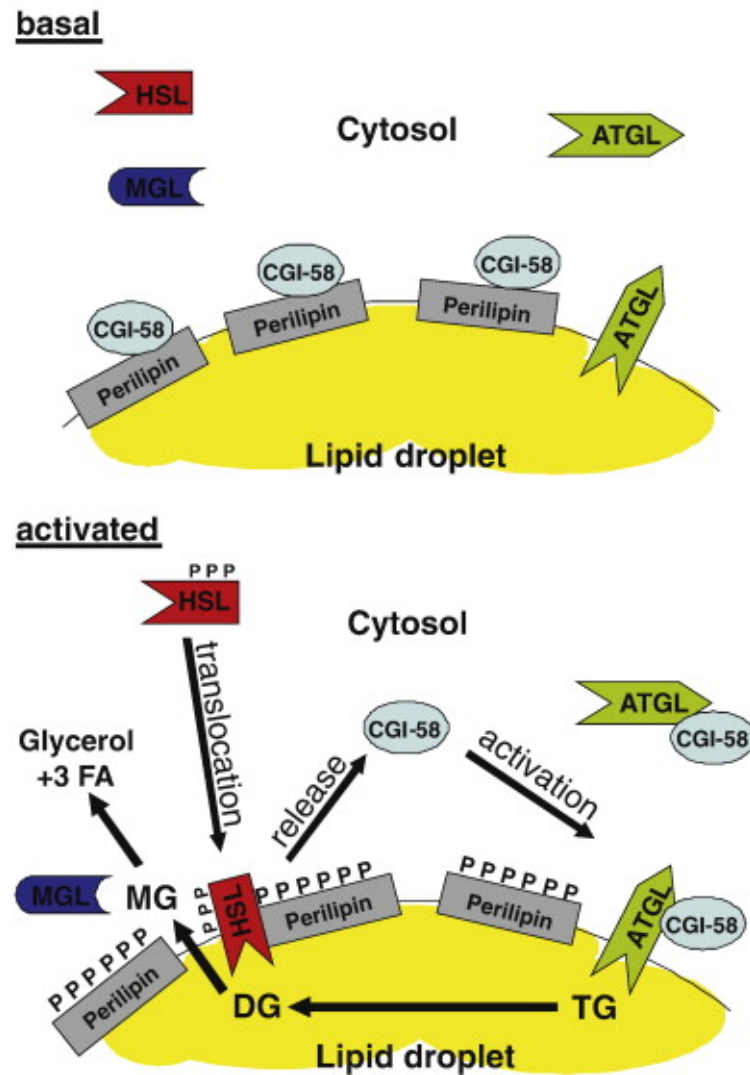


Figure 2.3.: Lipolysis

Perilipin regulates both ATGL and HSL activity by binding the ATGL activator CGI-58 and by controlling the access of HSL to the LD. In the basal state, CGI-58 is bound to perilipin and HSL is predominantly cytosolic resulting in low LD-associated ATGL and HSL activity. ATGL is present on LDs at similar amounts in non-stimulated and stimulated adipocytes excluding an activation mechanism based on translocation. In the activated state, phosphorylation of perilipin by PKA leads to the release of CGI-58, which then becomes available for ATGL activation. Activated ATGL generates diacylglycerol (DG), the preferred substrate of HSL. In parallel, HSL is phosphorylated by PKA and perilipin promotes the translocation of the enzyme resulting in efficient DG hydrolysis. The last step in triacylglycerol (TG) degradation is performed by cytosolic MGL finally resulting in the formation of free glycerol and FA. This figure is taken from [50].

The PAT family proteins on the surface of LDs are thought to represent key controllers in lipolysis, as they seem to shield TAG from lipolysis [51–53] and the phosphorylation of perilipin A is required to activate HSL and ATGL [54]. Additionally, they seem to be important for the dramatic morphological changes that LDs undergo during lipolysis. Chronic stimulation of lipolysis in adipocytes results in a fragmentation of large LDs into small LDs, which are dispersed throughout the cell [3, 9]. A similar fragmentation connected with increased lipolysis could be achieved by ablation of the fat specific protein 27 (Fsp27) in adipocytes. Fsp27 is reported to be involved in the formation of large LDs [55, 56]. Though many players in lipolysis are known, the regulation of lipolysis is not completely understood, especially as most data result from studies in adipocytes only.

2.2.5. Storage of lipids

Though the main lipid composition of LDs is known, and the synthesis pathways of most stored lipids have been investigated, relatively little is known about how lipids are stored within the LDs. Most enzymes for complex lipid synthesis localize to the ER, but how the synthesized lipids enter the LD is still a matter of debate (see section 2.5). The main storage lipid TAG derives from glycerol and FAs in several enzymatically catalyzed synthesis steps, which are described further in section 2.3.

The FAs for the synthesis of storage lipids can derive from different sources. FAs can be imported into the cell, they can be synthesized *de novo* within the cell or they derive from stored lipids via lipolysis (see section 2.2.4). FAs are generally synthesized in the cytosol by the multifunctional polypeptide proteins acetyl-CoA carboxylase (ACC) and fatty acid synthase (FAS) from acetyl-CoA and malonyl-CoA. *De novo* synthesis mainly takes place in mammary gland for milk production, and in liver and adipose tissue for the synthesis of TAG. It is tightly regulated by the nutritional status and hormones [57].

The cellular import of FAs has been studied intensively, but the exact mechanism still remains to be elucidated. One possibility is the transport of FAs via membranes by flip-flop [58, 59], the other possibility requires several FA transport and binding proteins. In particular, the FA translocase (FAT/CD36) was reported to play a major role in protein-facilitated FA uptake [60–62]. The driving force for FA uptake seems to be the sequestration of FFA within the cell [63, 64]. As large amounts of FFAs are cytotoxic, they are immediately bound to soluble intracellular transport proteins like fatty acid binding proteins (FABPs) [65–67] and fatty acid transport proteins (FATPs) [68] or after activation with CoA they are bound to acyl-CoA binding proteins (ACBPs) [69]. After their activation by acyl-CoA

synthetases ligases (ACSLs) FAs are degraded by β -oxidation or incorporated into complex lipids like phospholipids or TAG.

2.2.5.1. Acyl-CoA synthetases ligases (ACSLs)

The addition of FAs to a glycerol or cholesterol backbone requires energy. Therefore, FAs have to be activated with CoA in order to be used by enzymes for the synthesis of lipids. This activation is catalyzed by acyl-CoA-acyltransferases (ACSLs). The activation is a two-step reaction: first, ATP and magnesium are used to activate a FA to AMP-acyl accompanied by the release of pyrophosphate (PP), second, AMP-acyl is linked to Coenzyme A via its sulfide (SH) group following the release of AMP. This process results in acyl-Coenzyme A [70] that can be used in diverse lipid metabolic pathways.

In humans, at least five ACSL isoforms (ACSL1, ACSL3, ACSL4, ACSL5 and ACSL6) with different tissue distributions and subcellular localizations have been detected [71–73]. They are divided into two subgroups, one of which comprises ACSL1, 5 and 6, the other ACSL3 and 4 [74]. While ACSL3 was reported to be involved in LD formation, PC synthesis, lipoprotein secretion and control of lipogenic gene expression [75–78], ACSL4 seems to be involved in hepatocellular carcinoma growth [79, 80] and may be linked to TAG synthesis [71].

ACSL1 is very abundant in adipocytes and liver. It is reported to localize to the ER, mitochondria-associated membranes (MAM) [81] and cytosol [71] in hepatocytes and to the plasma membrane (PM) and mitochondria in 3T3-L1 adipocytes [82, 83]. ACSL1 expression is reported to be regulated by the transcription factors PPAR α and PPAR γ depending on cell type and study conditions [84]. These findings and studies from liver-specific knock-out mice implicate a function in lipogenesis as well as in β -oxidation [85]. In hepatocytes, ACSL1 promotes FA incorporation into TAG [86], channels FAs away from CE into DAG and phospholipid synthesis and increases FA reacylation [81]. In adipocytes, ACSL1 interacts with FATP1, a FA transporter at the PM. There, ACSL1 activity is necessary for the activity of FATP1 by directly activating and mitigating incoming FAs. This process of channeling is called vectorial acylation [83, 87]. In contrast, knock-down studies on ACSL1 in adipocytes did not confirm a role in FA uptake, but indicate a role in FA reesterification following lipolysis [88].

2.3. TAG biosynthesis

TAG synthesis combines the products of glycolysis, in particular glycerol-3-phosphate, with acyl-CoA. In a four-step reaction, glycerol is dephosphorylated and three FAs are esterified to the glycerol backbone (figure 2.4 and reviewed in Coleman et al. [89]). The first step, the formation of lyso-phosphatidate (LPA) or 1-acylglycerolphosphate, is catalyzed by glycerolphosphate acyltransferase (GPAT), which represents the rate-limiting step of TAG synthesis. The second step, the addition of another FA to yield phosphatidic acid or 1,2-diacylglycerolphosphate, is catalyzed by acylglycerolphosphate acyltransferase (AGPAT/LPAAT). In the third step, the phosphate is removed from 1,2-diacylglycerolphosphate by the action of phosphatidic acid phosphatase (PAP, lipin). In the last step, the resulting diacylglycerol is converted to TAG by the addition of another FA at the sn-3 position. This reaction is catalyzed by the diacylglycerol acyltransferases (see section 2.3.1), which determine whether DAG is used for TAG synthesis or whether it participates in phospholipid synthesis (see section 2.4).

2.3.1. Diacylglycerol acyltransferases (DGATs)

TAGs are mainly synthesized by the glycerol-3-phosphate pathway. The last step in the formation of TAG, the addition of an activated FA to diacylglycerol, is catalyzed by diacylglycerol acyltransferases (DGATs). In mammals, two isoforms are known, DGAT1 and DGAT2, which share no sequence homology and belong to different protein families. Both isoforms are ubiquitously expressed with highest expression in white adipose tissue, small intestine, liver and mammary gland [90]. Both proteins are membrane proteins. While DGAT1 has multiple transmembrane domains [91], DGAT2 possesses only one hydrophobic stretch and a monotopic topology (see section 4.3.2 and [92]).

In mice, DGAT1 knock-out led to reduced TAG levels, resistance to diet-induced obesity and increased sensitivity to leptin and insulin [93, 94] suggesting a role in the regulation of energy metabolism. Knock-out of DGAT2 led to lipopenic mice with impaired skin barrier permeability that died soon after birth, demonstrating that DGAT2 is essential for survival [95]. While DGAT2 mainly catalyzes the formation of TAG, DGAT1 accepts also other substrates like retinol, waxes and MAG, especially in the intestine [96, 97].

Expression of DGAT2 in adipocytes is regulated by the transcription factor C/EBP [98] and by leptin [99]. Leptin reduces DGAT2 expression, but has no influence on DGAT1. Similarly, suppression of DGAT2 in rats leads to a reduced expression of lipogenic genes, but increases

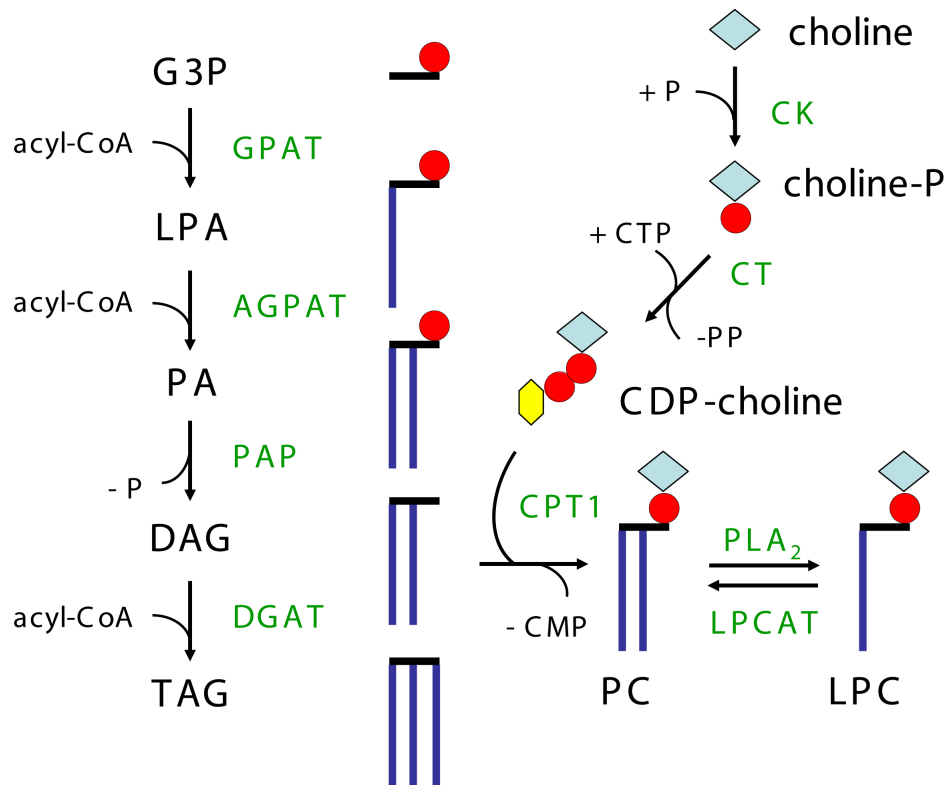


Figure 2.4.: Pathway of triacylglycerol and phosphatidylcholine synthesis

Synthesis of TAG is shown on the left side, synthesis of PC on the right side. Enzymes are labeled in green, phosphate in red, cytosine in yellow, choline in light blue, fatty acids in dark blue and glycerol in black. G3P, glycerol-3-phosphate; LPA, lyso-phosphatidic acid; PA, phosphatidic acid; DAG, diacylglycerol; TAG, triacylglycerol; choline-P, cholinephosphate; PC, phosphatidylcholine; LPC, lyso-phosphatidylcholine; GPAT, glycerolphosphate acyltransferase; AGPAT, acylglycerolphosphate acyltransferase; PAP, phosphatidic acid phosphatase; DGAT, diacylglycerol acyltransferases; CK, choline kinase; CT, CTP-phosphocholine cytidyltransferase; CPT, CDP-choline 1,2-diacylglycerol cholinephosphotransferase; PLA₂, phospholipase A₂; LPCAT, lyso-phosphatidylcholine acyltransferase.

expression of oxidative genes in the liver that reverses diet-induced hepatic steatosis and insulin resistance, whereas suppression of DGAT1 shows no similar effect [100].

DGAT1 and DGAT2 localize to the ER compartment and upon addition of oleate DGAT2 localizes to LDs (see section 4.1.1.1 and [28, 101]). Recently, a sequence was identified in DGAT2 that seems to be responsible to recruit DGAT2 to MAM within the ER compartment [101]. Furthermore, DGAT2 was reported to colocalize with the ER protein stearoyl-CoenzymeA desaturase (SCD) in Hela cells, which is also present in MAM and is important for the accumulation of TAG [102, 103].

2.4. PC biosynthesis

PC is synthesized by two different pathways (figure 2.4). One pathway is called the de novo or Kennedy pathway [104]. In this three-step reaction, choline is activated and transferred to DAG. First, choline is activated by phosphorylation to cholinephosphate by the

choline kinase (CK) and subsequent reaction with CTP, catalyzed by CTP-phosphocholine cytidyltransferase (CT), which yields CDP-choline and PP. In the last step, CDP-choline 1,2-diacylglycerol cholinephosphotransferase (CPT) catalyzes the transfer of cholinephosphate to DAG accompanied by the release of CMP, which results in the formation of PC.

The other pathway is called the membrane-remodeling pathway or Lands cycle [105]. The Lands cycle is crucial for the insertion of arachidonate into glycerophospholipids and the formation of platelet activating factor (PAF), both of which are important in inflammatory processes. Here, PC derives from LPC by the addition of acyl-CoA. LPC mainly originates from PC by the release of the FA at its sn-2 position. This reaction is catalyzed by phospholipase A₂. The reverse process, the formation of PC from LPC, is catalyzed by enzymes called lyso-phosphatidylcholine acyltransferases (LPCATs).

2.4.1. Lyso-phosphatidylcholine acyltransferases (LPCATs)

Recently, four LPCATs were cloned and characterized [106–111]. LPCAT1 and LPCAT2 belong to the lyso-phosphatidic acid acyltransferase (LPAAT) family, characterized by the presence of four conserved motifs [112], and possess a C-terminal ER retention motif. In contrast, LPCAT3 and LPCAT4 lack LPAAT motifs and are related to proteins of the membrane-bound O-acyltransferase (MBOAT) family [113], which includes the cholesterol acyltransferase ACAT1 and DGAT1. LPCAT1 is highly expressed in lung tissue, especially in type II alveolar cells [107], and it was also detected in red blood cells [109]. LPCAT2 expression is highest in resident macrophages and casein-induced neutrophils [108]. Both isoforms contain Ca²⁺-binding EF-hand motifs and LPCAT2 activity is Ca²⁺-dependent, whereas contradictory results were obtained for LPCAT1 activity [106, 107, 109, 114].

LPCAT1 is supposed to be important for the production of lung surfactant [106, 107, 115], a function that is reflected by its substrate specificity. It prefers medium-chain (C6–C14) saturated and long-chain (C18) unsaturated acyl-CoAs and catalyzes the formation of dipalmitoyl-PC [106, 107, 111, 116]. Increasing concentration of substrates shifts the preference towards unsaturated short-/medium-chain acyl-CoAs [114]. Recently, lyso-PAF acyltransferase activity of LPCAT1 was demonstrated [114]. The activity and expression of LPCAT1 is independent of any inflammatory stimulation, in contrast to LPCAT2. Upon acute inflammation LPCAT2 transfers acetyl-CoA to lyso-PAF to form PAF. Under resting conditions it participates in membrane-remodeling through insertion of arachidonyl-CoA into PC [108, 116]. Beside acetyl-CoA and arachidonyl-CoA, LPCAT2 exhibits a similarly broad substrate preference as LPCAT1 [111].

LPCAT3 is highly expressed in lung, thymus and adipocytes [117]. Additionally, it is the main LPCAT in liver cells [110]. As substrates it prefers long-chain unsaturated acyl-CoAs in vitro [110, 111, 117], but it seems to incorporate preferably saturated medium-chain FA in vivo, as was shown by overexpression in Sf9 insect cells or knockdown in HEK293 cells [118]. LPCAT4 is highly expressed in epididymis, brain, testis and ovary and utilizes preferentially oleoyl-CoA [111, 116].

2.5. Dynamics of lipids

Lipids are in a constant flux and are continuously converted into each other. Within cells, FAs are transported by FABPs and FATPs (see section 2.2.5). Also transport proteins for more complex lipids were reported for example the StAR-related lipid transfer (START) domain proteins [119]. Alternatively, lipids can be distributed by diffusion within membranes or between organelles via membrane continuities. Those continuities were reported between LDs and ER [13, 120, 121]. Additionally, LDs seem to stay in contact with other organelles like endosomes [122], peroxisomes [123], lysosomes, autophagosomes [124, 125] and mitochondria [126, 127] (figure 2.5). Furthermore, lipids can be exchanged between organelles by vesicular transport. LDs themselves are mobile. They can be transported along microtubules within cells [128, 129]. Additionally, LDs are able to fuse with each other [130, 131]. Also the TAG stored within LDs underlies a permanent turnover in cycles of lipolysis and reesterification.

Extracellularly, lipids are transported in lipoproteins. These lipoproteins are soluble complexes of proteins (apolipoproteins) and lipids that are transported in the circulation of vertebrates and insects and that are synthesized in the liver and intestine. They are classified into chylomicrons (CM), very low density (VLDL), low density (LDL) and high density (HDL) lipoproteins based on their apolipoprotein component and their density, which is determined by the lipid composition [57]. Like LDs, they contain a core of neutral lipids (TAG, CE) surrounded by phospholipids and cholesterol. TAG is secreted from the liver and intestine in apolipoproteinB (apoB) containing lipoproteins (CM and VLDL). In contrast to other apolipoproteins, apoB is not exchangeable between lipoproteins and resides in the plasma in a lipid-associated form only. While VLDL and CM contain apoE, apoC and apoB, LDL harbors exclusively apoB. ApoB is synthesized in the liver and is loaded with lipids in the ER and Golgi. Especially the neutral lipids are transferred to apoB by the luminal ER protein microsomal triacylglycerol transfer protein (MTP) [133]. In the absence of loaded lipids apoB cannot be secreted and is rapidly degraded [134, 135]. The TAG secreted as CM and VLDL mainly derives from TAG stored in cytosolic LDs [136].

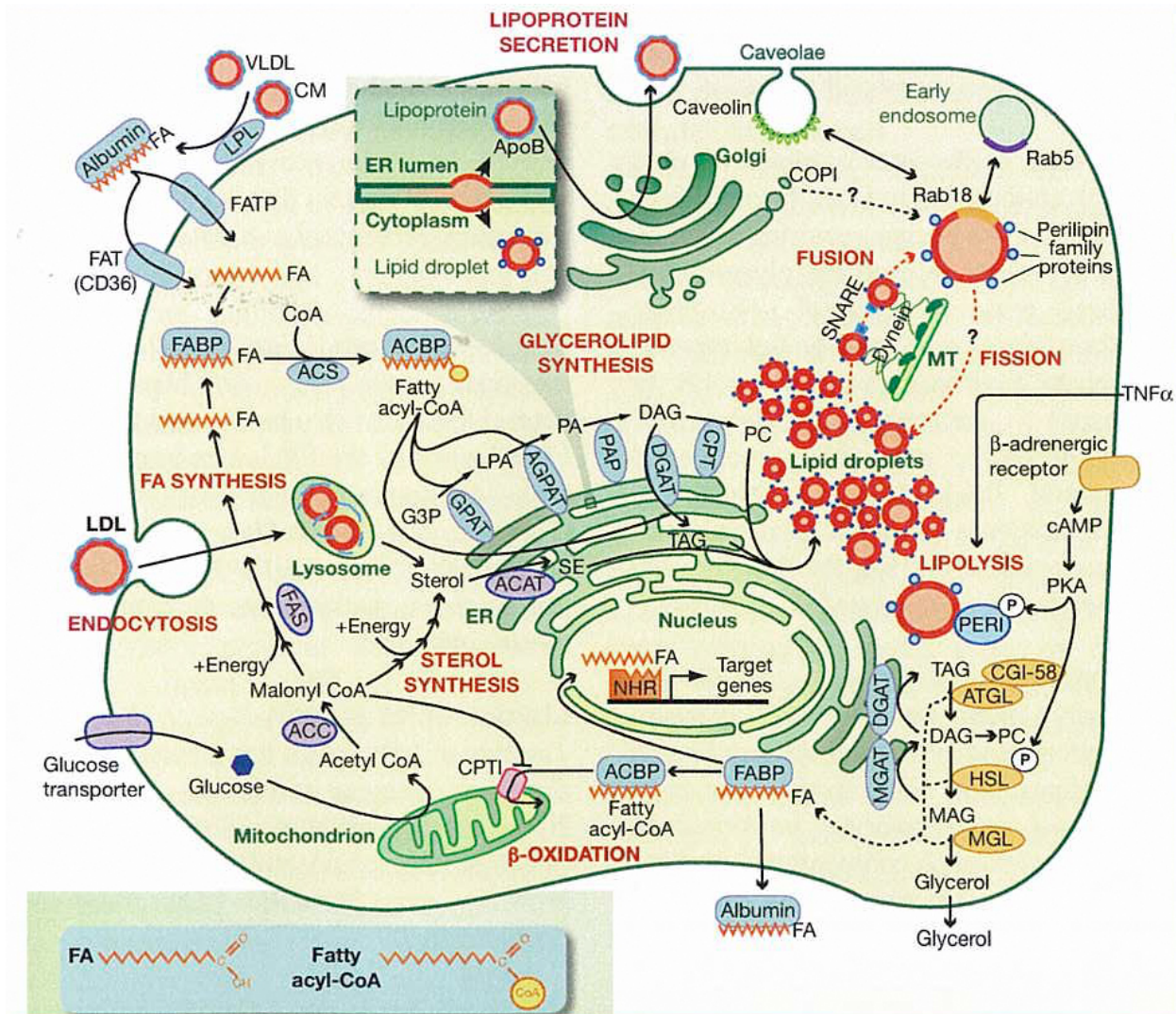


Figure 2.5.: Overview of the dynamics of LDs and their connection to different cellular processes
This figure is taken from [132]. For abbreviations of glycerolipid synthesis see section 2.3, for FA synthesis and transport proteins see section 2.2.5, for lipolysis see section 2.2.4 and for lipoprotein metabolism see section 2.5. CPT1, carnitine/acylcarnitine translocase 1; NHR, nuclear hormone receptor; TNF α , tumor necrosis factor α

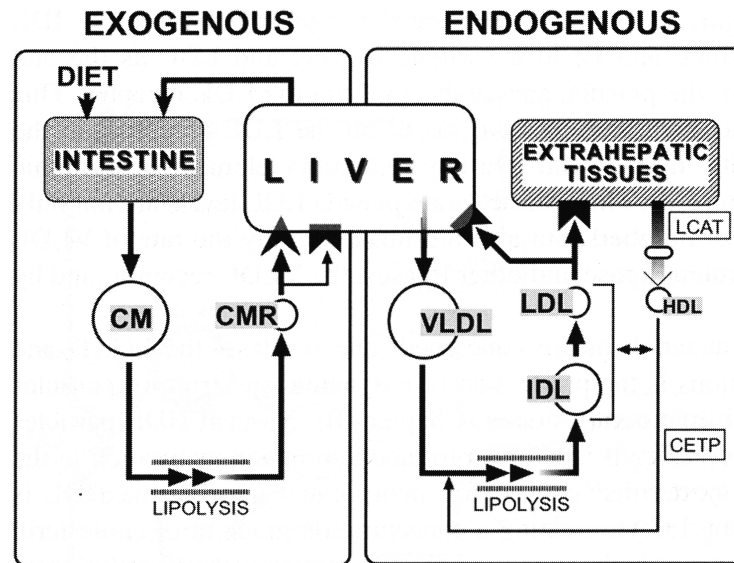


Figure 2.6.: Simplified receptor-mediated human lipoprotein metabolism

The liver is the crossing point between the exogenous pathway, which deals with dietary lipids, and the endogenous pathway that starts with the hepatic synthesis of very low density lipoprotein particles (VLDL). The endogenous metabolic branch starts with the production of chylomicrons (CM) in the intestine, which are converted to chylomicron remnants (CMR). VLDL are lipolyzed to low density lipoprotein particles (LDL), which bind to the LDL receptor. IDL, intermediate density lipoproteins; HDL, high density lipoproteins; LCAT, lecithin:cholesterol acyltransferase; CETP, cholesterol ester transferprotein; arrowhead, LDL receptor-related protein; arrowback, LDL-receptor. 'Lipolysis' denotes lipoprotein lipase-catalyzed TAG lipolysis in the capillary bed. This figure is taken from [57].

VLDLs and CMs are converted into intermediate density lipoproteins (IDL) and LDL by lipase activities within the circulation (figure 2.6). The major plasma TAG lipase is the lipoprotein lipase (LPL). While LPL is secreted mainly by adipose and muscle tissues, hepatic lipase is located to the liver. It converts VLDL remnants (IDLs) into LDLs by lipolysis of TAG. FAs released from lipoproteins are bound to serum albumin and taken up by cells (see section 2.2.5). Most lipoproteins are cleared from the circulation by lipoprotein receptors (VLDL-, LDL- and scavenger receptor).

2.6. Lipids and diseases

Storage and release of lipids, their consumption and uptake are regulated by several factors and signaling pathways. Already the deficiency of a single factor can cause an imbalance that results in the development of diseases. Mutations in CGI-58 cause the Chanarin-Dorfman Syndrome characterized by the accumulation of TAG in multiple tissues [45, 137]. A similar phenotype appears upon mutations in ATGL, which causes the so-called neutral lipid storage disease with myopathy [138]. In the Niemann-Pick disease type C, the Niemann-Pick C genes are disrupted. This leads to a defect in endosomal cholesterol transport following the accumulation of unesterified cholesterol in late endocytic organelles, which results in

neurodegeneration [139]. In contrast, the disruption of Berardinelli-Seip congenital lipodystrophy 2 (BSCL2, seipin) [140] and caveolin-1 [141] results in a complete or partial lack of adipose tissue.

Many metabolic disorders derive from additive defects in different pathways that can gradually progress into more severe diseases. The first step is usually the excess storage of lipids within different body tissues resulting in the development of obesity [142, 143]. Obesity is correlated to a set of metabolic disorders summarized as metabolic syndrome. This includes insulin resistance and type-2 diabetes [144, 145], hepatic steatosis [146], inflammation, atherosclerosis [147] and other cardiovascular diseases. Furthermore, it correlates with the development of neurological diseases like Alzheimer disease [148, 149].

3. Aim of the thesis

Lipids are stored within cells in organelles called lipid droplets (LDs). They consist of a hydrophobic core of neutral lipids like triacylglycerol (TAG), surrounded by a monolayer of phospholipids mainly containing phosphatidylcholine (PC). Excess storage of lipids is associated with cellular dysfunctions and the development of diseases. Treatment of these diseases requires detailed knowledge of the proper function of the processes and the key players involved. Though detailed but incomplete information on hydrolysis of storage lipids and lipoprotein metabolism was achieved, relatively little is known about the biogenesis and the liposynthetic metabolism of LDs. Most enzymes involved in lipid synthesis and degradation are identified, but their precise role in the synthesis and incorporation of complex lipids into LDs and subsequent LD growth still needs to be elucidated.

The aim of this thesis is to gain knowledge of the connection between lipid synthesis and growth of LDs. In particular, the following key questions will be addressed:

- Are LDs able to grow by local synthesis of their main components TAG and PC?
- What enzymes are responsible for this LD-localized synthesis?
- What is the localization and the topology of these enzymes?
- What is the physiological role of this LD-localized synthesis?
- Are other proteins like specific interaction partners involved in regulation of these enzymes?

In conclusion, this thesis will provide detailed new information on lipid metabolic processes closely linked to LDs.

4. Results

This chapter deals with the lipid droplet localized synthesis of triacylglycerol (TAG) and phosphatidylcholine (PC), which are the main components of lipid droplets (LDs). The first part focuses on the identification, localization and activity of enzymes that are responsible for the synthesis of these lipids. The second part goes further into detail about the importance of the LD surface, consisting mainly of PC, in the context of LD morphology and cell physiology. In the third part the membrane topology of the enzymes, responsible for the synthesis of these lipids, is investigated, especially with regard to the phospholipid monolayer surrounding LDs. The last part concentrates on the regulation of TAG synthesis by interactions between the responsible enzyme DGAT2 and other proteins.

4.1. LDs locally synthesize their lipid components

This first section presents the first evidence that LDs are able to locally synthesize the lipids of their core (TAG) and their surface (PC), which endows the LDs a more independent status than assumed before.

4.1.1. DGAT2 catalyzes the formation of TAG on LDs

TAGs are mainly synthesized by the glycerol-3-phosphate pathway (section 2.3). The last step in the formation of TAG, the addition of an activated fatty acid to diacylglycerol, is catalyzed by diacylglycerol acyltransferases (DGATs) [89]. The generation of knockout mice of the two DGAT iso-enzymes revealed that DGAT1 is important to maintain the skin and a normal energy metabolism, while DGAT2 is essential for survival [95]. In order to understand the *basic* regulation of lipid metabolism in the context of LDs, this thesis is therefore focused on the function of DGAT2.

4.1.1.1. Localization of DGAT2 in COS7 cells

Untreated COS7 cells contain an insufficient amount of DGAT2 for detection with our DGAT2 antibody. Additionally, tags at the termini of the DGAT2 protein interfere with a physiological localization of DGAT2 [28]. Therefore wildtype human DGAT2 was overexpressed in COS7 cells and its localization was analyzed under different nutritional conditions. Detection of DGAT2 results in the staining of a reticular structure representing the ER compartment, but upon the addition of oleate DGAT2 staining accumulates in ring-like structures surrounding LDs (figure 4.1). This localization to LDs is supported by data from another study [101]. Furthermore, endogenous DGAT2 can be found at the vicinity of LDs in mouse adipocytes [28].

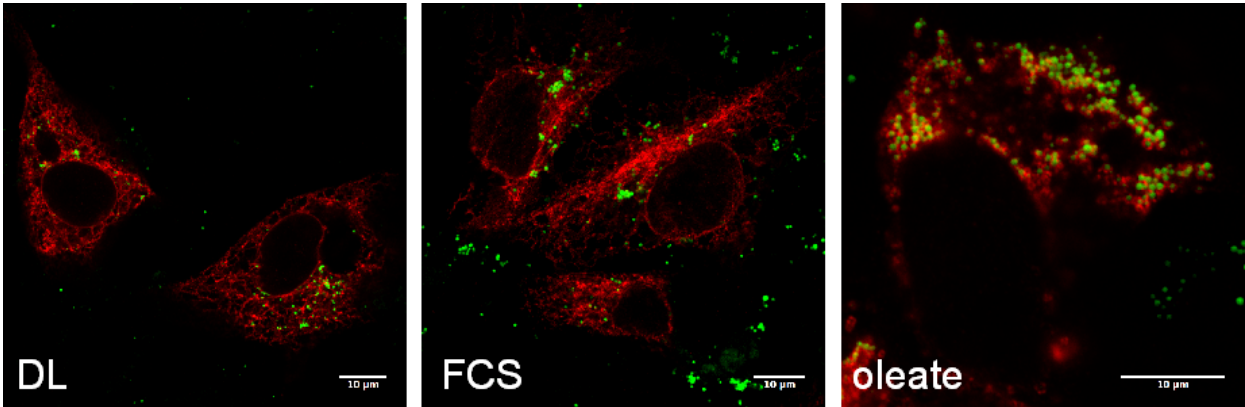


Figure 4.1.: Cellular localization of DGAT2

COS7 cells were transfected with wildtype human DGAT2 for 24 h. Cells were grown in DMEM medium supplemented with delipidated FCS (DL), normal FCS (FCS) or FCS and 100 μ M oleate (oleate). Cells were analyzed by immunofluorescence for LDs (green) and DGAT2 (red). See supplementary figure A.1 for the image (oleate) separated into single channels. Scalebar = 10 μ m

In order to distinguish, whether DGAT2 localizes to the ER compartment at the vicinity of LDs or directly to their surface, LDs were isolated from oleate-fed, DGAT2-overexpressing COS7 cells in a sucrose density gradient (see section 6.2.2.7). The western blot analysis of the abundance of DGAT2 and the ER membrane protein ACAT1 in the different fractions of the gradient revealed a signal for DGAT2 in the LD fraction, but no ACAT1 protein was detected (figure 4.2). This shows that DGAT2 localizes directly to the surface of LDs and not only to the ER compartment in their vicinity.

4.1.1.2. The activity of DGAT2 on LDs

The localization of DGAT2 to the surface of LDs, especially under fatty acid-rich conditions, raised the question, whether this enzyme is functional in the catalysis of TAG formation under these conditions. This activity would enable the LD to locally synthesize TAG, which

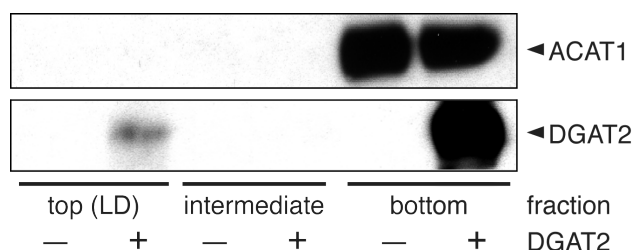


Figure 4.2.: DGAT2 localizes to LDs

Lysates of cells transiently overexpressing DGAT2 or of untransfected control cells were subjected to sucrose density gradient centrifugation. Fractions of the gradients were assayed by western blot analysis for expressed DGAT2 (lower row) and for the endogenous ER marker protein ACAT1 (upper row), which serves both as a loading control and to demonstrate absence of ER contamination from droplets.

might be advantageous for a fast response to excessive fatty acid supply. Additionally, it might participate in the acylation of DAG that is stored within the LDs [28]. Therefore, LDs isolated from wildtype or DGAT2-overexpressing COS7 cells were analyzed for their capacity to synthesize TAG from DAG and acyl-CoA. The data show that isolated wildtype LDs are capable to synthesize minor amounts of TAG. This LD-associated activity increases strongly upon overexpression of DGAT2 (figure 4.3).

4.1.2. LPCAT1 and LPCAT2 catalyze the formation of PC on LDs

Besides TAG, the major lipid of LDs is PC, which forms a monolayer that surrounds the TAG core. There are two possible pathways for the formation of PC. On the one hand it is formed from DAG and CDP-choline by the so called de-novo or Kennedy pathway, on the other hand it is formed from lyso-phosphatidylcholine (LPC) and acyl-CoA. This reaction is catalyzed by lyso-phosphatidylcholine acyltransferases (LPCATs) and is part of the so-called membrane-remodeling process or Lands cycle (see section 2.4). As shown in section 4.1.1, LDs are able to locally synthesize TAG. The growth of the LD surface must be coordinated with the growth of the LD core, suggesting a local mechanism for the synthesis of surface

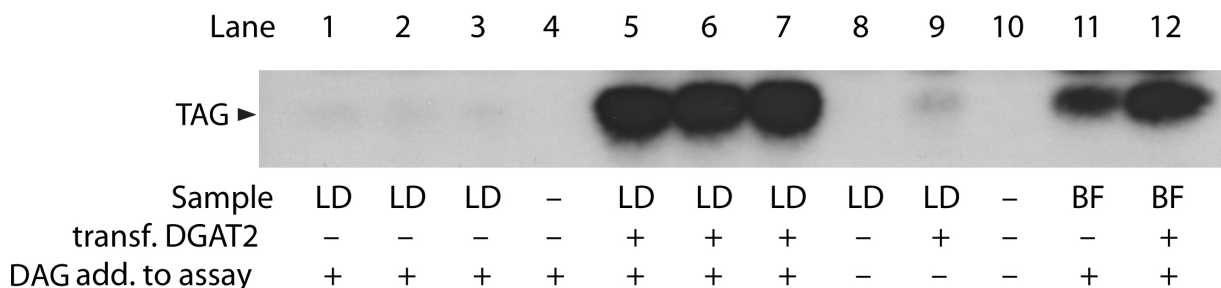


Figure 4.3.: DGAT2 enables LDs to locally synthesize TAG

Lysates of cells transiently overexpressing DGAT2 or of untransfected control cells were subjected to sucrose density gradient centrifugation. Samples of top fractions containing purified LDs and of bottom fractions (BF) were incubated for 1 h with radiolabeled acyl-CoA in the presence or absence of DAG in the assay buffer as indicated. Lipids were extracted and analyzed by TLC for radiolabeled TAG. Note that lanes 1-3 and 5-7 show triplicate measurements.

lipids like shown in section 4.1.1 for the core lipids. In order to identify candidates for local synthesis of PC on LDs the proteome of isolated LDs from A431 cells was dissected by protein mass spectrometry (supplementary figure A.2 and supplementary table B.1). This revealed the enzymes LPCAT1 and LPCAT2 as possible candidates.

4.1.2.1. Localization of LPCAT1 and LPCAT2

A specific antibody against human LPCAT1 and human LPCAT2 was raised by C. Thiele. The antibodies are isoform specific and recognize endogenous proteins (supplementary figure A.3). The western blot analysis of cell lysates from HuH7, A431 and COS7 cells revealed the expression of LPCAT1 and LPCAT2 in A431 and COS7 cells and the expression of LPCAT1 in HuH7 cells (figure 4.4). While A431 cells express large amounts of both proteins, COS7 cells in comparison show weaker expression of both proteins and HuH7 cells express only LPCAT1 in even lower amounts. The analysis of LPCAT1 and LPCAT2 localization in A431 cells (figure 4.5 and figure 4.6) and COS7 cells (figure 4.7) revealed, besides a reticular staining also a ring-like and patch-like staining pattern around LDs. These patterns were independent of the nutritional status of the cell and most likely reflect the available amount of both proteins. While in A431 cells the expression of large amounts of both proteins results in localization in ring-like structures, the lower expression in COS7 cells results in LD-associated patch-like structures. The amount of LPCAT1 in HuH7 cells was too low and the protein too dispersed for a specific staining in immunofluorescence.

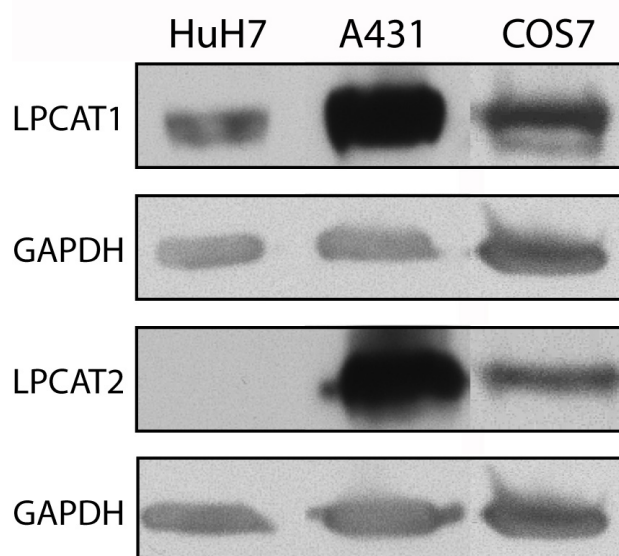


Figure 4.4.: Expression of LPCAT1 and LPCAT2 in HuH7, A431 and COS7 cells

Total lysates of HuH7 cells, A431 cells and COS7 cells were subjected to SDS-PAGE/western blot for LPCAT1, LPCAT2 and GAPDH (for normalization). Note that A431 cells contain abundant LPCAT1 and LPCAT2, whereas HuH7 cells contain a small amount of LPCAT1, but no detectable LPCAT2. Longer exposure times do not reveal any signal for LPCAT2 in HuH7 cells (data not shown).

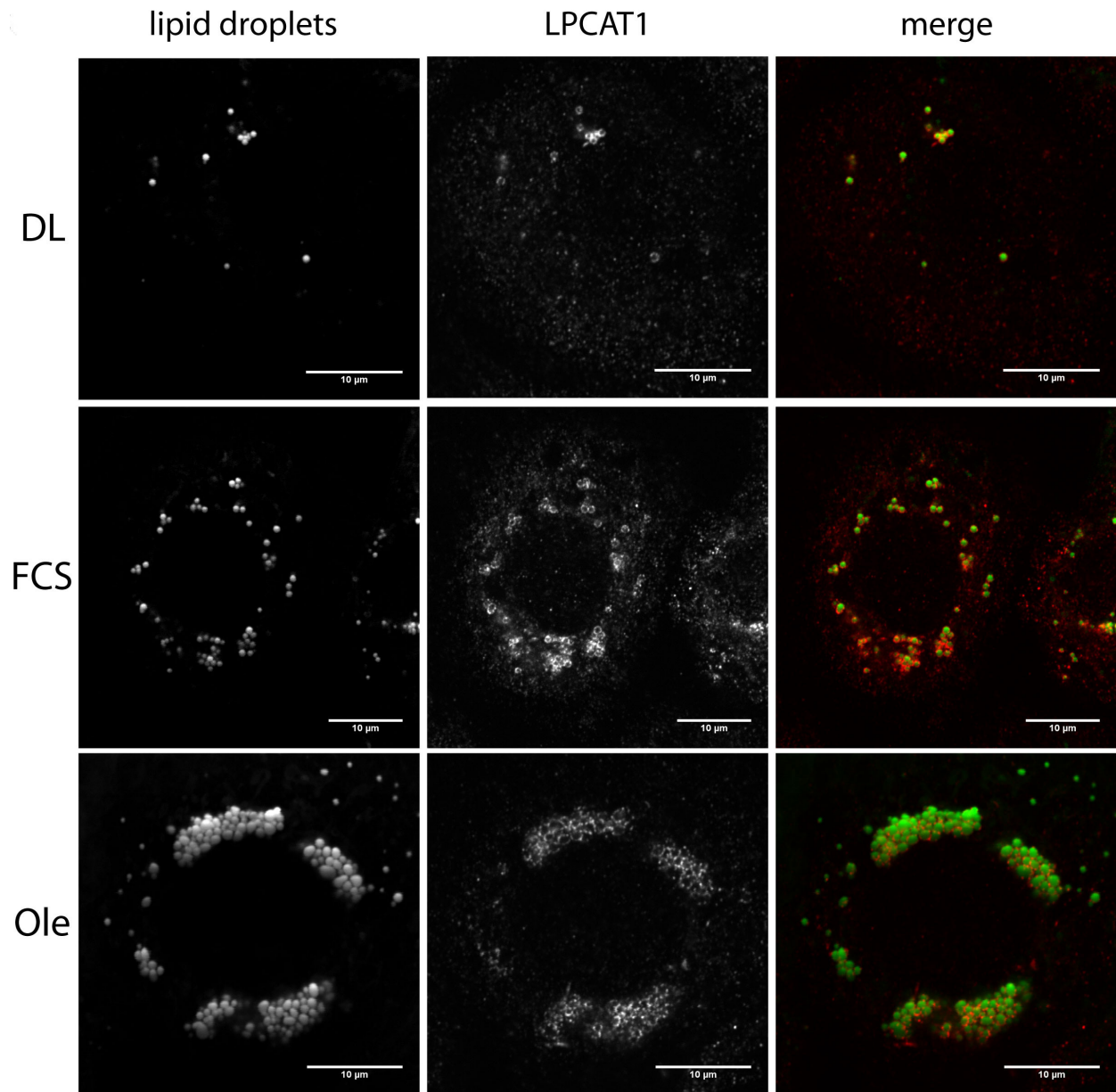


Figure 4.5.: Localization of LPCAT1 in A431 cells

A431 cells were cultivated for 20 h in DMEM supplemented with 10% of either delipidated FCS (DL), normal FCS (FCS), or normal FCS + 100 μ M oleate (Ole). Cells were fixed and processed for immunofluorescence microscopy using BODIPY 493/503 to stain neutral lipids (lipid droplets) and anti-LPCAT1 to stain the endogenous protein. In the merged pictures, BODIPY 493/503 staining is in green, anti-LPCAT1 in red. Scalebar = 10 μ m.

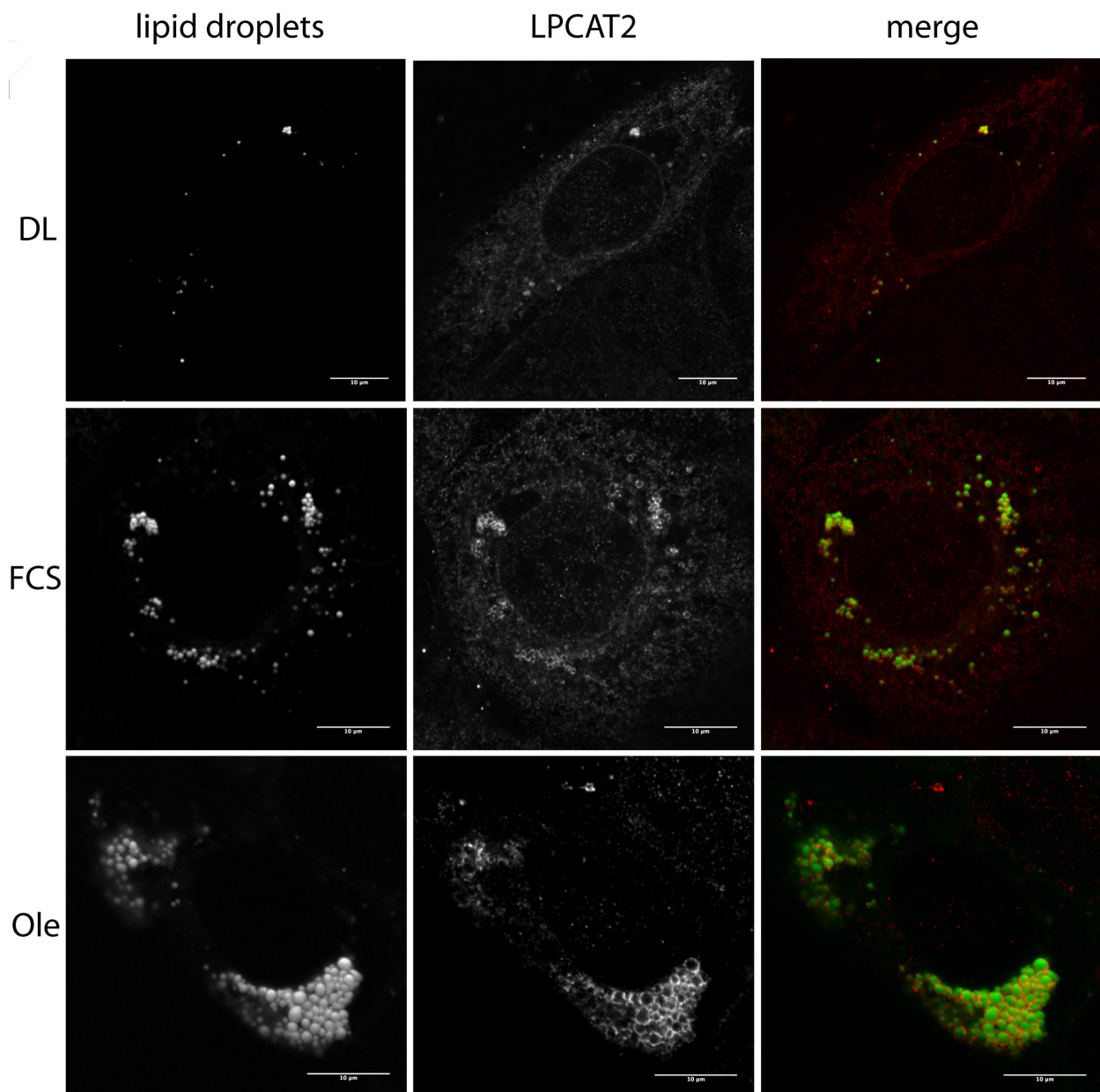


Figure 4.6.: Localization of LPCAT2 in A431 cells

A431 cells were cultivated for 20 h in DMEM supplemented with 10% of either delipidated FCS (DL), normal FCS (FCS), or normal FCS + 100 μ M oleate (Ole). Cells were fixed and processed for immunofluorescence microscopy using BODIPY 493/503 to stain neutral lipids (lipid droplets) and anti-LPCAT2 to stain the endogenous protein. In the merged pictures, BODIPY 493/503 staining is in green, anti-LPCAT2 in red. Scalebar = 10 μ m.

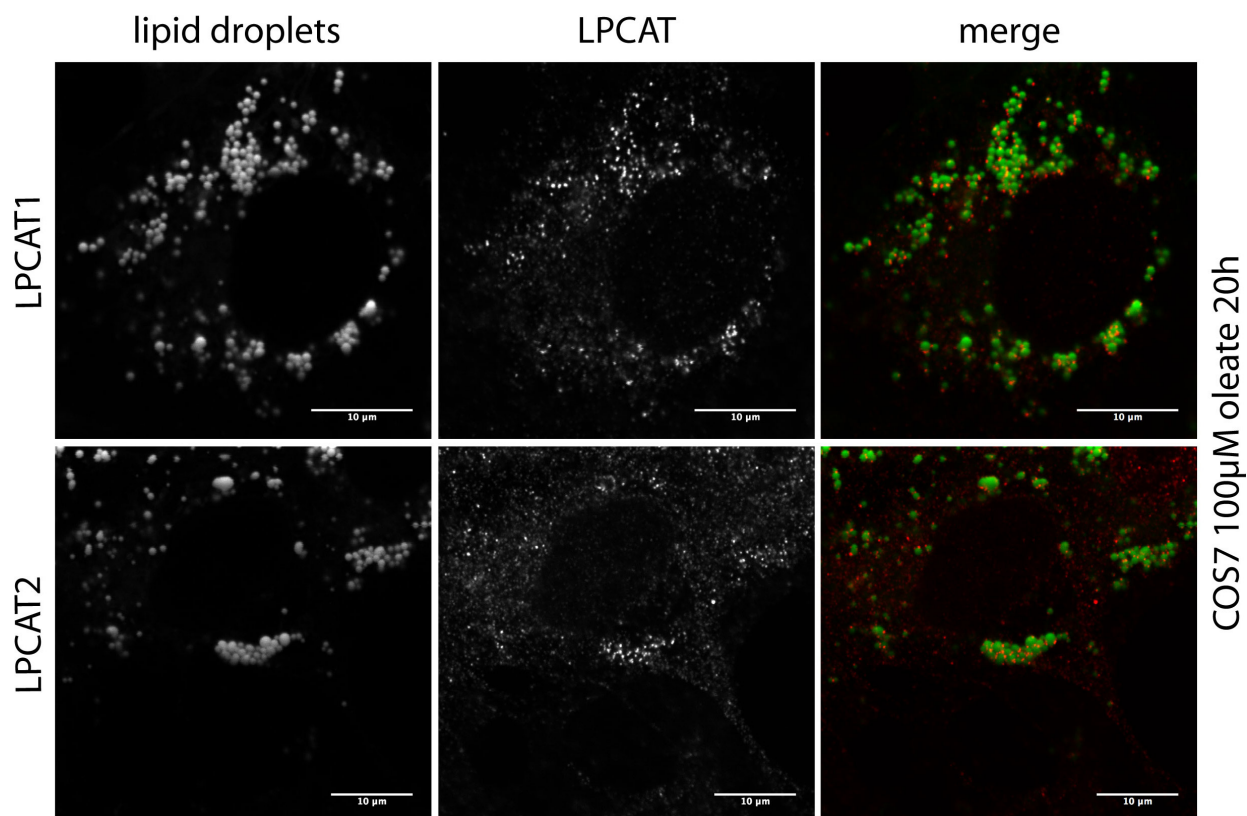


Figure 4.7.: Localization of LPCAT1 and LPCAT2 in COS7 cells

COS7 cells were cultivated for 20 h in DMEM supplemented with 10% normal FCS + 100 μ M oleate. Fixation, staining and imaging were performed as described in figure 4.5 and 4.6. Scalebar = 10 μ m.

In order to distinguish whether LPCAT1 and LPCAT2 localize to the ER compartment at the vicinity of LDs or directly to their surface, LDs were isolated from oleate-fed A431 and HuH7 cells in a sucrose density gradient (see section 6.2.2.7). The western blot analysis of the abundance of LPCAT1 and LPCAT2, the LD marker proteins ACSL3, TIP47, NSDHL and ADRP and the ER membrane proteins ACAT1 and calnexin in the different fractions of the gradient revealed a signal for LPCAT1 and LPCAT2 and the LD marker proteins in the LD fraction, but no or minor amounts of the ER markers calnexin and ACAT1 protein were detected (figure 4.8). This shows that LPCAT1 and LPCAT2 localize directly to the surface of LDs and not only to the ER compartment in their vicinity.

4.1.2.2. The activity of LPCAT1 and LPCAT2 on LDs

Similar to DGAT2 that enables LDs to locally synthesize TAG, LPCAT1 and LPCAT2 might enable LDs to locally synthesize PC. Therefore it was studied, whether LDs have the ability to synthesize PC via LPCATs, whether this activity is specific for LDs and whether it is a general property of LDs. LPCAT activity and LPAAT activity, which is abundant in the ER [150], were compared in three different cell lines (HuH7, COS7 and A431). While

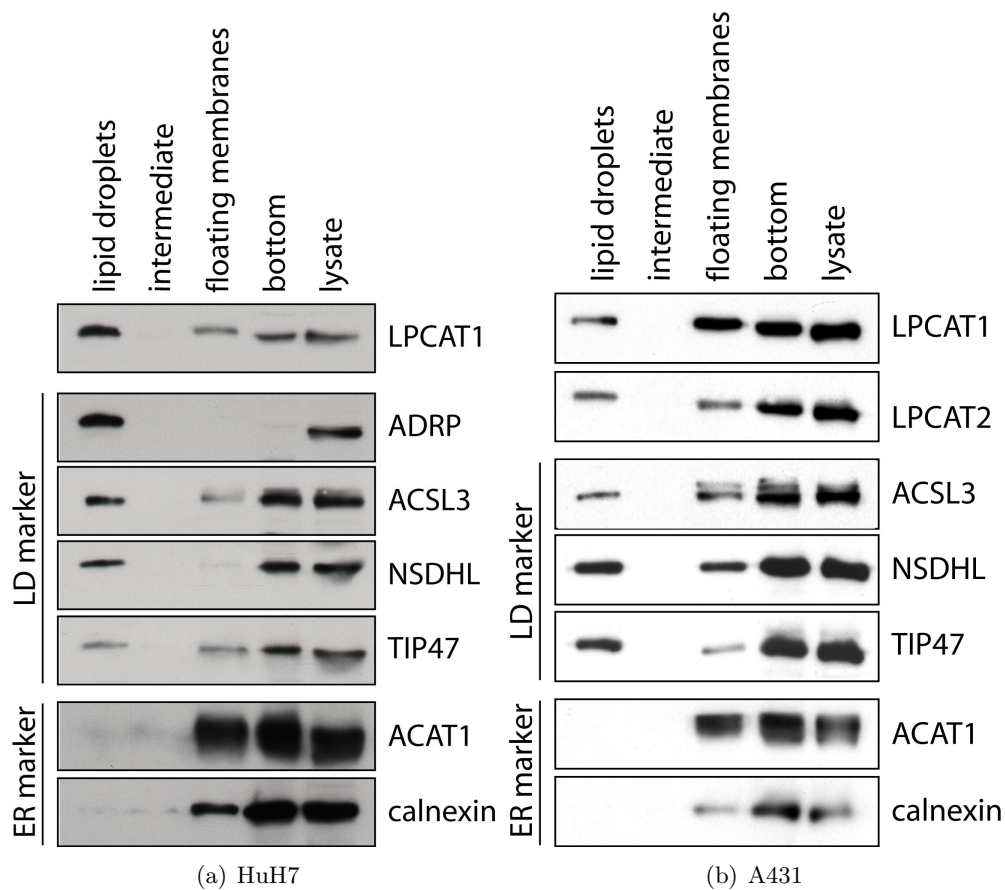


Figure 4.8.: LPCAT1 and LPCAT2 localize to LDs

Lysates of HuH7 cells (a) or A431 cells (b) that were grown in supplemented RPMI and DMEM with 10% FCS and 100 μ M oleate, respectively, were subjected to floatation in a sucrose density gradient. The gradient was fractionated from the top into lipid droplets, intermediate, floating membrane, and bottom fractions.

(a) Proteins were analyzed by SDS-PAGE/western blot for LPCAT1, the known integral droplet proteins ACSL3 and NSDHL, the peripheral droplet proteins ADRP and TIP47 and the integral ER membrane proteins ACAT1 and calnexin.

(b) Proteins were analyzed by SDS-PAGE/western blot for LPCAT1 and LPCAT2, the known integral droplet proteins ACSL3 and NSDHL, the peripheral droplet protein TIP47 and the integral ER membrane proteins ACAT1 and calnexin.

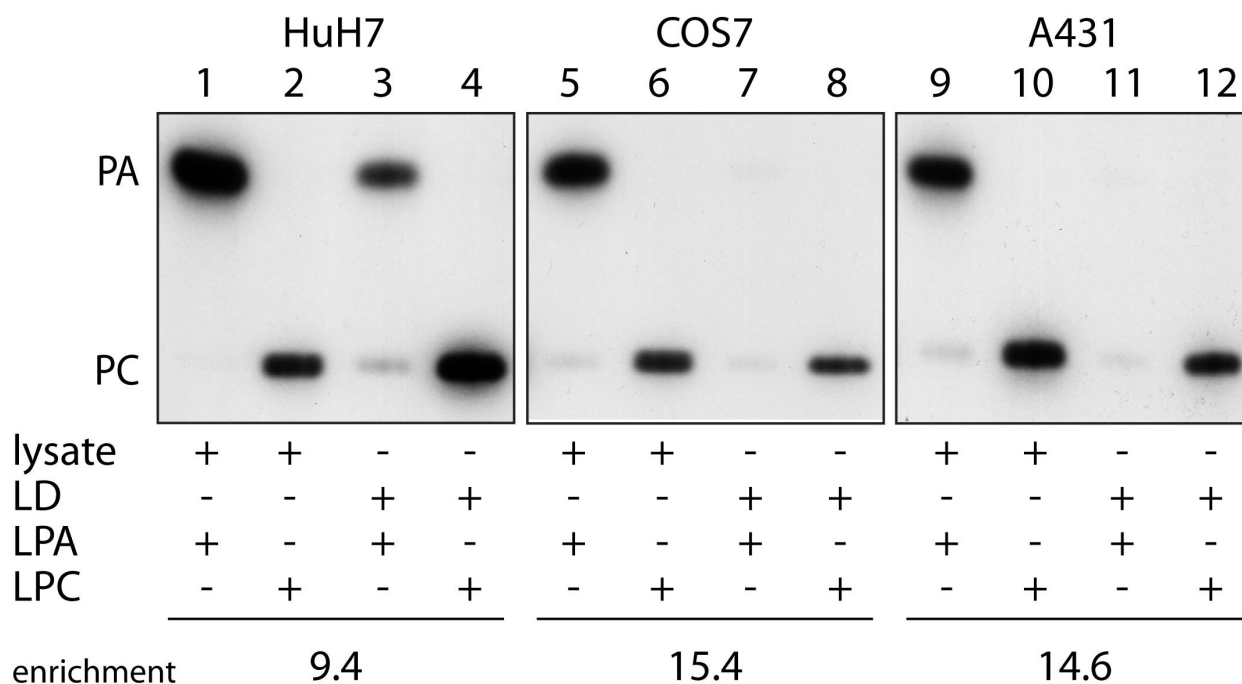


Figure 4.9.: LDs possess LPCAT activity

HuH7, COS7 and A431 cells were cultured in the presence of 100 μ M oleic acid for 16 h, lysed and the lysate subjected to floatation in a sucrose density gradient. Cell lysates (lysate) or purified lipid droplets (LD) isolated from the indicated cell lines were incubated in the presence of [3 H]acyl-CoA and lyso-phosphatidylcholine (LPC) or lyso-phosphatidic acid (LPA). Lipids were extracted and analyzed by TLC followed by autoradiography. Radioactive spots were identified by co-migrating standards; PC, phosphatidylcholine; PA, phosphatidic acid. To calculate enrichment of LPCAT activity on LDs, spots were scraped, lipids extracted and quantified by scintillation counting. Enrichment was defined as the ratio of radioactive PC/PA in the LDs, divided by the same ratio in the lysates.

cell lysates showed comparable LPCAT and LPAAT activities (figure 4.9, lanes 1+2, 5+6, 9+10), purified LDs displayed a much weaker activity for LPAAT, but a strong activity for LPCAT (4.9, lanes 3+4, 7+8, 11+12), resulting in an enrichment of LPCAT activity relative to LPAAT activity of about 9- to 15-fold.

As LPCAT1 and LPCAT2 localize to LDs, it is likely that the measured LPCAT activity relies on these proteins. Similar to the DGAT activity on LDs (section 4.1.1.2), overexpression of LPCAT1 or LPCAT2 in A431 cells increased LPCAT activity on isolated LDs: 17 ± 12 -fold ($p < 0.05$, $n = 5$) for LPCAT1 and 2.9 ± 1.8 -fold ($p < 0.1$, $n = 5$) for LPCAT2 overexpression.

Though only enzymes for PC synthesis by the Lands cycle were identified by protein mass spectrometry of isolated LDs (supplementary table B.1), it is possible that LDs also use the Kennedy pathway for local synthesis of PC. The amount of these enzymes on the LD might be too low to be identified by mass spectrometry or the localization of these enzymes to LDs might be transient and less stable than the localization of LPCAT1 and LPCAT2. By radioactive labeling combined with the measurement of the product from the enzyme reaction, higher sensitivity for detection is achieved than could be reached by direct detection

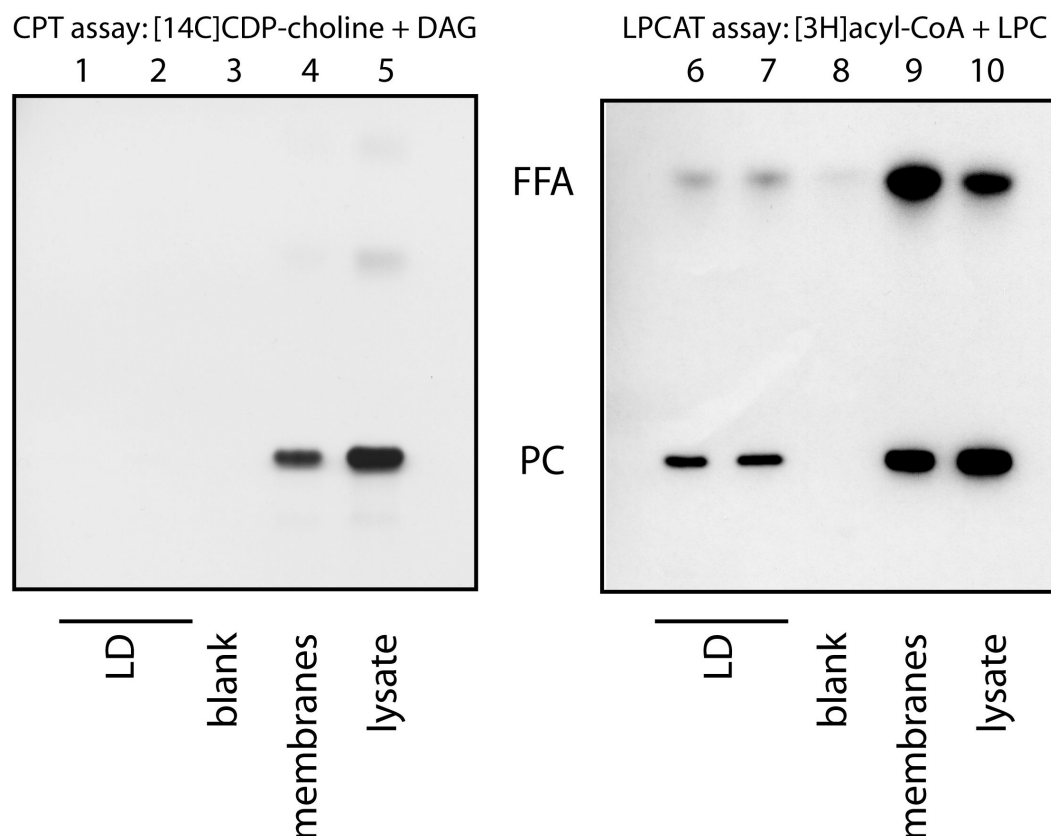


Figure 4.10.: LDs locally synthesize PC by the Lands cycle

A431 cells were cultured in the presence of 100 μ M oleic acid for 16 h, lysed and the lysate subjected to floatation in a sucrose density gradient. Samples of the lipid droplet fraction (LD), the floating membrane fraction (membranes), and the total lysates (lysate) of A431 cells were incubated in the presence of either [14C]CDP-choline plus diacylglycerol (left panel, CPT assay) or of [3H]acyl-CoA and LPC (right panel, LPCAT assay). Lipids were extracted and analyzed by TLC followed by autoradiography. Radioactive spots were identified by co-migrating standards. PC, phosphatidylcholine; FFA, free fatty acid.

of the enzyme. Therefore, LDs isolated from A431 cells were incubated with radioactively labeled substrates for the Lands cycle or for the Kennedy pathway. While lysates and membrane fractions displayed both CPT and LPCAT activity (figure 4.10, lanes 4, 5 and 9, 10), purified LDs showed only a strong LPCAT activity (figure 4.10, lanes 6, 7), but no significant CPT activity (figure 4.10, lanes 1, 2). Altogether, the experiments demonstrate that LPCAT activity on LDs is specific and general, and is not due to contamination by ER membranes.

4.2. Physiological role of LPCAT activities

This section presents the first evidence that the LD activities of LPCAT1 and LPCAT2 are reflected in the PC profile of LDs. Additionally, LPCAT1 and LPCAT2 participate in the adaptation and formation of the LD surface monolayer. Furthermore, evidence is presented that they influences the proper secretion of lipids from cells.

4.2.1. LPCAT1 and LPCAT2 participate in the synthesis of the LD surface

Though several enzymes catalyze the same reaction, they often show different substrate preferences. If the local activity of LPCAT1 and LPCAT2 contribute to the synthesis of the PC of the LD surface monolayer, their substrate preference should be reflected in the LD surface PC profile. Thus, they would participate in the formation of an organelle-specific composition of molecular PC species of the LD surface monolayer, which distinguishes it from the membranes of other cellular organelles. To characterize the molecular lipid composition of the LD surface monolayer we performed a comparative lipidomic analysis. For this experiment, it was necessary to obtain droplets with sufficient size for floatation without supplementation of oleic acid, which otherwise would dominate the lipid species composition. Therefore, A431 cells were grown with horse serum as a lipid donor. LDs were floated in a modified sucrose gradient (section 6.2.2.7 and [9]) to remove unspecific LD-associated membrane fragments and proteins. Western blots of the gradient fractions demonstrated that the LD preparation was enriched in integral LD proteins and devoid of plasma membrane, ER and endosomal contaminations (data not shown). The purity was further confirmed by mass spectrometry that showed an almost complete separation of TAG and PC in the LDs and the floating membrane fraction, respectively (supplementary figure A.4). Next, the molecular composition of the phosphocholine-containing lipids, PC and sphingomyelin (SM), in cell lysates, floating membranes and LDs were determined by lipid mass spectrometry (section 6.2.3.4).

LDs were enriched in PC species with saturated and mono-unsaturated fatty acid moieties (PC 28:0, 30:0, 32:0, 34:1, 34:2, 36:1, 36:2) as compared to floating membranes and cell lysates (figure 4.11). In contrast, PC species with poly-unsaturated fatty acid moieties (= 3 double bonds, e.g. PC 38:4), ether PC species and SM species were depleted from LDs (figure 4.11 insert). LPCAT1 has a substrate preference for medium-chain saturated LPC and for medium- and long-chain saturated fatty acids especially palmitate, but it uses also unsaturated C18 [106, 107]. LPCAT2 has a substrate preference for oleoyl-LPC and palmitoyl-LPC and short- and medium-chain saturated and C18 unsaturated fatty acids [108]. In conclusion, the PC profile of the LD monolayer reflects the substrate preferences of LPCAT1 [106, 107] and LPCAT2 [108]. However, a part of the LD PC profile also fits to the recently described substrate preferences of the ER-associated LPCAT3 [117, 118].

In comparison to the LD lipid profile of CHO-K2 cells [29] and of HepG2 cells [8], the surface of LDs from A431 cells is more similar to HepG2 than to CHO-K2 cells. The LD surface lipid composition of CHO-K2 cells resembles other cellular membranes except an

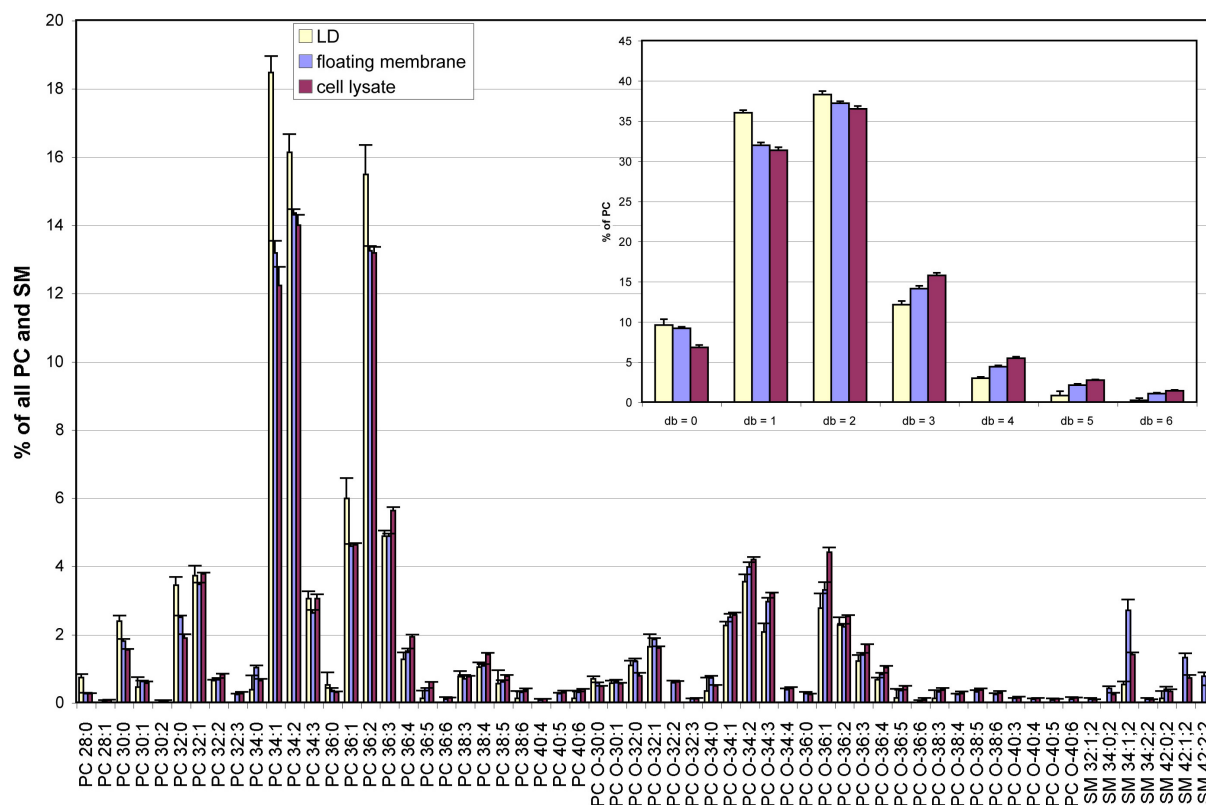


Figure 4.11.: Isolated LDs have a unique surface lipid profile

A431 cells were grown in DMEM with 10% normal FCS and additional 20% horse serum for 24 h. LDs were isolated in a modified sucrose gradient containing a pH 11.0 layer to remove all traces of LD-attached proteins and membrane fragments. Cell lysates, LDs and floating membrane fractions were collected. Total lipid extracts were analyzed in positive ion mode by precursor ions scanning for the fragment ion of phosphocholine (m/z 184.1), which specifically detects PC and SM. The amount of each lipid species is presented as percent normalized to the total abundance of PCs and SMs in each of the separate analysis. The insert shows the abundance of PC species with the indicated number of double bonds (db), as percent of total PC in the respective fraction. Bars coloured in amber, blue and red designate species detected in LD, floating membranes and whole cell lysate samples. PC, ester-linked phosphatidylcholine; PC O, ether-linked phosphatidylcholine; SM, sphingomyelin. Numbers indicate the total number of carbon atoms:double bonds in the fatty acid or fatty alcohol moieties. This figure is provided by Christer Ejlsing.

enrichment for PC, LPC and lyso-phosphatidylethanolamine (LPE) and a depletion for SM and phosphatidylserine (PS). In contrast, the lipid composition differs between LDs and ER or PM in HepG2 and also in A431 cells. While the PC of the LD surface of HepG2 cells was reported to be mainly enriched in mono-unsaturated fatty acids, the PC of LDs of A431 cells is also enriched in some saturated fatty acids compared to microsomal membranes and whole cell lysates.

4.2.2. LPCAT1 and LPCAT2 influence the morphology of LDs

The ability of LDs to synthesize their core lipid TAG and their surface lipid PC (section 4.1) might be beneficial for a fast adaptation to changes in the nutritional status. Concerning lipogenesis and lipolysis, the size of the LDs becomes an important factor. The same amount of TAG can be stored either in many small LDs or in few large LDs. Smaller droplets have a larger surface-to-volume ratio. This enables more lipid anabolic or catabolic enzymes to localize to the LD, enhancing the formation or degradation of lipids. The availability of surface and core material by the local activities of the LD will influence the surface-to-volume ratio of the LD. If local production of PC by LPCAT1 and LPCAT2 is functionally important for the dynamics of the LD monolayer, manipulation of LPCAT activity may result in a phenotypic alteration of the cellular LD pool. Therefore, siRNA-mediated gene silencing of LPCAT1 and LPCAT2 was performed in A431 cells followed by microscopic imaging of LDs.

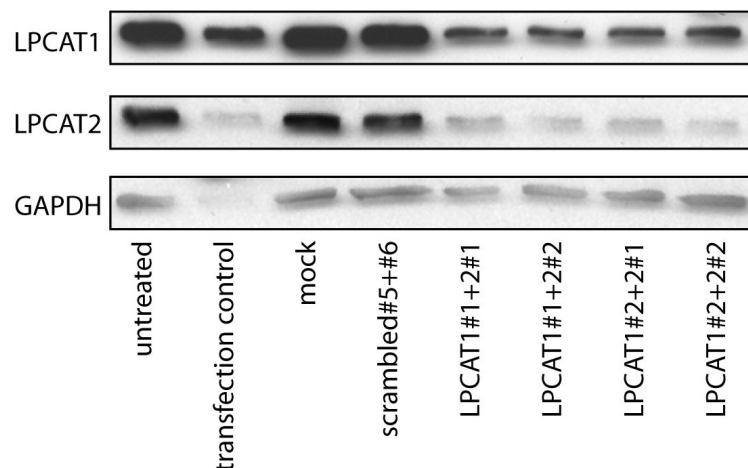


Figure 4.12.: Silencing of LPCAT1 and LPCAT2 by siRNA reduces the amount of the respective proteins in A431 cells

A431 cells were grown in DMEM with 10% normal FCS and were either left untreated (untreated or wt), mock transfected (mock), transfected with control siRNA (eg5 as transfection control, leads to cell death, or scrambled#5+#6 as non-targeting siRNAs) or the four possible combinations of two sequences each against LPCAT1 or LPCAT2 as indicated. After 48 h incubation in DMEM with normal FCS, cells were lysed and subjected to SDS-PAGE/western blot for LPCAT1, LPCAT2 and glycerol-3-phosphate dehydrogenase (GAPDH, as a loading control).

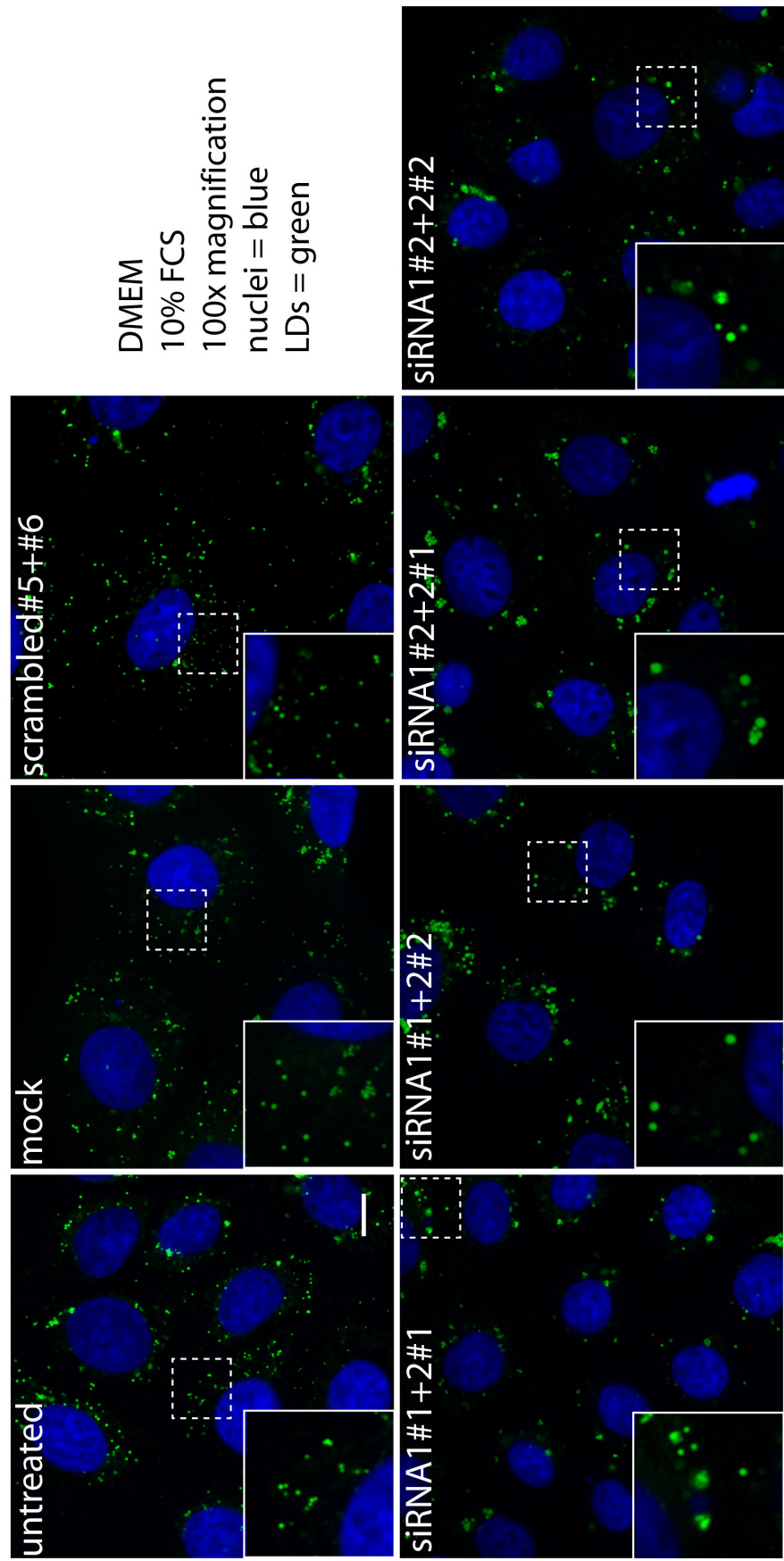


Figure 4.13.: Silencing of LPCAT1 and LPCAT2 by siRNA increases the size of LDs in A431 cells

Confocal images of controls and LPCAT1+LPCAT2 double knock-downs as described in figure 4.12. Inserts are the regions marked by dashed white squares in higher magnification. Nuclei (blue), LDs (green), scalebar = 10 μm

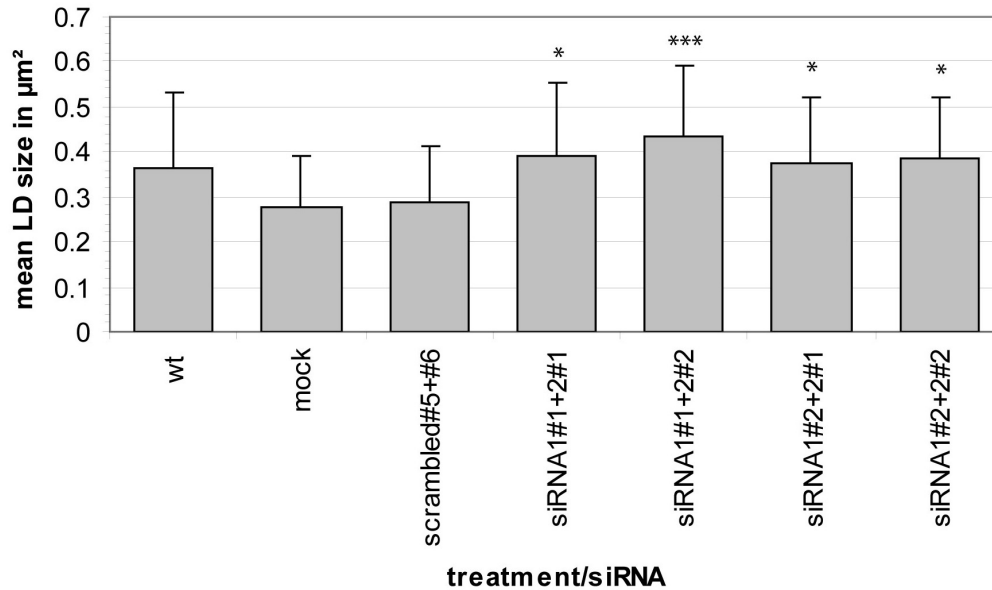


Figure 4.14.: Silencing of LPCAT1 and LPCAT2 by siRNA increases the mean size of LDs in A431 cells significantly

Confocal images as described in figure 4.13 from three different experiments were quantified with Image J and the mean LD size from the LD size distribution is compared between controls and double knock-downs as described in figure 4.12. Significances were calculated by unpaired two-sided t-test analysis relative to scrambled#5+#6 and standard deviation is shown for each dataset.

Double knock-down of LPCAT1 and LPCAT2 with various combinations of siRNA sequences results in a decrease of LPCAT1 and LPCAT2 proteins compared to controls (figure 4.12). In the LPCAT1-LPCAT2 double knock-down cells, LDs are slightly enlarged (figure 4.13). Quantification of these images confirms a significant increase in mean LD size upon LPCAT1-LPCAT2 knockdown (figure 4.14 and supplementary table B.2). However, there is no increase in the rate of TAG synthesis as measured by [3H]oleate-labeling (supplementary figure A.5), nor in the total TAG content of the cells as determined by mass spectrometry (supplementary figure A.6). In addition, the abundance of other neutral lipids (DAG, CE) and phospholipids (PC, PE and SM) is unaffected.

To corroborate the observed increase in LD diameter, the siRNA knock-down experiment was repeated under modified conditions. The cells were kept under choline-free conditions during the knock-down. This limits PC biosynthesis, leading to channeling of fatty acids towards the production of TAG, as described for the inhibition of the pathway for de novo PC synthesis (supplementary figure A.7 and [151]). Although these experimental conditions lead to overall larger LDs, the knock-down of LPCAT1 and LPCAT2 results in a further increase of LD size (supplementary figure A.8) without changes in TAG biosynthetic rates (supplementary figure A.9) or total TAG amount (supplementary figure A.10). This shows that the increase in LD size upon knock-down of LPCAT1-LPCAT2 results from another mechanism, than the LD size increase following choline-depletion. Nevertheless, the LD

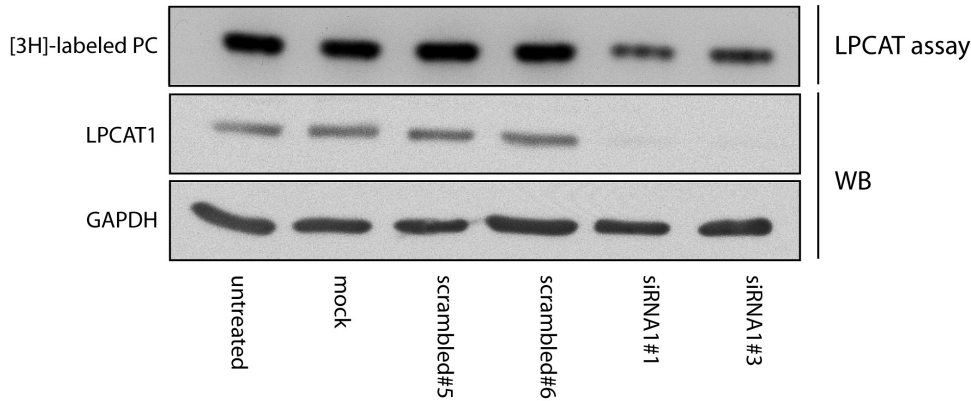


Figure 4.15.: Silencing of LPCAT1 in HuH7 cells reduces cellular LPCAT1 protein and activity

HuH7 cells were grown in supplemented RPMI medium with 10% normal FCS and were either left untreated (untreated or wt), mock transfected (mock), transfected with control siRNA (scrambled#5 and scrambled#6 as non-targeting siRNAs) or the two different siRNA sequences against LPCAT1 as indicated. After 72 h incubation in supplemented RPMI with normal FCS, cells were scraped and subjected to a LPCAT activity assay or lysed and subjected to SDS-PAGE/western blot for LPCAT1 and GAPDH (loading control).

size increase upon LPCAT1-LPCAT2 knock-down is weak due to partial compensation of the iso-enzymes (data not shown) and insufficient reduction of the LPCAT1 and LPCAT2 proteins.

Therefore, results were confirmed in the human hepatoma cell line HuH7 and in vivo in the model organism *Drosophila melanogaster*. In contrast to A431 and COS7 cells, HuH7 cells express detectable amounts of LPCAT1 only, but no LPCAT2 (figure 4.4). Similarly, LPCAT1 is associated with LDs (figure 4.8). Knock-down of LPCAT1 in HuH7 cells with two different siRNA sequences results in a decreased LPCAT activity in whole cell lysates and in a remarkable decrease in LPCAT1 protein (figure 4.15). Morphologically, this knock-down results in the appearance of larger LDs (figure 4.16). A quantification of the microscopic images revealed a significant increase in the mean LD size upon LPCAT1 knock-down of about 100 - 200 nm² (figure 4.17 and supplementary table B.3). This increase is due to a shift from small LDs (50 - 300 nm²) to large LDs (400 nm² - >1 μm²) (figure 4.18). Similar to A431 cells, the increase in LD size upon LPCAT1 knock-down is neither caused by an increase in TAG synthesis rate (figure 4.19) nor is it based on an enhanced accumulation of neutral lipids (figure 4.20).

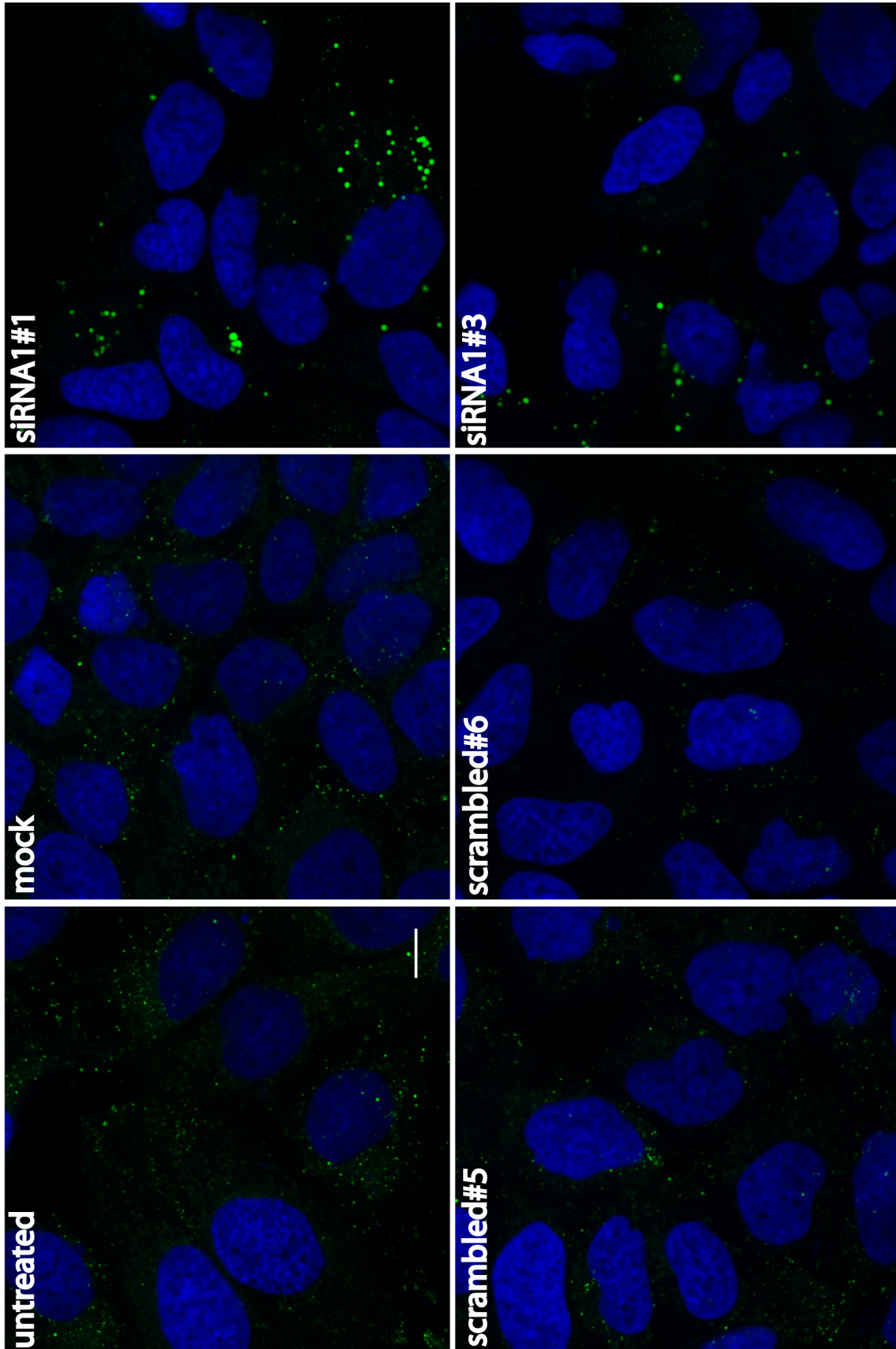


Figure 4.16.: Silencing of LPCAT1 by siRNA increases the size of LDs in HuH7 cells
Representative confocal images of controls and LPCAT1 knock-downs as described in figure 4.15. Nuclei (blue), LDs (green), scalebar = 10 μ m

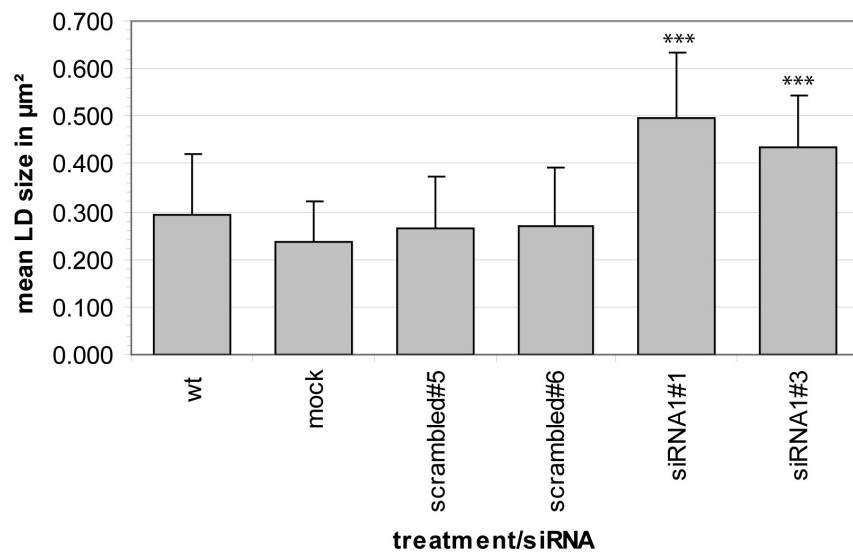


Figure 4.17.: Silencing of LPCAT1 by siRNA increases the mean size of LDs in HuH7 cells significantly
Confocal images as described in figure 4.16 from three different experiments were quantified with Image J and the mean LD size from the LD size distribution is compared between controls and knock-down as described in figure 4.15. Significances were calculated by unpaired two-sided t-test analysis relative to wt and standard deviation is shown for each dataset.

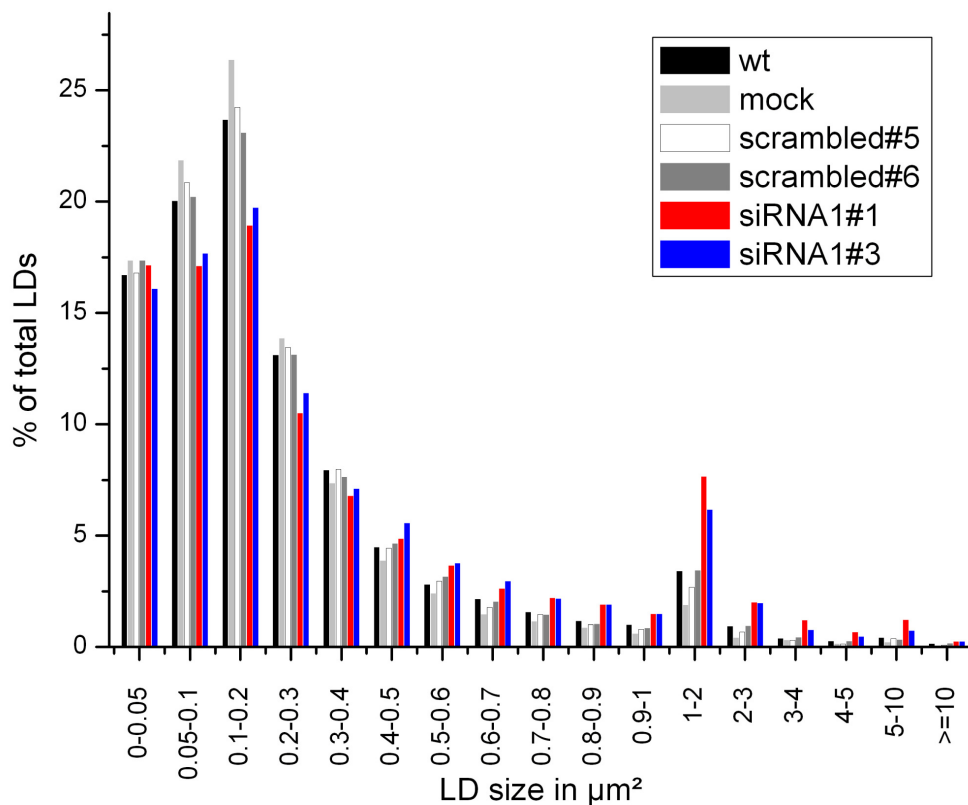


Figure 4.18.: Changes in LD size distribution in HuH7 cells upon LPCAT1 knock-down
Confocal images as described in figure 4.16 from three different experiments were quantified with Image J and the LD size distribution is displayed as percentage of total LDs analyzed per treatment. Measured LDs were grouped into size classes displayed as LD size in μm^2 . Controls (black, light and dark grey and white), siRNAs against LPCAT1 (red, blue)

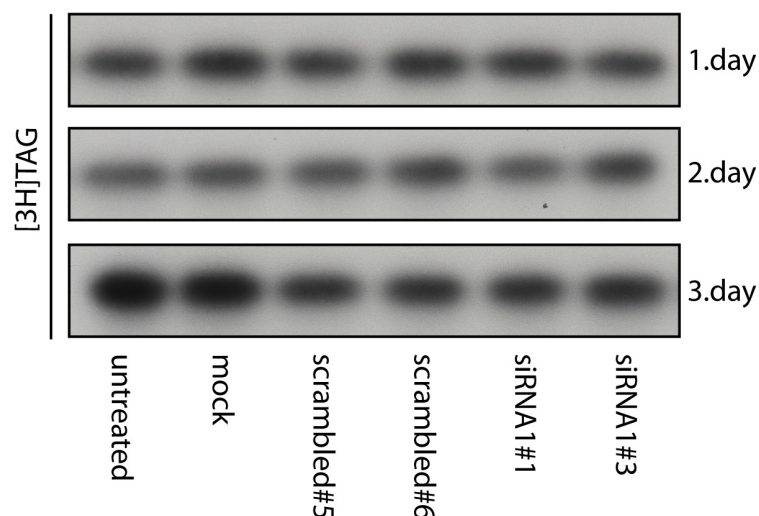


Figure 4.19.: Knock-down of LPCAT1 in HuH7 cells has no influence on TAG synthesis rate

HuH7 cells were grown and transfected with siRNA as described in figure 4.15. [^3H]oleate was added for further 24 h to the cells either directly (1.day), 24 h (2.day) or 48 h (3.day) after transfection. Lipids were extracted, separated by TLC and visualized by autoradiography. Only the region of newly synthesized [^3H]TAG is shown.

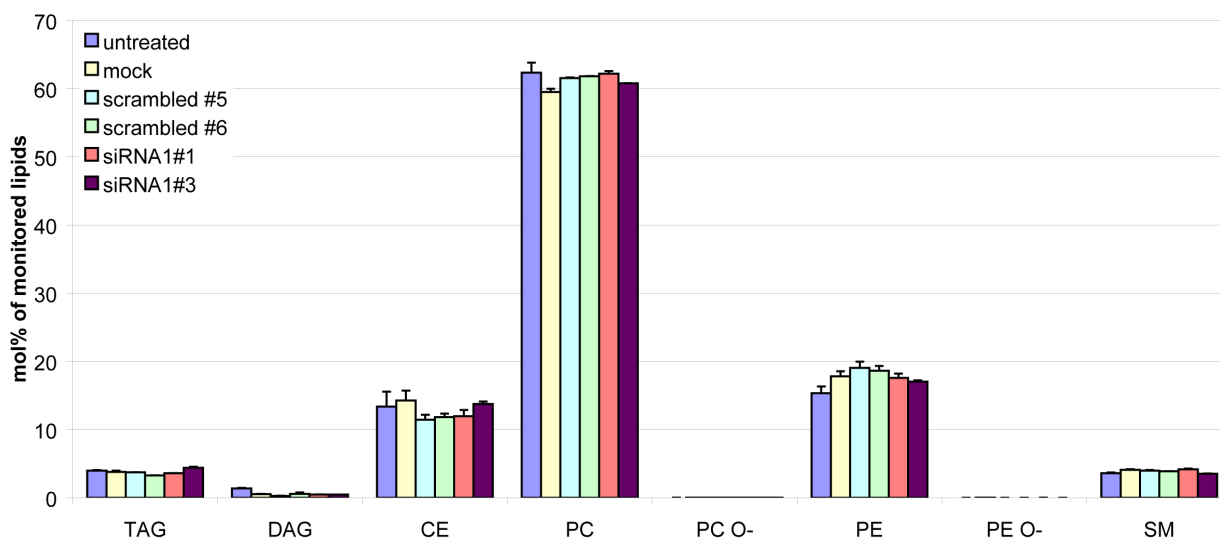


Figure 4.20.: Silencing of LPCAT1 in HuH7 cells does not influence the amount of stored neutral lipids

HuH7 cells were transfected as described in figure 4.15. After 72 h, total lipid extracts were analyzed by mass spectrometry. Each sample was measured in duplicate, and species abundances were normalized to the corresponding internal standard. The molar contents of each species of the same class were summed up and normalized to the total content of all detectable lipids. This diagram and lipid mass spectrometry is provided by Christer Ejlsing.

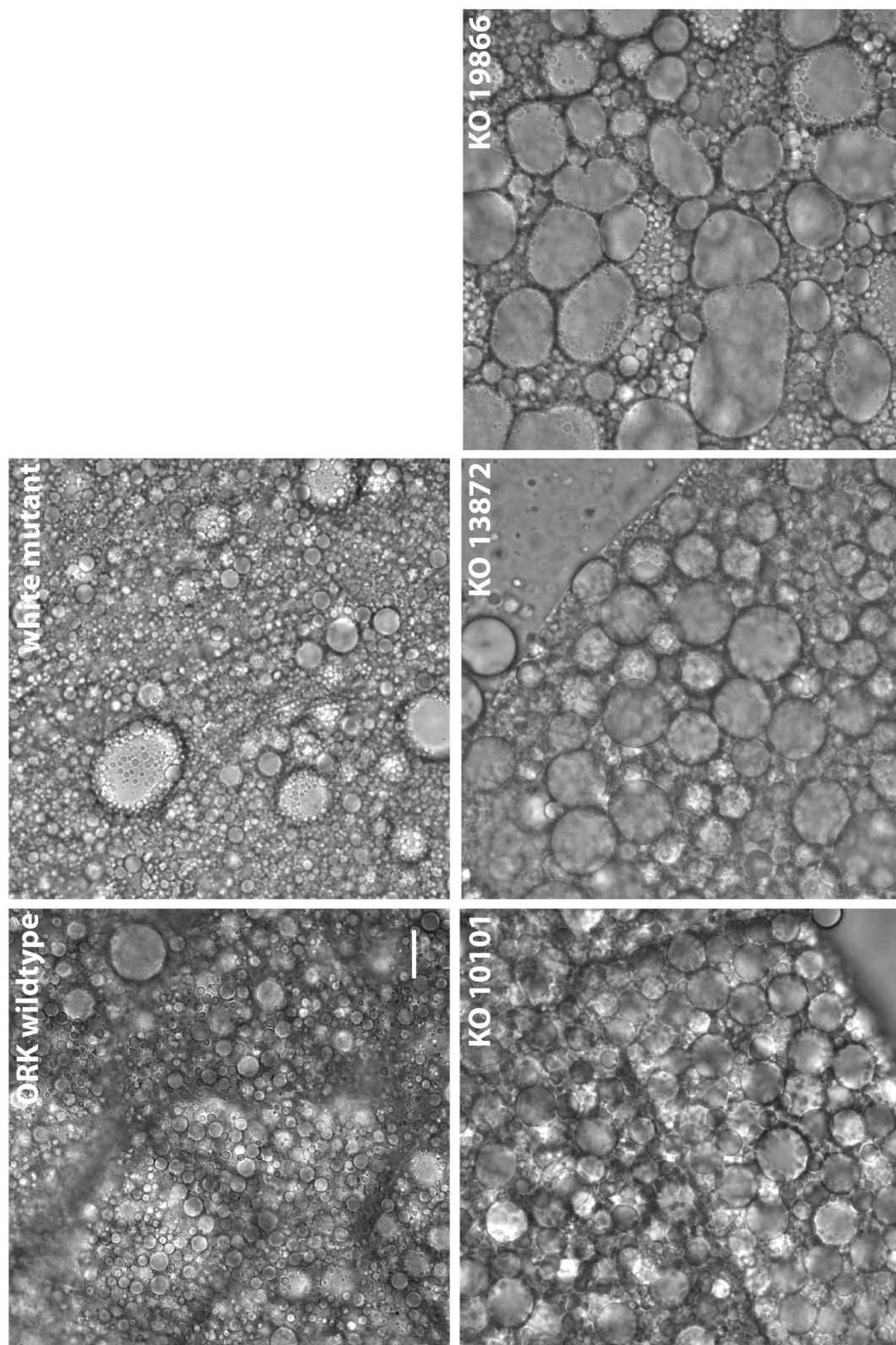


Figure 4.21.: Knockout of the LPCAT1/2 *Drosophila melanogaster* homologue CG32699 leads to enlarged LDs in the fat body of L3 larvae
 Fat bodies of L3 larvae of *Drosophila melanogaster* were isolated and representative bright field images of those fat bodies are shown for wildtype, white mutant and three CG32699 knockout (KO) strains 10101, 13872 and 19866. Scalebar = 10 μ m

The LPCAT activity is not only important for LDs in isolated cell lines, but also seems to play a role within complex organisms. LPCAT1 and LPCAT2 have one homologue in *Drosophila melanogaster*, which is annotated as *CG32699* and is predicted to be a LPC acyltransferase. The investigation of three knockout strains, which harbor three different P-elements in the 5'-UTR region of *CG32699* for silencing in a white mutant background, confirmed the influence of LPCAT activity on the size of LDs. LDs in the fat body [152] of L3 larvae of these knockout strains are larger than the LDs in the comparable white mutant or wildtype fly larvae (figure 4.21). Additionally, crosses between these knockout strains exclude an influence of the P-elements on the LD phenotype (supplementary figure A.11).

4.2.3. LPCAT1 is important for lipoprotein particle secretion

Since LDs serve as energy storage organelles, their functionality, morphology and composition influences both cell and systemic energy metabolism [93]. From the intestine and the liver, TAG, CE and phospholipids are transported by lipoprotein particles to adipose tissues and muscles. It was reported that HuH7 cells synthesize and secrete apoB containing VLDL and LDL particles (supplementary figure A.12, [124], [134] and [153]) and that their assembly requires the long-chain acyl-CoA synthetase ACSL3 [77]. This protein is also involved in the incorporation of fatty acids into PC in this cell line and localizes to LDs [76]. Since LPCAT1 and LPCAT2 localize to LDs and catalyze PC synthesis, they might also be important for lipoprotein assembly and secretion. Therefore, the secretion of apolipoproteinB (apoB) containing lipoprotein particles from HuH7 cells was measured, quantifying the amount of secreted apoB, which is associated with lipoprotein particles of a similar density as LDL (supplementary figure A.12). As HuH7 cells contain LPCAT3 [110] and LPCAT1, but no LPCAT2 (figure 4.4), only LPCAT1-specific siRNAs were used for knock-down. The knock-down with two distinct siRNAs resulted in a significant reduction of apoB-containing lipoprotein particle secretion (figure 4.22a and b) monitored by western blot and ELISA. Furthermore, the knock-down of LPCAT1 results in a decreased release of [3H]labeled lipids from HuH7 cells (figure 4.22c), which indicates that, in connection to reduced apoB secretion, less lipoprotein particles are secreted. Nevertheless, the reduction of secreted lipids seems to be caused mainly by reduced secretion of neutral lipids (for lipid profile see supplementary figure A.13). As hepatitis C virus (HCV) relies on lipoprotein particle release to exit hepatocytes [154], virus replication and release was analyzed upon LPCAT1 knock-down. LPCAT1 knock-down did not influence virus replication (data not shown), but one LPCAT1 siRNA sequence significantly reduces HCV release from transfected HuH7 cells (figure 4.22d), corroborating the connection between LPCAT1 and lipoprotein particle secretion.

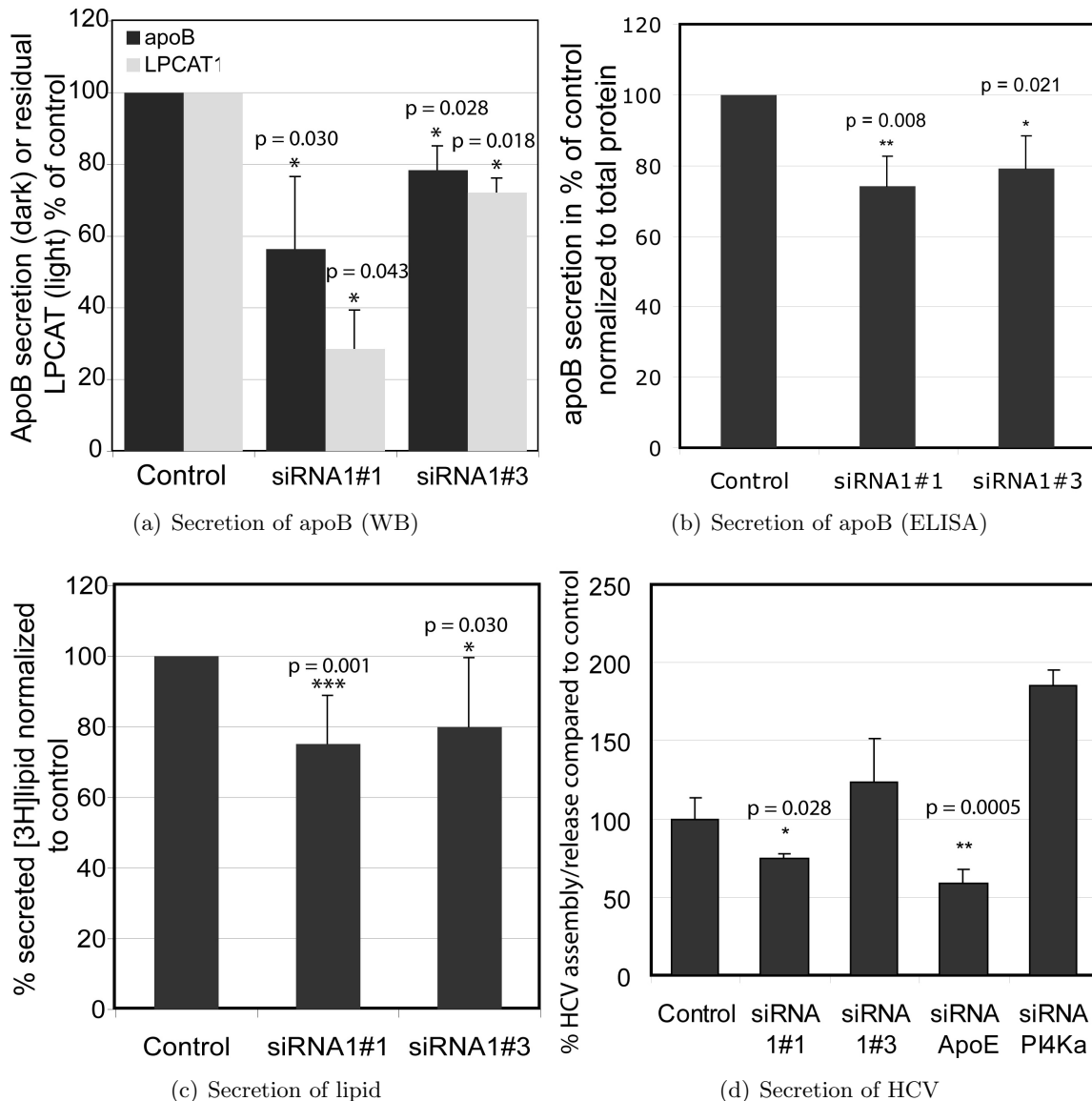


Figure 4.22.: LPCAT1 is important for lipoprotein particle secretion in HuH7 hepatoma cells

HuH7 cells were grown in serum-free medium and transfected with non-targeting siRNA (control) or one of two different siRNA sequences targeting LPCAT1.

(a) After 72 h, supernatants and cell lysates were collected and subjected to SDS-PAGE/western blot (WB). Supernatants were analyzed for apolipoproteinB, cell lysates for GAPDH and LPCAT1. Secreted apoB and cellular LPCAT1 were first normalized to GAPDH and then to control. The panel shows the mean result of five experiments; dark grey, apolipoproteinB; light grey, LPCAT1.

(b) After 24 h siRNA was removed and cells were grown for further 48 h in fresh serum-free medium. Supernatants were analyzed for apolipoproteinB with an apoB specific ELISA. Cells were collected and protein content was measured. ApoB released was normalized to the protein content and then to control. The panel shows the mean results of four experiments.

(c) The siRNA transfected cells were labeled with [3H]oleate for 24 h. Then, radioactivity and siRNAs were removed and cells were grown for further 48 h in fresh serum-free medium. Lipids of supernatant (S) and cells (C) were extracted and quantified by scintillation counting. The ratio between secreted radioactive lipid (S) and total radioactively labeled lipid (S + C) was normalized to control. The panel shows the mean results of four experiments.

(d) HuH7.5 firefly cells were transfected with siRNA for 24 h and then medium was replaced by fresh medium for 40 h. Next, cells were infected with Jc2Ra reporter hepatitis C virus (HCV) at MOI 0.21 for 24 h. The medium was replaced by fresh medium and 48 h later supernatants were collected and used for reinfection of HuH7 cells. HuH7 cells were lysed and assayed for Renilla Luciferase activity, to calculate the levels of HCV assembly/release. ApoE targeting siRNA was used as control for disruption of VLDL assembly/secretion; PI4Ka siRNA was used as control for HCV replication. The mean values of three independent experiments are shown. The analysis of HCV replication and secretion (d) is provided by Gualtiero Alvisi.

In all four subfigures the standard deviations are shown and the p-values were obtained by unpaired t-test, indicating the significance relative to the respective control.

4.3. Monotopic topology is a common feature of LD membrane proteins

In this section the topology of LD-localizing membrane proteins is investigated and compared to a typical single-span ER membrane protein. Though several membrane proteins were reported to localize to LDs and several proteins with monotopic conformation were described, it is still not clear to which extent the topology influences LD localization.

The comparison of the protein sequence of LPCAT1, LPCAT2 and DGAT2 with the typical LD-localizing membrane proteins NSDHL and caveolin 1 and the typical ER single-span membrane protein calnexin reveals a long hydrophobic stretch in the LD-localizing proteins (figure 4.23). This stretch spans about twice the length (about 35 amino acids) of the hydrophobic membrane domain of single-span membrane proteins (15 to 25 amino acids) and it is sufficient to pass a membrane two times. The middle of this domain is marked by a charged, small or helix-breaking amino acid that may force a kink into the structure. Thus, the features of the LD-localizing membrane proteins point towards a monotopic hairpin conformation. Additionally, all of these proteins display complex multiple localizations to LDs and other cellular organelles [28, 155–158].

In NSDHL [159] and caveolin 1 [160] the long hydrophobic domain does not fully span a membrane, but forms a turn with both N- and C-terminus facing the cytoplasm. This monotopic mode of membrane insertion allows protein integration into the surface monolayer of LDs [161] and explains, how membrane proteins can localize to a phospholipid bilayer like the ER membrane and at the same time to a phospholipid monolayer surrounding a hydrophobic core like LDs (see figure 4.1 and figure 4.6). Furthermore, in comparison to calnexin, the LD-localizing membrane proteins show no typical ER localizing sequence, although they also localize to the ER. It has to be mentioned that some LD-localizing proteins contain a C-terminal KKXX-ER-retrieval motif that seems to positively influence LD localization [157]. Also phosphorylation can be involved in LD targeting, as Nir2 is targeted to LDs upon phosphorylation on a threonine [162].

As described in section 2.3 and 2.4 many reactions are catalyzed by different iso-enzymes, which belong to different protein families and differ in protein sequence and structure. Though some proteins like the AAM-B methyltransferase contain a N-terminal hydrophobic sequence that seems to be crucial to target these proteins to LDs [163], this sequence motif is not common to all LD-localizing proteins and is lacking in LPCAT1, LPCAT2 and DGAT2. A more widespread feature of LD-localizing proteins is the existence of hydrophobic do-

membrane	1	10	20	30	40	50
domain						
LPCAT1	..LSALQKAQVALMTLTLFVRLLVAAAMMLLAWFLALVASLGS	AEKEPEQFP..				
LPCAT2	..IGSARRVQIVLLGIILLPIRVLLVALILLLAWPFAAIS	TVCCPEKLTHFIT..				
DGAT2	..RSKVEKQLQVISVLQWVLSFLVLGVACSAILMYIFCTDCW	LIAVLYFTWLVDWNTFKKGGRR..				
NSDHL	..NYEAPKYHIPYVWVAYYLALLLSLLVMVISFVIQLQPTFT	PMRVALAGTFHYYSCE	RAKK..			
CAV1	..KYWFYRLLSALFGIPMALIWGIYFAILSFLHIWAVVPCIK	SFLIEIQCISRVYSIYVHTVC	DPLFE..			
CALX	..AAEERPWLWVVYILTVALPVFLVILFCCSGKKQTS..					
N-terminus						
LPCAT1	MRLRGCGPRAAPASSAGASD..					
LPCAT2	MSRCAQAAEVAATVPGAGVG..					
DGAT2	MKTLLIAAYSGVLRGERQAEA..					
NSDHL	MEPAVSEPMRDQVARTHLTE..					
CAV1	MSGGKYVDSEGHLYTVPIRE..					
CALX	MEGKWLCLMLLVLTGTAIVEA..					

Figure 4.23.: LD-localizing membrane proteins contain a long hydrophobic stretch

Sequence comparison between the single long hydrophobic sequences of LPCAT1, LPCAT2 and DGAT2 and the hairpin hydrophobic domains of the well-characterized LD proteins, NSDHL and caveolin 1 (CAV1) and the ER transmembrane protein calnexin (CALX). The LD monotopic membrane proteins have a single long hydrophobic sequence with regular interspaced helix-breaking amino acids and lack N-terminal hydrophobic leucine-rich signal sequences. Position 1 indicates the first residue of the hydrophobic stretch or the N-terminal methionine. Color code in the membrane domains: charged residues (blue), helix breaking (P,G,S,C)(red); color code for N-termini: charged residues (blue), leucine (green). Sequences are taken from Swissprot with the following accession numbers: LPCAT1 Q8NF37, LPCAT2 Q7L5N7, DGAT2 Q96PD, NSDHL Q15738, CAV1 Q03135, CALX P27842. This figure is provided by Christoph Thiele.

mains, with which the cytosolic PAT family proteins can attach to LDs [164, 165] or integral proteins can insert into LDs (figure 4.23). The integral membrane proteins of LDs show a monotopic, presumably hairpin, topology that might selectively target some iso-enzymes to LDs.

4.3.1. Topology of LPCAT1 and LPCAT2

The hydrophobicity plots of both LPCAT1 and LPCAT2 show a strongly hydrophobic region starting at amino acid position 44 in LPCAT1 and 58 in LPCAT2 (supplementary figure A.14). This region is predicted to form a hairpin (TTHM prediction Expasy) so that both proteins should be inserted into membranes with both termini targeting the cytosol. To characterize the topology of LPCAT1 and LPCAT2, fusion constructs with either a N- or C-terminal 3HA-tag were expressed. Cells were permeabilized using saponin (permeabilizes all cellular membranes) or digitonin (permeabilizes the plasma membrane, but not the ER membrane) [166] and stained with anti-HA antibody to detect the termini of the expressed LPCAT proteins, and an antibody against the luminal ER protein disulfide isomerase (PDI) to monitor the selective permeabilization of the plasma membrane by digitonin. While anti-HA detected the LPCAT constructs irrespective of the mode of permeabilization or the position of the tag, the anti-PDI only showed specific staining after saponin permeabilization (figure 4.24). This result indicates that both termini of LPCAT1 and LPCAT2 are directed towards the cytoplasm.

This was confirmed in a biochemical analysis. A431 cells were transfected with N-terminally 3HA-tagged LPCAT1 or LPCAT2, and microsomes were isolated and treated with proteinase K. The integrity of the microsomes was analyzed with the antibody against PDI. The accessibility of the N-terminus of LPCAT1 and LPCAT2 towards proteinase K was detected by anti-HA antibody, the accessibility to the C-terminus by our specific LPCAT1 and LPCAT2 antibodies. Though microsomes remained mainly intact after the isolation and digestion procedure, the signal of both LPCAT1 and LPCAT2 termini vanished or was strongly reduced after proteinase K digestion (figure 4.25). In conclusion, LPCAT1 and LPCAT2 display a monotopic conformation with both termini facing the cytoplasm.

4.3.2. Topology of DGAT2

DGAT2 contains a hydrophobic stretch of about 46 amino acids starting at amino acid 67. The properties and length of the transmembrane domain is similar to caveolin 1 (figure 4.23) and is very conserved in different species (figure 4.29). Caveolin 1 predominantly localizes to the plasma membrane and it can bind free cholesterol. LD-targeting of caveolins is achieved by overexpression, BrefeldinA treatment, insertion of a KKXX-ER-retrieval sequence or deletions in the N-terminus [157, 158, 167]. It has been shown that caveolin is inserted into the membrane in a hairpin topology and that both termini face the cytoplasm [160].

If DGAT2 is also a monotopic hairpin membrane protein like caveolin 1 with both termini directed towards the cytoplasm, tags at both termini of DGAT2 must be detectable by antibodies, even though the ER lumen is not accessible. Therefore, similar fusion constructs as described for LPCAT1 and LPCAT2 (section 4.3.1) were cloned for DGAT2 with either a N- or C-terminal 3HA-tag. These constructs were expressed in COS7 cells, which were permeabilized using saponin or digitonin [166] and stained with anti-HA antibody to detect expressed DGAT2 protein, and an antibody against the luminal ER protein PDI. While anti-HA detected the DGAT2 construct irrespective of the mode of permeabilization or the position of the tag, the anti-PDI only showed specific staining after saponin permeabilization (figure 4.26). This result indicates that both termini of DGAT2 are directed towards the cytoplasm like it was shown for LPCAT1 and LPCAT2 in section 4.3.1.

This was confirmed in a biochemical analysis. COS7 cells were transfected with N- or C-terminally 3HA-tagged DGAT2, and microsomes were isolated and treated with proteinase K. The integrity of the microsomes was analyzed with the antibody against PDI. The accessibility of the termini of DGAT2 towards proteinase K was detected by anti-HA antibody and the digestion pattern was compared to the C-terminally 3HA-tagged hairpin protein

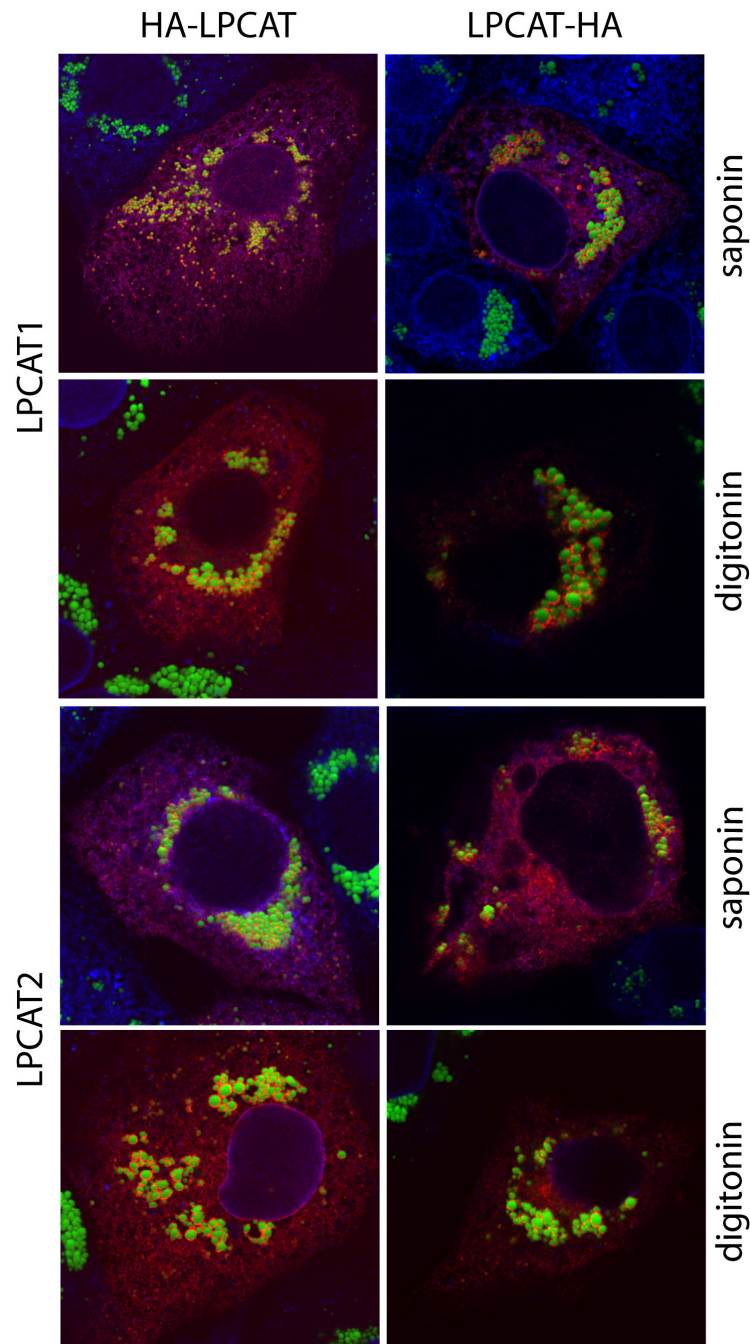


Figure 4.24.: LPCAT1 and LPCAT2 insert into LDs and membranes in a monotopic conformation

A431 cells were transfected with vectors coding for LPCAT1 or LPCAT2 as indicated, both with either N-terminal 3HA-tag (HA-LPCAT) or C-terminal 3HA-tag (LPCAT-HA) and were cultivated for 16 hours in the presence of 100 μ M oleate. Cells were fixed and processed for immunofluorescence microscopy using either saponin (permeabilizes all membranes) or digitonin (permeabilizes plasma membrane, but not the ER membrane) for permeabilization. Cells were stained with BODIPY 493/503 to stain LDs (green), anti-HA to detect transfected LPCAT proteins (red) and anti-PDI (blue) as a luminal ER marker. Only merged pictures are shown. Note that LPCAT proteins are stained irrespective of the position of the tag or the detergent used for permeabilization. In contrast, the luminal PDI epitope is stained only after saponin permeabilization. See supplementary figure A.15 and A.16 for pictures split into the single channels.

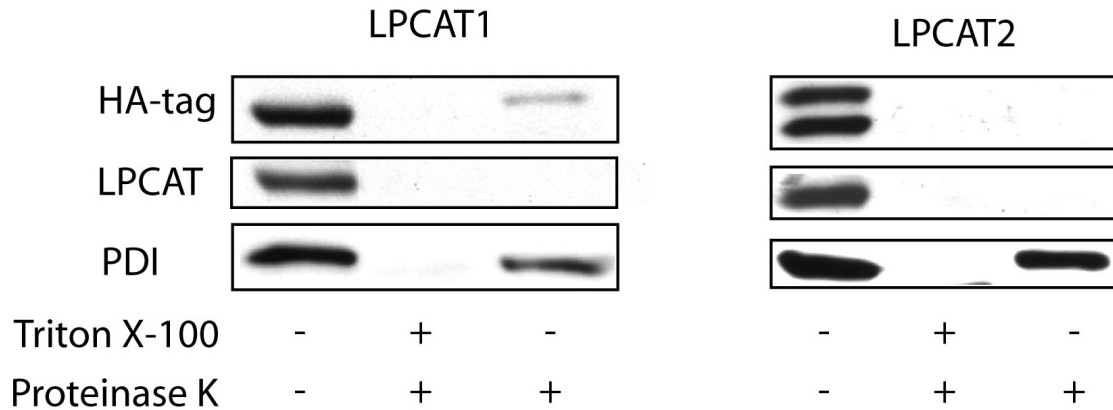


Figure 4.25.: LPCAT1 and LPCAT2 insert into membranes in a monotopic conformation

N-terminally 3HA-tagged LPCAT1 or LPCAT2 were expressed in A431 cells for 16 h. Cells were cracked and microsomes were collected by centrifugation. Microsomes were incubated in PBS with either no addition (negative digestion control), addition of 1% Triton-X100 and proteinase K (positive digestion control) or addition of proteinase K alone. The integrity of the microsomes was analyzed by western blot with the luminal ER marker PDI, the N-terminus of LPCAT1 and LPCAT2 was detected with a HA-specific antibody (HA-tag) and the C-terminus with our specific LPCAT1 and LPCAT2 antibodies (LPCAT). Note that either end of the protein is destroyed in the absence of detergent. No smaller fragments were detected on the blots (data not shown).

caveolin 1. Though microsomes remained mainly intact after the isolation and digestion procedure, the signal of both termini of DGAT2 vanished after proteinase K digestion similar as to caveolin 1 (figure 4.27). In conclusion, DGAT2 displays a monotopic conformation with both termini facing the cytoplasm. This data are in line with a study to DGAT2 topology by Stone et al. [92] and Shockey et al. [168].

In order to corroborate that the monotopic conformation reflects a hairpin protein that inserts into the membrane rather than a strongly membrane-associated, but peripheral membrane protein, the mode of membrane association was assayed in COS7 cells overexpressing DGAT2. Therefore, membranes were isolated and incubated with high NaCl concentrations or carbonate to disrupt electrostatic membrane interaction, with urea to disrupt structural interaction of peripheral membrane proteins, with the detergents TritonX-100 or dodecyl-maltoside to disrupt the membranes or with PBS as control. The analysis by western blot of the differently treated membrane pellets and the corresponding supernatants reveals that DGAT2 can be totally released from membranes only by treatment with detergents, that also release the single-span membrane protein calnexin (figure 4.28). This shows that DGAT2 integrates into the membrane.

4.4. Regulation of DGAT2 localization and activity

In this section the TAG metabolism is further investigated regarding the regulation of DGAT2 by interacting proteins. It is shown that DGAT2 interacts with the enzyme ACSL1 and that these proteins influence the cellular packaging of TAG.

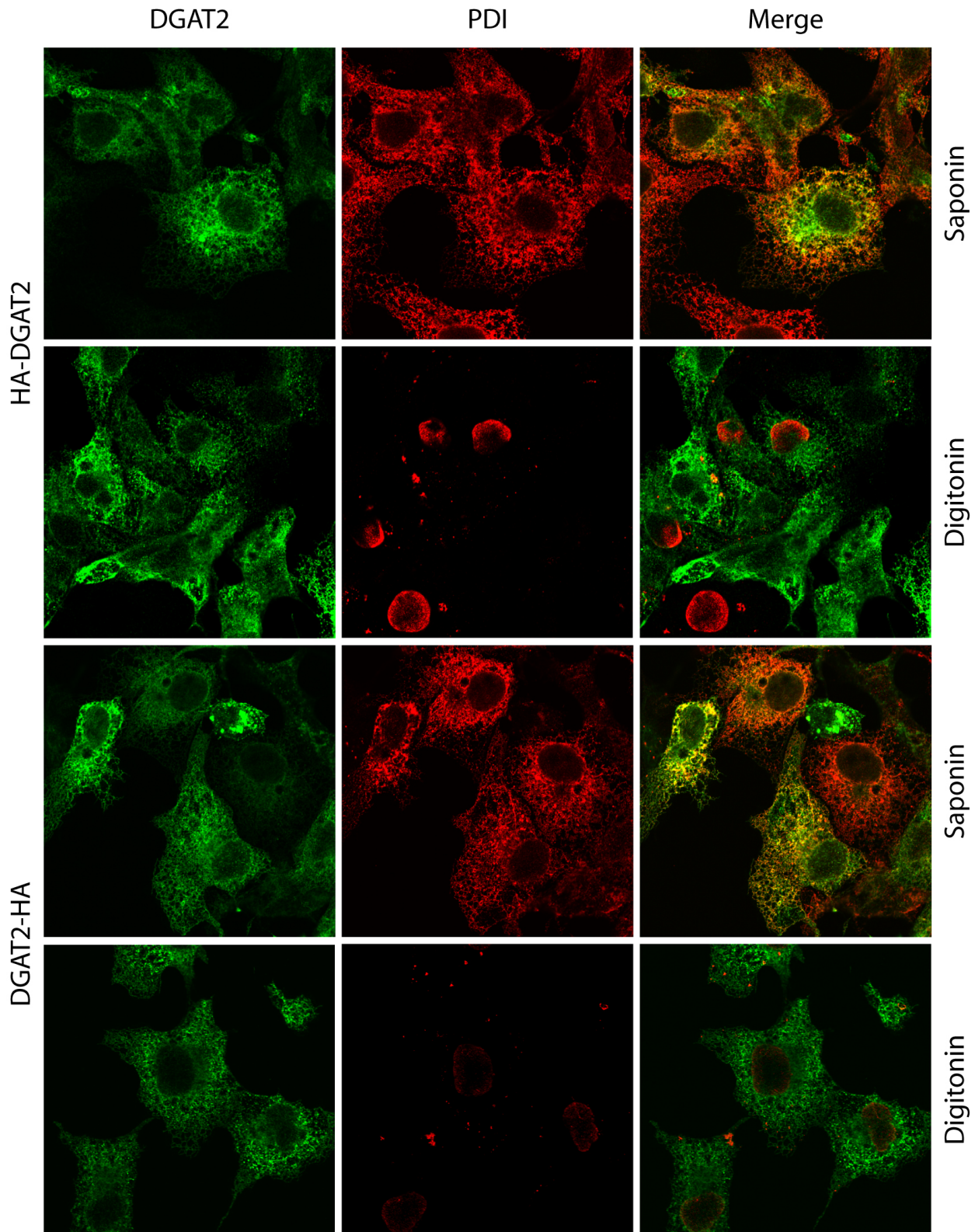


Figure 4.26.: Topology of DGAT2

COS7 cells were transfected with vectors coding for human DGAT2 with either N-terminal 3HA-tag (HA-DGAT2) or C-terminal 3HA-tag (DGAT2-HA). Cells were fixed and processed for immunofluorescence microscopy using either saponin (permeabilizes all membranes) or digitonin (permeabilizes plasma membrane, but not the ER membrane) for permeabilization. Cells were stained with anti-HA to detect transfected DGAT2 protein (green) and anti-PDI (red) as a luminal ER marker. Note that DGAT2 protein is stained irrespective of the position of the tag or the detergent used for permeabilization. In contrast, the luminal PDI epitope is stained only after saponin permeabilization.

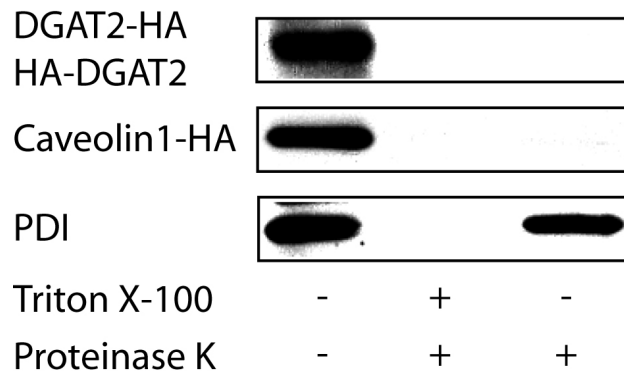


Figure 4.27.: DGAT2 is a monotopic membrane protein

N-terminally and C-terminally 3HA-tagged DGAT2 together with C-terminally 3HA-tagged Caveolin1 were expressed in COS7 cells for 16 h. Cells were cracked and microsomes were collected by centrifugation. Microsomes were incubated in PBS with either no addition (negative digestion control), addition of 1% Triton-X100 and proteinase K (positive digestion control) or addition of proteinase K alone. The integrity of the microsomes was analyzed by western blot with the luminal ER marker PDI, the N- and C-terminus of DGAT2 was detected with a HA-specific antibody and compared to the signal of the HA-tag of the known monotopic membrane protein Caveolin1. Note that either end of the protein is destroyed in the absence of detergent. No smaller fragments were detected on the blots (data not shown).

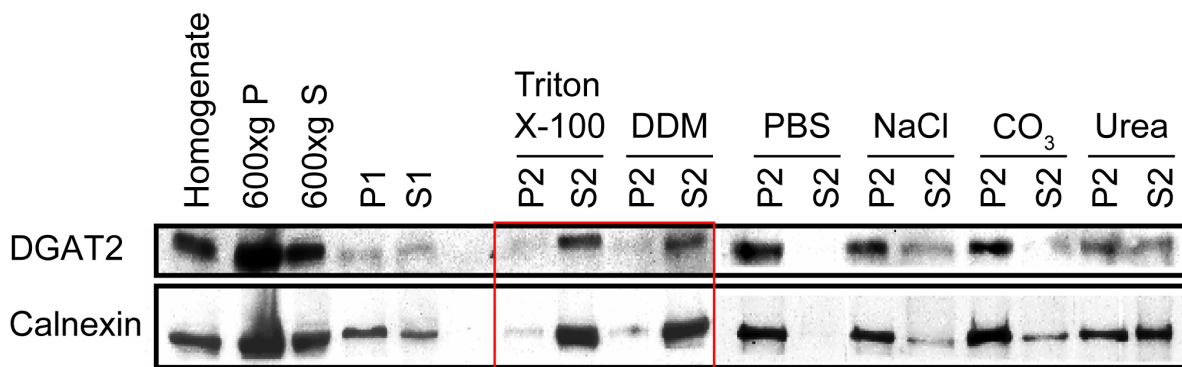


Figure 4.28.: DGAT2 behaves like a single-span membrane protein

DGAT2 was expressed in COS7 cells for 16 h. Cells were cracked (Homogenate), crude membranes and nuclei were pelleted (600xg P and 600xg S; P = pellet, S = supernatant) and membranes were collected by centrifugation (P1 and S1). Membranes were incubated with PBS (PBS), 1% TritonX-100 in PBS (TritonX-100), 1% dodecylmaltoside in PBS (DDM), 1 M NaCl in PBS (NaCl), 0.1 M Sodiumcarbonate in PBS (CO₃) pH 11 and 6 M Urea in PBS (Urea). Membranes were again collected by centrifugation and the abundance of DGAT2 in the pellet and the corresponding supernatant was analyzed by western blot and compared to the single-span membrane protein Calnexin. The red square marks the conditions under which DGAT2 is totally released from membranes.

4. Results

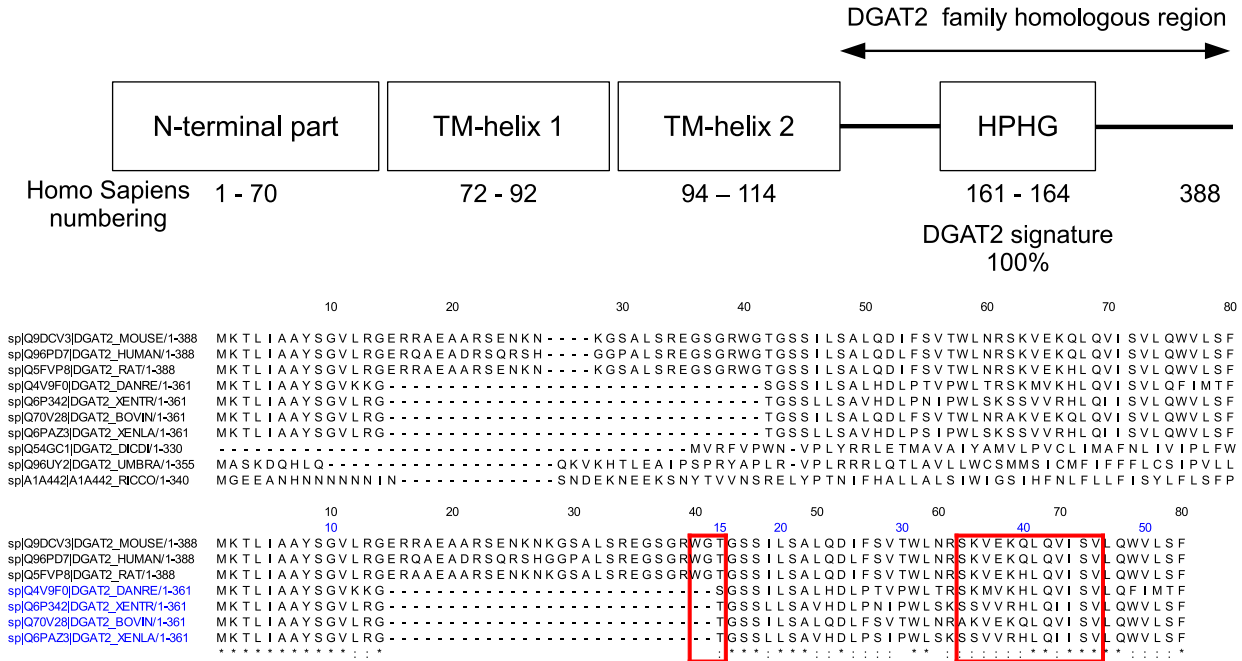


Figure 4.29.: Domain structure and conservation of DGAT2

Protein sequences of DGAT2 from different species were aligned with ClustalW. The upper part describes the domains of human DGAT2, which are representative for all DGAT2 from different species, and highlights the catalytic motif, which is conserved to 100%.

The middle part displays the sequence alignment of the N-terminal part of DGAT2 from different species. Sequences from mouse (MOUSE), human (HUMAN), rat (RAT), zebrafish (DANRE), xenopus (XENTR and XENLA), bovine (BOVIN), dictyostelium (DICDI), fungus (UMBRA) and ricinus plant (RICCO) were used for the alignment. The numbering of amino acid position refers to the human DGAT2 protein sequence.

The lower part displays the vertebrate sequences and the coloured numbering of amino acid position refers to the sequences in the same colour. Absolute conserved residues are marked by stars, highly conserved residues by colons. The red boxes mark potential binding motifs for DGAT2-ACSL1 interaction calculated with hmmer. This figure is provided by Anne Tuukkanen.

As DGAT2 plays an important role in the synthesis of the storage lipid TAG and is linked to LDs, it is of growing interest to obtain a deeper knowledge of the regulation of DGAT2 and its connection to the lipid homeostasis of the cell. The localization of DGAT2 seems to be subject to regulation. Figure 4.1 shows a change in localization from the ER membrane to the LD surface in oleate-rich conditions. This change in localization might directly or indirectly influence the activity of DGAT2. The localization and activity of DGAT2 might be regulated by direct modifications like phosphorylation and ubiquitination or it could be controlled by the interaction with other proteins.

Proteins interact with each other via specific binding motifs. These motifs are often very conserved across different species. DGAT2 is structured into three domains: the N-terminus, the membrane domain (see figure 4.23) and the C-terminal catalytic domain (figure 4.29). Though the N-terminus lacks an obvious function, the amino acid sequence is conserved between different species, which makes it a good candidate as binding site for other proteins.

4.4.1. DGAT2 interacts with ACSL1

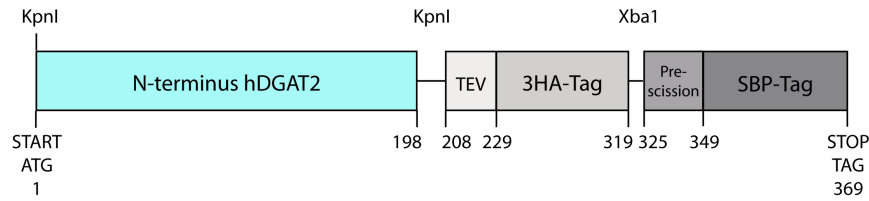
Besides very transient interactions with modifying proteins like kinases, enzymes can be part of multi-enzyme complexes [169]. Enzymatic activities that belong to the same metabolic pathway often cluster in the same cellular locations, like the enzymes for cholesterol biogenesis [159]. Especially in multi-step reactions, this might lead to a faster and more efficient use of substrates to yield a certain end product [170]. Additionally, these complexes can interact with activating or repressing proteins to efficiently activate or deactivate a complete metabolic pathway instead of all the single participating enzymes.

4.4.1.1. Identification of DGAT2 interaction partner

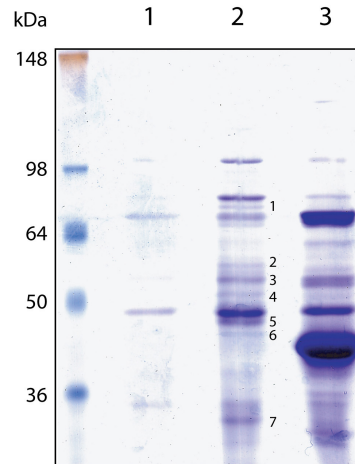
The structural analysis and the comparison of DGAT2 sequences of different organisms (figure 4.29) revealed that the N-terminal part of DGAT2 contains a highly conserved hydrophobic motif that might function as recognition and binding site for interaction partners. In order to find an interaction partner of DGAT2, the first 66 amino acids of human DGAT2 were coupled to an SBP (Streptavidin Binding Protein)-tag (figure 4.30a) and after bacterial expression of the construct at conditions to obtain natively folded protein, it was purified on a streptavidin-sepharose column (see section 6.2.3.6). EGFP coupled to the same tag was used in parallel to control for unspecific interaction with the tag and for binding and elution dynamics. For the pull-down of specific interaction partners, a pig liver cytosol fraction, the corresponding liver membrane fraction and, in order to study cooperative binding, a one to one mixture of liver membranes and cytosol was used as protein source. The eluates of the columns were separated by SDS-PAGE, stained with Coomassie (figure 4.30b) and bands specifically appearing in the eluates of the DGAT2 containing column were analyzed by MALDI-TOF mass spectrometry (figure 4.30c, supplementary figure A.17 and supplementary table B.4).

Besides ATP-synthases and actin, the main liver metabolic enzymes like aldehyde dehydrogenase and epoxide hydrolase were identified. These proteins most probably represent unspecifically bound proteins that were detected because of their high abundance. An exception is ACSL1 (Long Chain Acyl-CoA Synthetase 1), which could be identified in the membrane fraction and the mixed fraction (figure 4.30, supplementary figure A.17 and supplementary table B.4). ACSL1 activates fatty acids by coupling them to CoA. These FAs can be used for oxidation in order to obtain energy or to build up storage lipids or phospholipids. ACSL1 was reported to localize to the ER, to mitochondria-associated membranes (MAM) [81] and to the cytosol [71] in hepatocytes and to mitochondria, PM and LDs in

4. Results



(a) Construct used as bait for identification of DGAT2 interaction partner



(b) Coomassie gel of the eluates obtained from the columns used for the study of specific and cooperative binding to DGAT2

Spot No.	SwissProt entry	Protein	Predicted MW (kDa)	MS/MS (Score)	PMF Score	Matched Peptides	Sequence Coverage
1	ACSL1_CAVPO (Guinea pig)	Long-chain-fatty-acid-CoA ligase 1	77.65	2 (25,47)	-	4/30	5%
2		Keratin					
3	ATPB_BOVIN	ATP synthase subunit beta, mitochondrial	56.25	-	70	9/41	26%
	ATPB1_BOVIN	ATP synthase subunit alpha heart isoform, mitochondrial	59.68	-	63	10/41	21%
4	HYEP_PIG	Epoxide hydrolase 1	52.36	-	129	13/40	27%
5	ACTB_BOVIN	Actin, cytoplasmic 1	41.71	-	108	11/36	31%
6	ACTB_XENLA (Xenopus laevis)	Actin, cytoplasmic 1	41.74	2 (31,15)	-	4/12	14%
7	ADH1_MOUSE	Alcohol dehydrogenase 1	39.62	1 (49)	-		

(c) List of potential interaction partner of DGAT2

Figure 4.30.: Identification of ACSL1 as interaction partner of DGAT2

(a) The conserved N-terminus of human DGAT2 was cloned in front of a tag consisting of a TEV protease cleavage site (TEV), a triple hemagglutinin-tag (3HA-Tag), a Prescission protease cleavage site (Prescission) and a streptavidin binding protein-tag (SBP-Tag). The cleavage sites allow the removal of parts or the whole tag, the HA-tag allows localization studies with tag-specific antibodies and the SBP-tag allows specific binding of the expressed construct to streptavidin. Restriction enzymes used for construction of the construct are labeled above, the position and length of the elements of the construct are labeled in base pairs below.

(b) The coomassie gel shows the proteins accumulating in the eluates of the columns used to isolate specific interaction partner of DGAT2. In lane 1 the proteins in the eluate of the column loaded with lysates of bacteria transfected with an empty vector (control for unspecific binding to column material), in lane 2 the eluate of the column loaded with the lysates of bacteria expressing the N-terminus hDGAT2 construct described in (a) and in lane 3 the eluate of the column loaded with the lysates of bacteria expressing the EGFP control construct (EGFP cloned in front of the tag described in (a) as control for unspecific binding to the tag) are shown. Bands labeled with numbers only appeared in lane 2 and were cut out and analyzed by mass spectrometry. Only results for the columns incubated with a mixture of cytosolic and membrane liver proteins for competitive binding are shown. For complete results see supplementary figure A.17.

(c) In the table the proteins identified by mass spectrometry in the bands cut from the coomassie gel shown in (b) are listed. The numbering of the hits corresponds to the numbering of the bands in (b). For the complete hit list see supplementary table B.4. The mass spectrometric analysis and the table is provided by Cornelia Czupalla.

3T3-L1 adipocytes [9, 82, 83]. In 3T3-L1 cells, ACSL1 interacts with the FATP1 protein and promotes fatty acid import in a process called vectorial acylation [83, 87] or it is involved in reesterification of fatty acids released by lipolysis [88]. In hepatocytes, it is reported to be involved in the synthesis of phospholipids, DAG and TAG [81, 85, 86]. As DGAT2 and ACSL1 are both involved in anabolic lipid metabolism, an interaction might be physiologically beneficial.

4.4.1.2. DGAT2 and ACSL1 partially localize to the same compartments

DGAT2 localizes to the ER compartment [28, 101], to MAM [101] and to the surface of LDs (see section 4.1). In comparison, ACSL1 was reported to localize to the PM, the cytosol, the ER compartment, MAM and mitochondria. The localization of these proteins to the same compartments supports the possibility of a specific interaction. Within COS7 cells localization by immunofluorescence of both proteins showed that the major portion of DGAT2 resides in the ER or accumulates on LDs upon oleate feeding, whereas ACSL1-HA strongly accumulates in the mitochondria, though also a staining of the ER compartment and the cytosol is visible (figure 4.31 and supplementary figures A.18 and A.19). The localization of DGAT2 or ACSL1-HA was not influenced by the coexpression of both proteins. To further analyze the localization of both proteins lysates of COS7 cells overexpressing human wildtype DGAT2 and human C-terminal HA-tagged ACSL1 were fractionated by centrifugation in a stepwise sucrose density gradient. The fractions were analyzed for the abundance of DGAT2 and ACSL1-HA by western blotting and compared to markers for ER, mitochondria and LDs (figure 4.32). ACSL1-HA strongly accumulates in the fractions 14 to 16 and three to seven and colocalizes with the markers for ER (fraction three to 18), LDs (fraction one to six) and mitochondria (fraction 14 to 16). DGAT2 accumulates mainly in fraction four and five, where it colocalizes with the ER marker and the LD marker. Furthermore, some signal can be detected in fraction 15 and 16, where it colocalizes with the ER and the mitochondria marker. About 19% of the total ACSL1-HA colocalizes with 62% of total DGAT2 in the LD or light ER fractions that represent most likely smooth ER. A minor amount of DGAT2 colocalizes with the heavy ER and mitochondria, presumably representing a localization to MAM. In conclusion, DGAT2 and ACSL1 might interact in the ER compartment, at MAM and at LDs.

4.4.1.3. Validation of the interaction between DGAT2 and ACSL1

For the identification of ACSL1 as an interaction partner of DGAT2 (see section 4.4.1.1), only the N-terminus of DGAT2 was used as bait and pig liver proteins as prey. Though

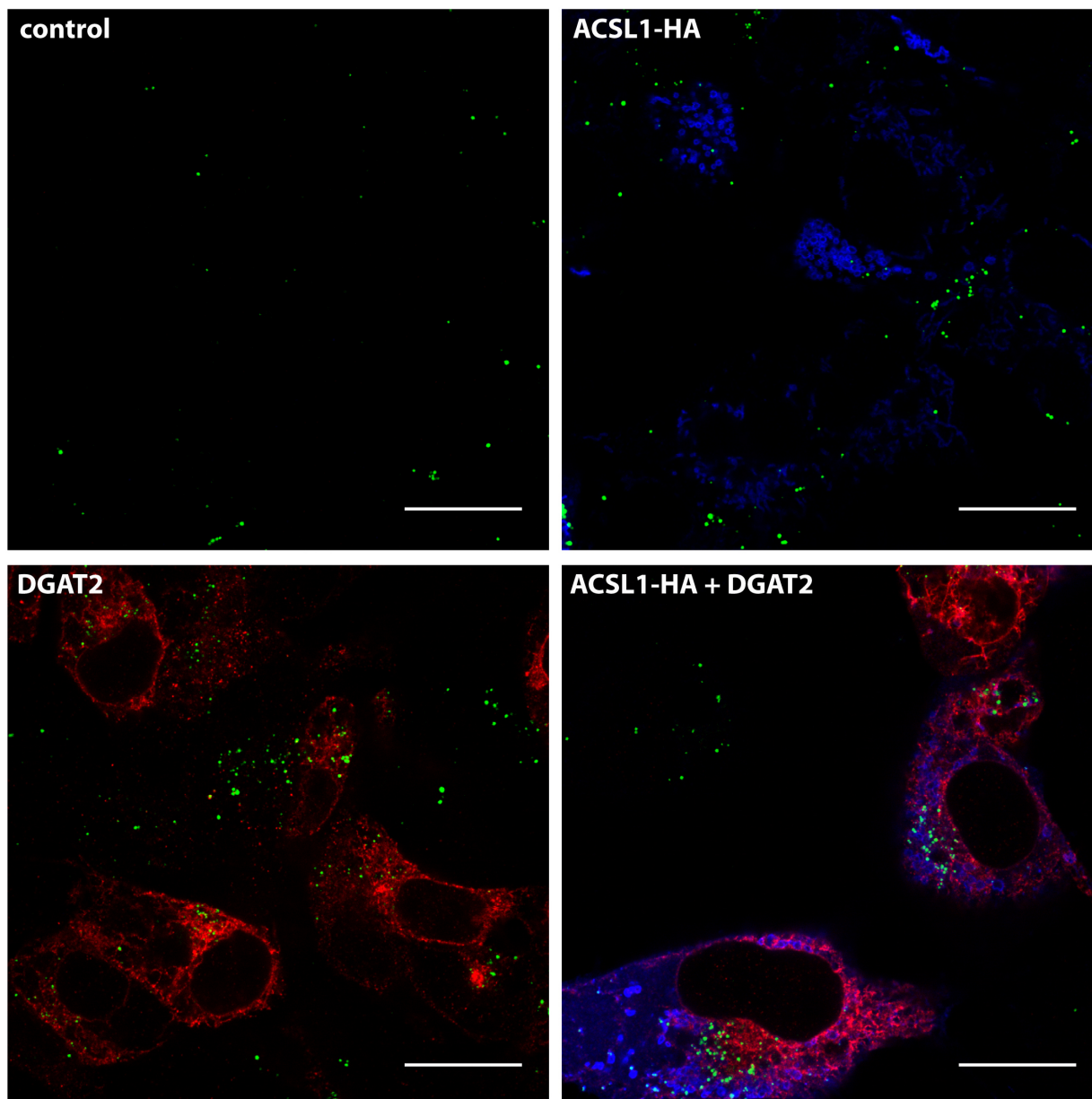


Figure 4.31.: Cellular localization of DGAT2 and ACSL1

COS7 cells were transfected with empty vector (control), human C-terminal HA-tagged ACSL1 (ACSL1-HA), wild-type human DGAT2 (DGAT2) or wildtype human DGAT2 and human C-terminal HA-tagged ACSL1 (ACSL1-HA + DGAT2) for 24 h. Cells were grown in DMEM medium supplemented with FCS. Cells were analyzed by immunofluorescence for lipid droplets (green), ACSL1 (blue) and DGAT2 (red). Scalebar = 10 μ m. For immunofluorescence data for delipidated FCS or FCS and 100 μ M oleate conditions see supplementary figure A.18 and A.19.

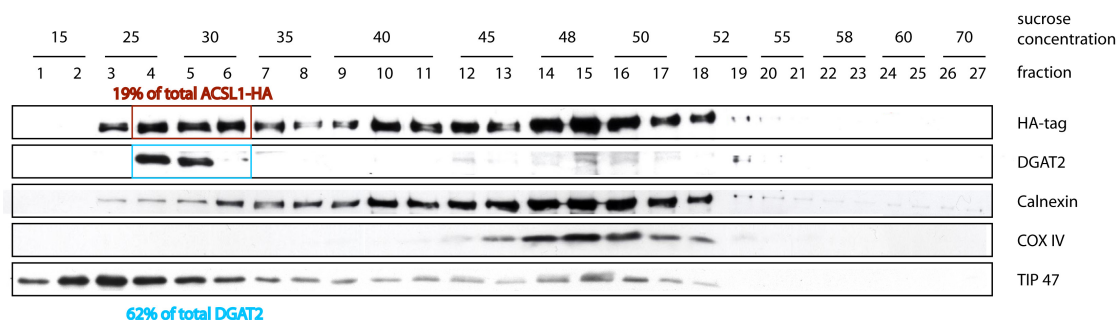


Figure 4.32.: DGAT2 and ACSL1 partially localize to the same compartments

COS7 cells were grown in DMEM medium supplemented with normal FCS and transfected with wildtype human DGAT2 and human C-terminal HA-tagged ACSL1 for 24 h. Cell lysates were floated in a stepwise sucrose density gradient ranging from 15 to 70% sucrose and fractions were analyzed by SDS-PAGE/western blot. The abundance of ACSL1 (HA-tag) and DGAT2 (DGAT2) in the different fractions was compared to the localization of marker proteins for ER (Calnexin), mitochondria (COX IV) and LD (TIP 47). The red and turquoise square mark the main fractions, where both, DGAT2 and ACSL1, are detected. The coloured labeling indicates the amount of DGAT2 (turquoise) or ACSL1 (red) protein in the marked fractions related to the total protein detected in the gradient.

controls for unspecific binding to the column material and to the tag were included in the experiment, the interaction could still be unspecific or not transferable to living cell systems and other species. Therefore, full-length human wildtype DGAT2 and human C-terminal HA-tagged ACSL1 were expressed either each alone or together in COS7 cells and coimmunoprecipitated with the DGAT2 antibody or the HA antibody (figure 4.33). It was possible to coimmunoprecipitate DGAT2 with ACSL1 and vice versa in cells overexpressing both proteins, but no signal for the coimmunoprecipitated protein was detected in SDS-PAGE/western blot for single expression, showing that the signal obtained in coimmunoprecipitation was specific. A quantification of the amount of DGAT2 or ACSL1-HA that was recovered by coimmunoprecipitation from total expressed DGAT2 or ACSL1-HA revealed that 25% of total ACSL1-HA coimmunoprecipitated when DGAT2 was used as bait and 9% of total DGAT2 was coimmunoprecipitated when ACSL1-HA was used as bait.

A comparison with the amounts of DGAT2 and ACSL1-HA protein that localize to the same compartment (see figure 4.32) suggests that all DGAT2 comes from a compartment where it can colocalize with ACSL1-HA. Furthermore, nearly all ACSL1-HA that colocalizes with DGAT2 at the smooth ER (19%) and additional some ACSL1-HA at the MAM compartment seems to be recovered by coimmunoprecipitation with DGAT2 (25% ACSL1). In contrast to DGAT2, only about 50% of the ACSL1-HA protein immunoprecipitated comes from a compartment, where DGAT2 and ACSL1-HA colocalize. Additionally, although they may colocalize on MAM, ACSL1-HA seems to be much more abundant than DGAT2, therefore the chance to immunoprecipitate an ACSL1-HA molecule that has a DGAT2 molecule bound instead of an unbound ACSL1-HA molecule is much lower. Taken together, this explains why only 9% of DGAT2 protein was recovered by immunoprecipitation of ACSL1-HA. In

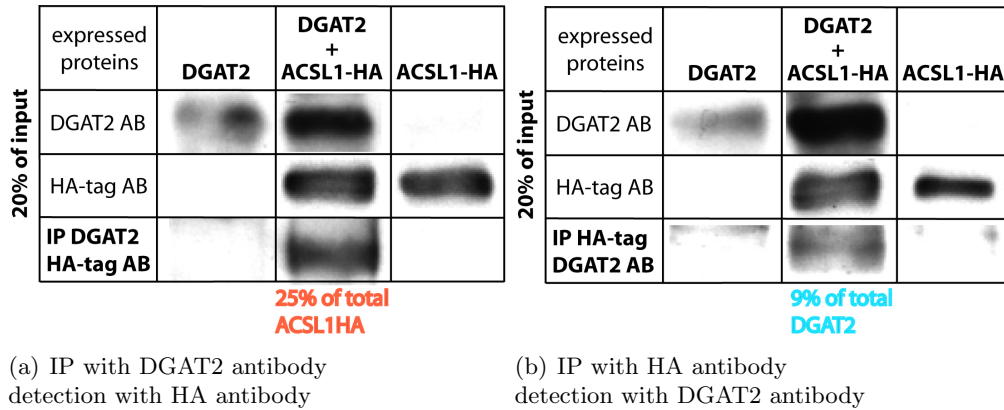


Figure 4.33.: DGAT2 interacts with ACSL1 in COS7 cells

COS7 cells were grown in DMEM medium supplemented with normal FCS and transfected with wildtype human DGAT2 (DGAT2), wildtype human DGAT2 and human C-terminal HA-tagged ACSL1 (DGAT2 + ACSL1-HA) or human C-terminal HA-tagged ACSL1 (ACSL1-HA) for 24 h.

(a) Cell lysates were used for immunoprecipitation with DGAT2 antibody (IP DGAT2). Coimmunoprecipitated proteins were analyzed by SDS-PAGE/western blot with the HA-tag antibody (HA-tag AB). The upper first two horizontal lanes show the amount of DGAT2 (DGAT2 AB) or ACSL1-HA (HA-tag AB) in the cell lysates used for the immunoprecipitation of DGAT2 (IP DGAT2).

(b) Cell lysates were used for immunoprecipitation with HA-tag antibody (IP HA-tag). Coimmunoprecipitated proteins were analyzed by SDS-PAGE/western blot with the DGAT2 antibody (DGAT2 AB). The upper first two horizontal lanes show the amount of DGAT2 (DGAT2 AB) or ACSL1-HA (HA-tag AB) in the cell lysates used for the immunoprecipitation of ACSL1-HA (IP HA-tag).

The coloured labeling indicates the amount of ACSL1-HA (red) or DGAT2 (turquoise) protein related to the total protein used that is coimmunoprecipitated with DGAT2 and ACSL1, respectively.

summary, all ACSL1-HA protein of the smooth ER fraction seems to interact with DGAT2 and additionally, all DGAT2 in the MAM fraction seems to interact with ACSL1-HA.

The coimmunoprecipitation of DGAT2 and ACSL1 showed that both proteins can specifically interact with each other. Nevertheless, it might be an artefact of overexpression or the interaction could be less frequent and of minor importance. The amount of DGAT2 per cell is very low, so that it can not be visualized by detection with our antibody. Additionally, no antibody for the detection of untagged wildtype ACSL1 protein was available. Therefore, DGAT2 was immunoprecipitated from wildtype COS7 cells and the coimmunoprecipitated ACSL proteins were detected by their enzymatic activity. The use of radioactively labeled substrates enabled to detect even minor amounts of ACSL activity. The experiments reveal that DGAT2 interacts specifically with an ACSL activity in wildtype COS7 cells, which most likely represents ACSL1 activity (figure 4.34).

4.4.2. Physiological role of the DGAT2-ACSL1 interaction

DGAT2 and ACSL1 both participate in lipid metabolism and they interact under physiological conditions (see section 4.4.1.3). As ACSL1 catalyzes the formation of acyl-CoAs, which are substrates for DGAT2, an interaction might speed up the formation of TAG by

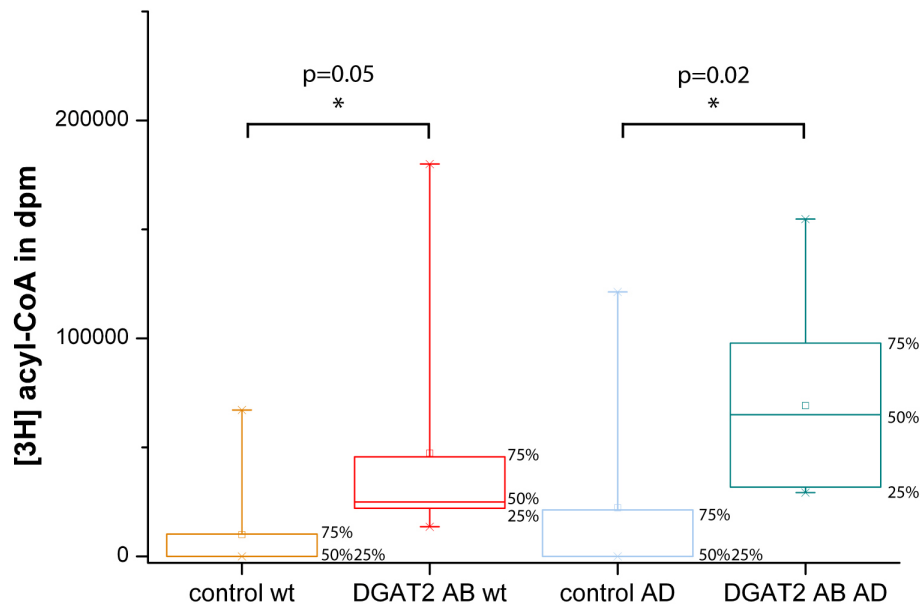


Figure 4.34.: DGAT2 associates with an ACSL activity in COS7 cells

COS7 cells were grown in DMEM medium supplemented with normal FCS. Cell lysates from untreated COS7 cells (wt) or COS7 cells transfected with wildtype human DGAT2 and human C-terminal HA-tagged ACSL1 (AD) for 24 h were used for a modified immunoprecipitation of DGAT2 (DGAT2 AB). Precipitates were subjected to an ACSL activity assay and the amount of the synthesized product $[3H]$ acyl-CoA was measured by scintillation counting. As control for unspecific binding, empty beads (control) were used in parallel in the immunoprecipitation procedure and ACSL assay. The results from ten experiments are shown as box blots. The box describes the range of values that contains half of the values measured. The crosses describe the maximum and minimum values measured and the square represents the mean of all experiments. Significances were calculated by unpaired two-sided t-test; * $p \leq 0.05$.

vectorial acylation. This process of substrate channeling was described in 3T3-L1 adipocytes, where FATP1, a fatty acid transporter, and ACSL1 interact at the PM. There, ACSL1 activity is necessary for the activity of FATP1 by directly activating and metabolizing incoming fatty acids [83, 87]. Therefore, COS7 cells overexpressing an empty vector, C-terminal HA-tagged ACSL1, wildtype DGAT2 or both proteins were fed with $[3H]$ oleate for 6 h or 24 h under normal growth conditions or supplemented with 100 μM oleate. Lipids were extracted, separated by TLC and quantified with ImageGauge. Though overexpression of DGAT2 increases TAG synthesis, the results show that coexpression of ACSL1 and DGAT2 has no further effect on de novo TAG synthesis compared to DGAT2 overexpression alone (supplementary figure A.20). In rat primary hepatocytes [81], overexpression of ACSL1 led to a channeling of FAs towards DAG and phospholipids and an increase in reacylation of hydrolyzed FAs into TAG. In order to investigate whether ACSL1 has a similar role in kidney fibroblasts, COS7 cells overexpressing an empty vector, C-terminal HA-tagged ACSL1, wildtype DGAT2 or both proteins were fed with $[14C]$ acetate for 6 h under normal growth conditions. Lipids were extracted, separated by TLC and quantified with ImageGauge. Neither single ACSL1 expression nor coexpression with DGAT2 revealed changes in the flux of fatty acids to certain lipids (supplementary figure A.21). If ACSL1 and DGAT2 interaction has no effect on acceleration or channeling in lipid metabolism, it might be beneficial

for the stability of DGAT2 and thus control the duration of DGAT2 activity. Labeling of DGAT2 with [35S]methionine and quantification of labeled DGAT2 protein after different chase times revealed a half time of about three hours under normal growth conditions. The half time of DGAT2 was not influenced by the coexpression of ACSL1 (supplementary figure A.22).

Though the interaction of ACSL1 and DGAT2 does not influence the direct speed of lipid metabolism, the lipid species synthesized or the stability of DGAT2, it seems to have an influence on the packaging of the synthesized lipids in LDs. The immunofluorescence data on the morphology of LDs in COS7 cells overexpressing an empty vector, C-terminal HA-tagged ACSL1, wildtype DGAT2 or both proteins (figure 4.31) indicate an increase in LD number upon overexpression of DGAT2 and a slight enlargement in LD size upon ACSL1 overexpression. The analysis of different immunofluorescence pictures from several experiments with Image J displays significant differences in the number and size of LDs. DGAT2 expression leads to more but smaller LDs, whereas ACSL1 expression shifts the mean droplet size towards larger droplets (figure 4.35). Overexpression of both proteins leads to a similar size distribution of the droplets, but a higher number. Differences were most prominent under delipidated conditions.

In order to confirm these size differences, LDs from COS7 cells grown in DMEM with 10% FCS and overexpressing an empty vector, C-terminal HA-tagged ACSL1, wildtype DGAT2 or both proteins were isolated by modified sucrose density gradient centrifugation and analyzed by electron microscopy. The LD diameter was analyzed manually on several pictures from three independent experiments (see figure 4.36). The measurements reveal a mean LD diameter of 105 nm for control cells. The mean LD diameter decreases significantly in DGAT2 overexpressing cells (40 nm, $p=2.79427E-12$) and increases significantly in ACSL1 overexpressing cells (267 nm, $p=9.05731E-19$). The expression of both proteins induced a slightly enlarged mean LD diameter compared to control cells (171 nm, $p=3.72301E-07$). All measured LDs from the EM pictures from three experiments are displayed as LD size distributions in figure 4.37. The size distribution reveals that more small LDs were measured upon DGAT2 overexpression and more large LDs were measured upon ACSL1 overexpression compared to control cells. Though the expression of both proteins ends up in a mean LD diameter similar to control, the distributions reveal that more small and more large LDs are measured upon coexpression of DGAT2 and ACSL1 than in the control. The distribution obtained for coexpression of DGAT2 and ACSL1 most likely represents the addition of both individual phenotypes.

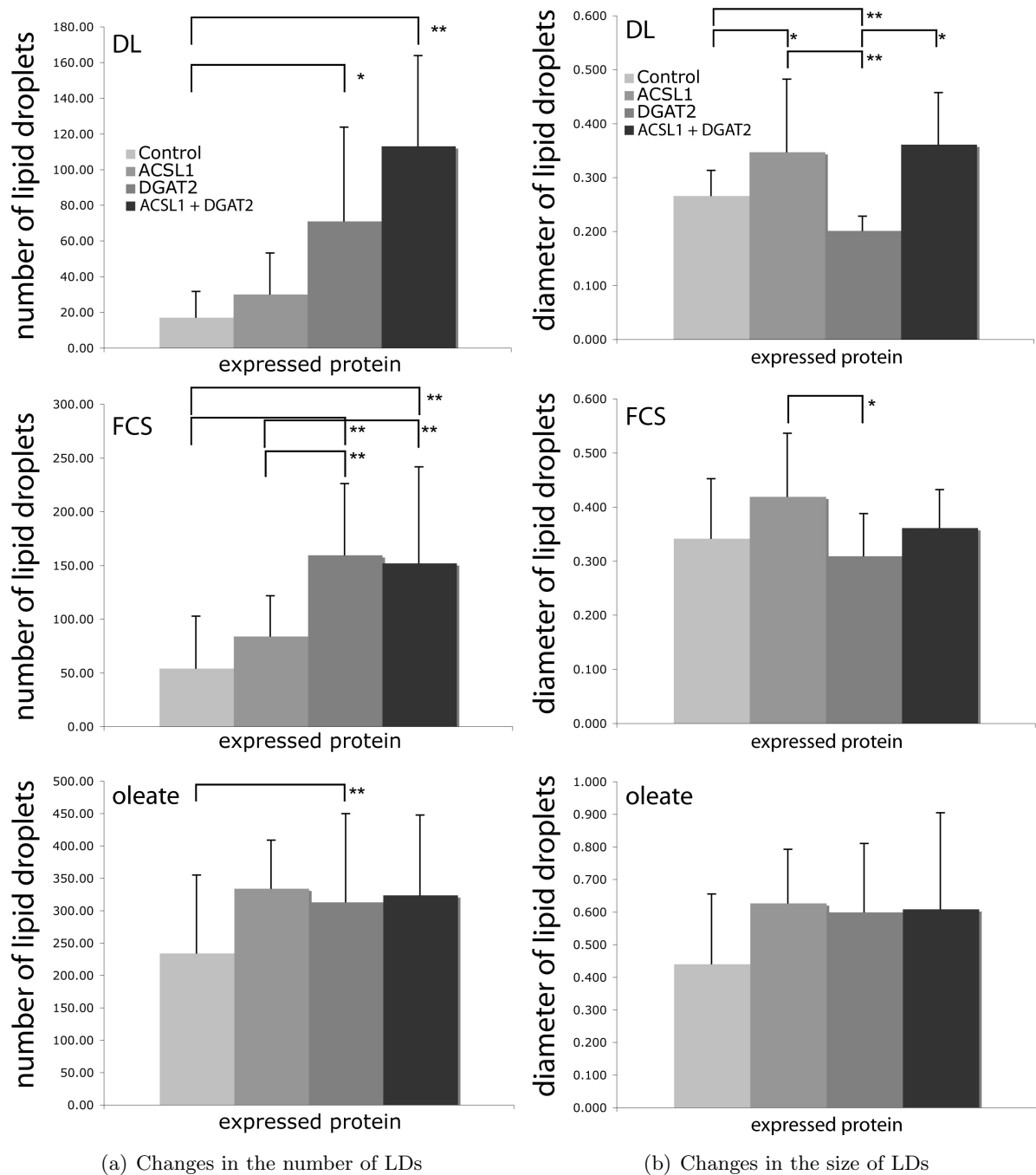


Figure 4.35.: The ratio between DGAT2 and ACSL1 influences the packaging of stored TAG

COS7 cells were transfected with empty vector (Control), human C-terminal HA-tagged ACSL1 (ACSL1), wildtype human DGAT2 (DGAT2) or wildtype human DGAT2 and human C-terminal HA-tagged ACSL1 (ACSL1 + DGAT2) for 24 h. Cells were grown in DMEM medium supplemented with delipidated FCS (DL), normal FCS (FCS) or FCS and 100 μ M oleate (oleate). Cells were analyzed by immunofluorescence (see figure 4.31) and several images from three different experiments were analyzed with Image J. The mean number of LDs (a) and the mean LD diameter (b) for all four expressed constructs and for all three conditions are shown. Significances were calculated by unpaired two-sided t-test relative to control; * $p \leq 0.05$; ** $p \leq 0.01$.

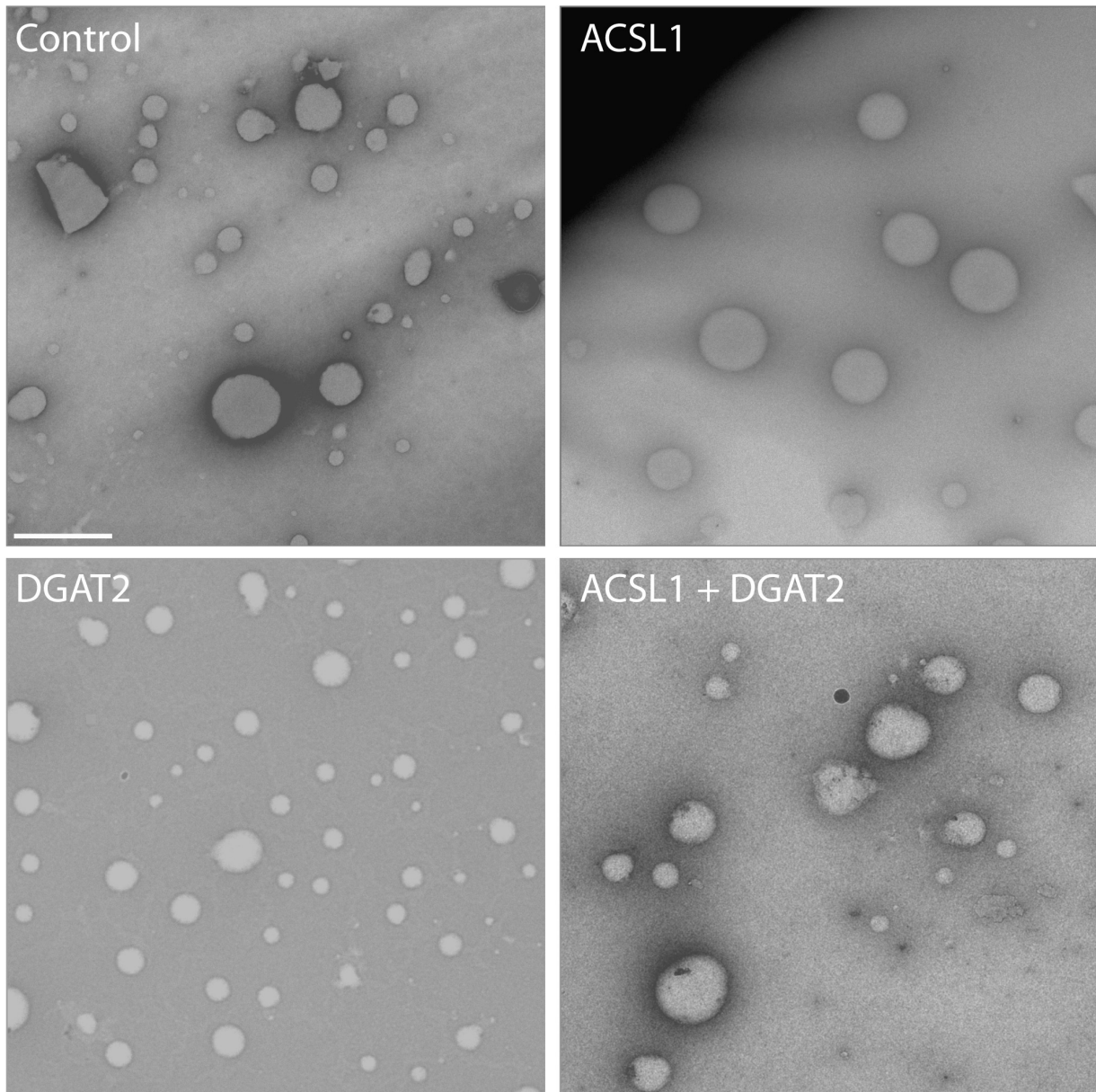


Figure 4.36.: ACSL1 and DGAT2 influence the size of LDs

COS7 cells grown in DMEM with 10% FCS and overexpressing an empty vector (Control), C-terminal HA-tagged ACSL1 (ACSL1), wildtype DGAT2 (DGAT2) or both proteins (ACSL1 + DGAT2) were isolated by modified sucrose density gradient centrifugation and analyzed by electron microscopy. Representative images are shown; scalebar = 1 μ m. Images were acquired by Kevin Manygoats and Daniela Vorkel.

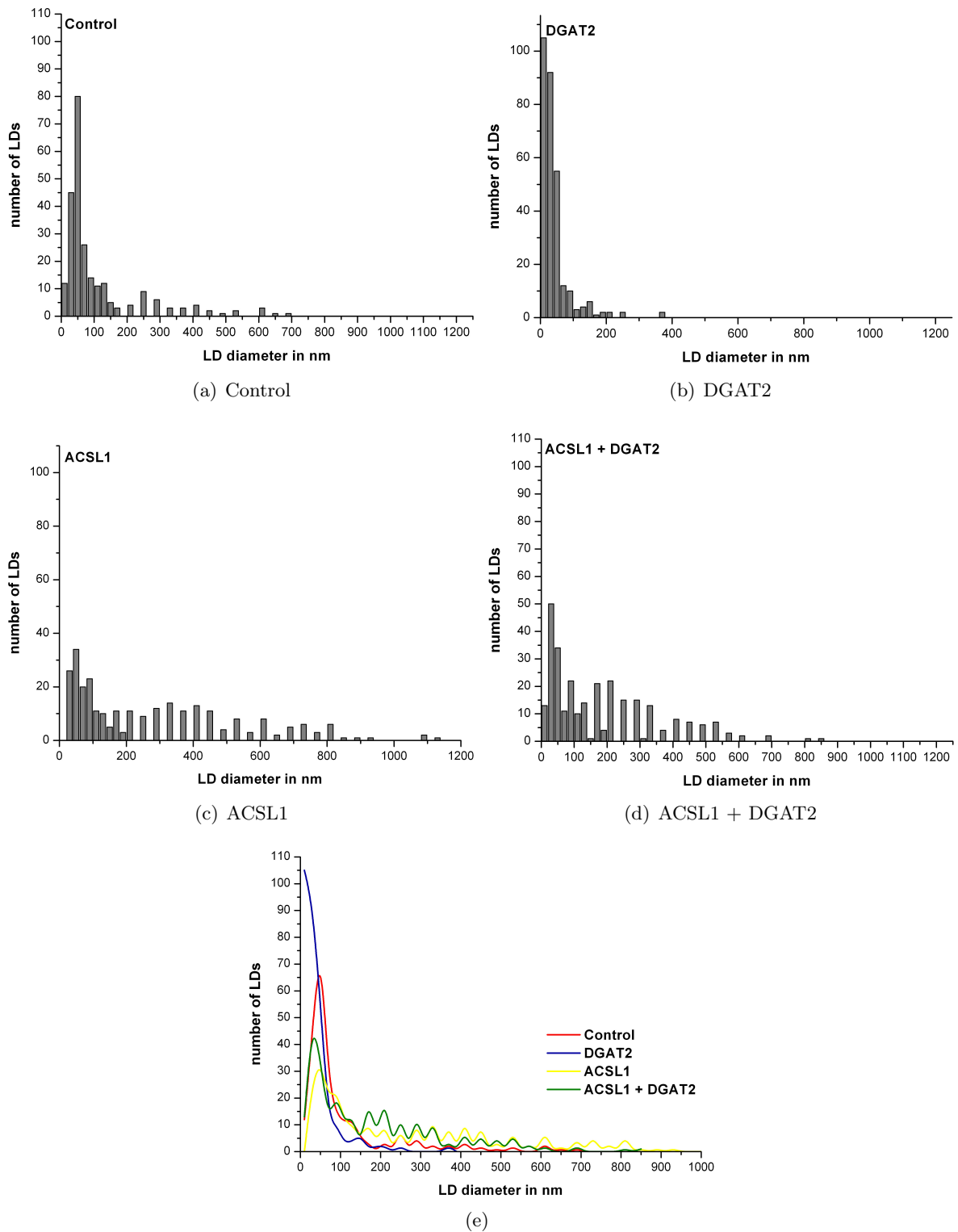


Figure 4.37.: The ratio between DGAT2 and ACSL1 influences the size distribution of LDs

COS7 cells grown in DMEM with 10% FCS and overexpressing an empty vector (Control), C-terminal HA-tagged ACSL1 (ACSL1), wildtype DGAT2 (DGAT2) or both proteins (ACSL1 + DGAT2) were isolated by modified sucrose density gradient centrifugation and analyzed by electron microscopy. The diameter of the isolated LDs was measured manually from several electron microscopy pictures obtained for each condition (see figure 4.36). The size distribution of LDs for Control is displayed in (a), for DGAT2 in (b), for ACSL1 in (c) and for ACSL1 + DGAT2 in (d). All four size distributions are summarized in (e); Control (red), DGAT2 (blue), ACSL1 (yellow), ACSL1 + DGAT2 (green).

5. Discussion

The results obtained in chapter 4 are discussed with respect to methodological aspects and they are compared with the observations of others. Additionally, they are set into broader context regarding their physiological significance and their involvement in diverse metabolic processes and disorders.

5.1. LDs grow by local synthesis of TAG and PC

The growth of LDs requires expansion of volume and surface area. LDs can gain additional lipids by different mechanisms, which are probably not exclusive and might promote each other. Four mechanisms are possible, which might be used depending on the need and cell type: LDs can grow (i) by homotypic fusion of LDs, (ii) by facilitated monomeric diffusion of lipids, (iii) by localized synthesis at the LD surface or (iv) by transport via continuities of the LD monolayer with the ER membrane. The growth of LDs and the incorporation of FAs into TAG is a fast event, typically taking just a few minutes [28, 171]. Homotypic fusion was recently observed in NIH-3T3 fibroblasts [130, 131]. Since it was not reported by others, who investigated LD growth, it seems to be a rather rare event that is unlikely to account for the rapid biosynthetic transport of droplet constituents [25, 28]. Additionally, recent data negate the formation of new small LDs and fusion to bigger LDs upon FA supply, but rather show the growth of already existing LDs supposedly by local synthesis of TAG [171]. Transporters for FAs and PC binding proteins have been reported [65, 69, 119], but their role remains unclear and no similar proteins were discovered for TAG so far. It has been shown that membrane continuities can exist [13, 120, 121], but it is uncertain whether they occur frequently or rather represent a rare intermediate state of LD biogenesis.

The data presented in section 4.1 show that TAG synthesis as well as PC synthesis can occur on LDs, which enables them to grow by local synthesis. The origin of the long-chain acyl-CoA species that are used by LPCAT1, LPCAT2 and DGAT2 is likely local production by ACSL3, an abundant constituent of LDs [76, 77] or by ACSL1, which can interact with DGAT2 (section 4.4.1) and was found in the vicinity of LDs and in adipocytes even on LDs [9]. The other precursor of TAG, DAG, could be produced at the ER by phosphatidic

acid phosphatase or derives from lipolysis of TAG. As shown in section 4.1.1.2, LDs contain sufficient DAG to produce measurable amounts of TAG [28]. For the other precursor of PC, LPC, the most likely source is production by action of PLA₂ either at the LD [14] or on other membrane compartments, probably the ER, followed by transport to the LD. Potential candidates for the PLA₂ activity are iPLA₂, the key activity in the Lands cycle of membrane lipid remodeling and involved in stress response of LDs [172] or cPLA₂, an important player in LD biogenesis [173]. Another possibility is the recently discovered adipocyte-specific PLA₂ [174], whose genetic ablation in mice results in strongly reduced TAG storage [175]. LPC is spontaneously released from membranes with a half-time of 13-20 milliseconds [176]. Desorption from membranes and transport in the cytosol are supported by binding to fatty acid binding proteins (FABPs) [65]. It should be noticed that the same principle, i.e. monomeric transport of a lyso-phospholipid followed by vectorial acylation at the target membrane, is used for the synthesis of PA. LPA is produced in mitochondria, transported to the ER by FABP [177] and converted to PA by an ER-resident LPAAT activity [150].

Local synthesis of TAG and PC has several advantages over the other mechanisms. In case of diffusion via membrane continuities, the surface lipid composition of LDs should resemble that of the ER. This would make it difficult to distinguish LDs and ER as separate targets for example for transport, signaling or metabolic activities. Additionally, it would not be possible to enrich the LD in certain lipids, if free diffusion existed between ER and LD. It was shown that the LD surface has a different lipid composition than the ER [8]. The local activity of LPCAT1 and LPCAT2 provide a unique LD surface lipid profile and enables to specifically enrich the LD in certain lipids (see section 4.2.1). Thus, local synthesis provides specificity and directionality to lipid synthesis. Fusion of LDs requires a change in LD surface lipids or protein composition to modulate surface tension and curvature to promote fusion [178, 179]. Furthermore, this growth mechanism requires the synthesis of new LDs prior to delivery to already existing LDs, which does not seem to be the case in 3Y1 fibroblasts or 3T3-L1 adipocytes [171]. Fusion between old and new LDs might be problematic, as it was reported that the protein composition changes during LD growth [25]. Though lipid binding and transfer proteins exist, they are often not specific for a certain lipid and a certain transport route [119]. For transport as well as fusion it might be difficult to regulate the magnitude and the directionality of the reaction, especially, as already existing LDs are not loaded equally with newly synthesized lipids [28, 171]. Therefore, local synthesis of the major LD lipids, TAG and PC, allows the independent and precise regulation of LD loading. Additionally, it enables the LD to rapidly respond to nutritional changes or to adapt its size.

5.2. Physiological significance of local TAG and PC synthesis

The local activity of DGAT2, LPCAT1 and LPCAT2 might be important to maintain a low level of toxic lipid intermediates, such as FFAs or LPC. Upon supply with exogenous FAs DGAT2 localizes to LDs and imported FAs can be rapidly incorporated into different lipids [28]. In this process not only TAG is formed and stored in LDs, but already measurable amounts of DAG accumulate in LDs. The DAG pool may therefore act as a reservoir to support the import of FAs while keeping the cellular pool of FFAs low [63, 64]. At later timepoints the DAG can be converted to phospholipids and to the long-term storage form TAG by the DGATs or FAs can be released for β -oxidation. The local synthesis of TAG at LDs makes additional transporters for transport of DAG to the ER and TAG back to the LD unnecessary, thereby accelerating lipid metabolism. FFAs and LPC are known to disrupt membranes and to function in cell death [180]. In order to prevent unwanted accumulations they can be incorporated into PC molecules. As LDs can store LPC [8], are usually disconnected from membranes and are able to synthesize PC, they are good locations for the detoxification of LPC and FFAs.

The activity of DGAT2, LPCAT1 and LPCAT2 might also be involved in the regulation of fusion between LDs and in LD budding from the ER during LD biogenesis. As LPC and DAG change the curvature of membranes and modulate fusion [178, 179], regulation of local DGAT and LPCAT activity of LDs might be crucial for the regulation of budding or fusion events. Furthermore, as the activities of LPCAT1, LPCAT2 and DGAT2 seem to determine the lipid composition of the LD, their regulation might be involved in the specific recruitment of certain proteins. Supporting this hypothesis, LDs in adipocytes are reported to change protein composition during maturation [25] or upon lipolytic stimulation [9]. Recently, it was shown that the accumulation of DAG in a membrane promotes the recruitment of TIP47, S3-12 and OXPAT to this membrane [181], which suggests a link between lipid composition and protein composition that might be favorable to adapt lipid metabolism to the cellular metabolic state.

5.2.1. Size regulation of LDs

Regarding the growth of LDs, two LD components have to increase in size: the LD core, mainly consisting of neutral lipids, and the LD surface, mainly consisting of PC. The LD grows upon synthesis of TAG, either by DGAT1 [93] or by DGAT2 [95], but only DGAT2 can localize to LDs and was reported to be crucial for TAG synthesis. Concerning the growth of LDs the LD surface layer has to expand with similar kinetics as the LD volume, otherwise

the surface-to-volume ratio will change. This requires a coordination between TAG and PC synthesis. The inhibition of PC synthesis reduces the amount of available LD surface. This leads to a change of the surface-to-volume ratio by concomitant unchanged or increased amounts of TAG and it results in the formation of larger LDs.

Interestingly, both, the inhibition of *de novo* PC synthesis and the inhibition of the membrane-remodeling pathway, result in the formation of larger LDs, but this is achieved by different mechanisms. Inhibition of the *de novo* pathway shifts FAs determined for PC production towards the production of TAG (supplementary figure A.7, [151]). In this case LDs enlarge, because the growth of their volume exceeds the growth of their surface. In contrast, inhibition of the membrane-remodeling pathway does not change the amount of neutral lipids, but restricts only the amount of available LD surface material. This leads to a reorganisation of the LD pool, which results in the formation of larger LDs (see section 4.2.2) in order to reduce the surface-to-volume ratio.

The magnitude, with which the different LPCATs participate in LD surface formation, has still to be dissected. LPCAT1 and LPCAT2 localize to the LD surface and to the ER and a knock-down does not provide information, whether both enzyme pools participate equally in the LD surface formation. Additionally, the role of LPCAT3 activity in this process is still unclear. Though *in vitro* studies revealed a preference for FAs that are rare at the analyzed LDs [110, 111, 117], a recent study reported similar FA preferences for LPCAT3 as for LPCAT1 and LPCAT2 *in vivo* [118]. Nevertheless, it might be possible that the acquired profile after LPCAT3 knock-down or overexpression results from concomitant changes in the activities of LPCAT1 and LPCAT2 rather than from direct effects of LPCAT3 decrease.

Besides direct modulation of the LD surface and indirect modulation of the LD volume by shifts in the FA metabolism, the LD size can be influenced by direct changes of the LD volume. Activation of DGAT results in enhanced formation of TAG [90], which is stored in LDs. This does not necessarily result in bigger LDs. Instead, overexpression of DGAT2 leads to the formation of more, but smaller LDs (see 4.4.2). This suggests that enhanced presence and activation of DGAT2 could upregulate the quantity or activity of LD surface forming enzymes. In conclusion, LD size regulation seems to depend on the interplay of different enzymes, in particular their abundance and activity.

5.2.2. LD size influences the lipid metabolism

Lipogenesis and lipolysis are multi-step processes that require the action of different enzymes (see chapter 2). Several of these enzymes attach directly to the surface of LDs. Therefore,

the size of LDs and the availability of surface is one determining factor for the availability of substrates for these enzymes. If more surface is available, more enzymes can bind to the LD and faster synthesis or degradation of lipids can occur. This suggestion is supported by the finding that LD fragmentation seems to be connected to lipolysis [3, 9]. Though fragmentation is not necessary for lipolysis, the finding that fragmentation of LDs promotes lipolysis [55, 56] further supports the importance of LD size for the lipid metabolism.

Changes in the cellular lipid metabolism can shift the cellular balance between lipid storage, lipid oxidation, lipid release, lipid uptake and lipid-carbohydrate metabolism. It was reported that a decrease in DGAT2 leads to a reduction in lipoprotein particle secretion [182], but this reduction is mainly due to reduced amounts of TAG available in the cells. Recently, a more surprising regulation of lipoprotein particle secretion was reported. It was shown that a decrease in ACSL3 protein results in a secretion defect for VLDL particles from hepatic cells [77]. The defect was mainly due to reduced availability of PC. In this thesis, a similar phenotype was observed upon reduction of LPCAT1 protein levels in hepatic cells (see section 4.2.3). Similar to LPCAT3 reduction, reduction in LPCAT1 results in decreased LPCAT activity and therefore also decreased availability of PC. This reduction leads to a decreased release of apoB, of radioactively labeled lipids, and of with lipoprotein particles associated hepatitis C virus particles.

The reduction in apoB secretion from HuH7 cells upon LPCAT1 knock-down seems to result from a simple decrease in lipoprotein particle secretion and not from a modification of the lipoprotein particles. The reduction of LPCAT1 leads to only minor changes in the composition of secreted lipids (see supplementary figure A.13), but reduces the amount of secreted lipids significantly. Decreased release of lipoprotein particles is supported by a decreased release of HCV particles. HCV particles are reported to depend on VLDL secretion for their release from hepatic cells [154]. The phenotype was only detected with one of the two LPCAT1 targeting siRNAs, which might depend on the less efficient reduction of the LPCAT1 protein with the other sequence and the need of a certain threshold to influence virus particle release. Differences in the strength of the reduction phenotype (apoB analyzed by western blot or ELISA, lipid secretion and HCV release) most likely result from differences in the methods and incubation times.

Interestingly, though large amounts of PC are available in the ER, the assembly locus for lipoprotein particles, the secretion is influenced by the modification of a small PC pool within the cells. Taking into account the influence of PC availability on lipolysis, it is suggested that the availability of PC modulates the lipoprotein particle secretion efficiency by slowing down the release of lipids from LDs by lipolysis. These lipids are required for lipoprotein

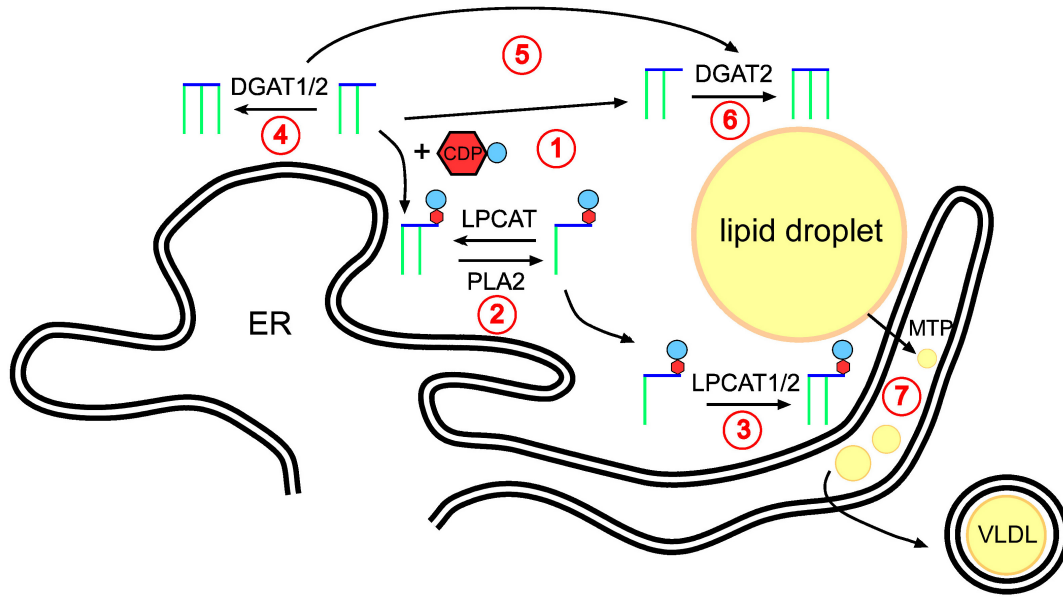


Figure 5.1.: A model to integrate triglyceride and phospholipid metabolism

The cellular homeostasis of PC is a complex process, in which PC biosynthesis via the Kennedy pathway (No.1) and PC turnover by the Lands cycle (No.2) are key elements. The Lands cycle consists of degradation by PLA_2 and re-acylation by LPCAT. Re-acylation does not take place exclusively in the ER (LPCAT1-3), but also on the LD surface (LPCAT1+2, No.3). Reduced PC biosynthesis via the Kennedy pathway results in increased production of TAG, likely a compensatory mechanism to deposit the excess FAs that are not used for membrane expansion. The specific reduction of PC biosynthesis on LDs by knock-down of LPCAT1 and/or LPCAT2 results in an increase of LD size, which can be explained by an imbalance of the synthesis of LD surface PC relative to LD volume. Likewise, TAG biosynthesis is compartmentalized in the same way between ER (DGAT1 and DGAT2, No.4) and LDs (DGAT2, No.6), where DGAT2 concentrates in response to excess fatty acids (No.5). DGAT2 and LPCAT1 are both important for normal secretion of lipoprotein particles, which are assembled in the ER by microsomal triglyceride transfer protein (MTP, No.7). This demonstrates a close connection between synthesis of LD surface, LD volume and secreted lipoproteins.

particle assembly (summarized in figure 5.1). In conclusion, the results show that already small changes like the different packaging of TAG can have severe consequences beyond the cell level. As the development of many diseases is connected to the lipid level in the circulation and the hepatitis C virus release relies on the secretion of lipoprotein particles [154], it will be of interest to study these findings in more detail.

5.3. Formation and regulation of subcellular lipid pools

In lipid metabolism most reactions are catalyzed by enzyme families. Usually several iso-enzymes that catalyze the same reactions, belong to these families, but they differ in structure and subcellular localization [64, 111]. This allows compartmentalization of synthesis and maintenance of separate pools with different fates. But as these iso-enzymes are often unable to substitute for each other, it makes cells susceptible for defects in one of the enzymes. This explains why the activity of LD-associated LPCAT1 is important for secretion of lipoprotein particles in HuH7 cells, although the cell contains abundant ER-associated

LPCAT activity provided by LPCAT3 [110]. The compartmentalization of the PC biosynthesis between ER and LD parallels the TAG biosynthesis. In order to obtain a separation of iso-enzymes, they must contain recognition motifs or structures. These motifs would enable the cell to target certain iso-enzymes to the LD (DGAT2, LPCAT1 and LPCAT2), while others remain in the ER (DGAT1, LPCAT3 and LPCAT4).

Concerning the DGAT iso-enzymes, DGAT1 is a polytopic transmembrane protein localizing to the ER [91], while DGAT2 is a monotopic protein (see section 4.3.2, [92]) with localization to both ER and LDs (see section 4.1.1, [28], [101]). Likewise, the biosynthesis of PC via acylation of LPC can either take place at the ER by the action of the polytopic enzymes LPCAT3 and LPCAT4 [111], which actually belong to the same protein family as DGAT1, or at the LDs by the activity of the monotopic proteins LPCAT1 and LPCAT2 (see section 4.3.1). The principle behind is the same: the different physical properties of bilayer and monolayer membranes lead to separation of iso-enzymes with polytopic and monotopic mode of membranes insertion.

5.3.1. Interaction of DGAT2 and ACSL1

The importance of the subcellular localization and the ratio of the amounts of enzymes in lipid metabolism is demonstrated by the interaction of DGAT2 and ACSL1. While ACSL1 shows broad distribution in various membranes and organelles, DGAT2 seems to be restricted to certain regions in the ER and the LDs (see figure 4.31 and 4.32). ACSL1 and DGAT2 specifically interact with each other (see section 4.4.1.3). The interaction is likely mediated via one of two potential sequence motifs revealed by bioinformatical analysis (see figure 4.29). Concerning the conservation of these motifs in different species, the motif at amino acid position 62 to 73 is highly conserved and therefore more likely to account for the specific interaction. Interestingly, this motif was found to be involved in targeting of DGAT2 to mitochondria-associated membranes (MAM) [101]. As a significant amount of ACSL1-HA is suggested to localize to MAM (see figure 4.31 and 4.32), but the amount of DGAT2 in this location is low, it is possible that ACSL1 traps DGAT2 at MAM via specific binding. This is supported by the finding that a disruption of the putative ACSL1-DGAT2 binding site reduced DGAT2 association to MAM drastically [101]. Whether the localization of DGAT2 to MAM is accidental, as it get trapped by ACSL1, which is abundant in this compartment, or whether it represents a physiological relevant localization needs to be further investigated. In contrast, as most DGAT2 localizes to specific ER regions (see figure 4.31 and 4.32) and nearly all ACSL1-HA coimmunoprecipitated seems to interact with DGAT2 there, it is likely that the localization of ACSL1-HA into DGAT2-containing

ER regions depends on the specific targeting of DGAT2. Via the potential binding motif ACSL1 might be recruited to these membrane regions together with DGAT2. The functional analysis of the potential binding motifs is currently under way and a localization study of mutated DGAT2 and ACSL1 might answer the question, to which extent ACSL1 localization depends on DGAT2.

The role of the interaction between DGAT2 and ACSL1 in lipid metabolism also remains to be analyzed further. Though ACSL1 is likely involved in providing activated FAs for the formation of TAG by DGAT2, coexpression of both proteins does not seem to influence TAG synthesis beyond the rates obtained by overexpression of DGAT2 alone. Nevertheless, this does not exclude a supporting effect of ACSL1 on TAG synthesis by DGAT2. ACSL1 might just not be the limiting factor in this system or another regulating component is missing. This is supported by the finding that the highly conserved sequence at the extreme N-terminus of mammalian DGAT2 (see figure 4.29) does not seem to be involved in ACSL1-DGAT2 interaction, but presumably mediates a specific interaction with other regulating factors. Additionally, several specific mass spectrometric profiles were obtained in the analysis of potential DGAT2 interaction partners, which could not be allocated to a certain protein. This can be explained by the use of pig liver and the existence of an only incomplete protein mass spectrometry profile database for the pig proteome. Furthermore, ACSL1 does not seem to influence the cellular lipid profile, though it was reported that ACSL1 increases FA incorporation into TAG and shifts FAs into DAG and phospholipids [81, 85, 86, 88]. The discrepancies might be due to the use of different radioactively labeled lipid precursors ([^{14}C]acetate versus [^{14}C]oleate), the different transfection conditions (transient vector transfection, adenovirus-based transfection for overexpression versus knock-down or liver-specific knockout) and the use of different cell lines (african green monkey kidney fibroblasts, rat primary hepatoma cells, mouse 3T3-L1 adipocytes and primary hepatocytes from liver-specific knockout mice).

Though ACSL1 shows no direct influence on lipid synthesis rates, it influences the packaging of lipid into LDs, as it promotes the formation of larger LDs (see figure 4.35, 4.36 and 4.37). One possibility, how ACSL1 influences LD morphology, might be via the control of DGAT2 mobility. As DGAT2 can change localization from ER to LDs upon oleate-feeding and preliminary data from FRAP (fluorescent recovery after photobleaching) experiments suggests a high mobility of DGAT2 within the ER (data not shown), it is possible that ACSL1 traps DGAT2 for a longer timeperiod at a certain location, which leads to the formation of larger LDs. Overexpression of DGAT2 alone leads to the formation of many, but small LDs. This can be explained by suggesting that DGAT2 resides at the location of

LD formation and fills the LD with TAG. In combination with the high DGAT2 mobility, the time that a DGAT2 molecule stays at this location and fills a LD with TAG instead of moving and starting the formation of a new LD elsewhere is shorter than when it is associated with ACSL1. However, the analysis of the LD size profile upon coexpression of DGAT2 and ACSL1 revealed a combination of many small and many big LDs, whereas control cells mainly exhibit medium sized LDs. This might result from differences in the expression of DGAT2 and ACSL1 over the whole cell population, as some cells will only overexpress one of both enzymes or in different ratios.

Another possibility, how ACSL1 might influence LD morphology could result from channeling of FAs and control of other enzymatic activities. Though changes in FA incorporation could not be detected in this thesis, they were reported to occur by others. ACSL1 overexpression might channel FAs towards TAG and away from PC formation, which would influence the surface-to-volume ratio of LDs and lead to enlarged LDs as discussed in section 5.2.1. Besides this indirect influence, ACSL1 might participate in the direct regulation of other enzymes, for example LPCATs, by blocking interaction sites of the DGAT2 molecule, by influencing its localization or by the modification, recruitment or release of an unknown regulator.

5.4. Impact of DGAT2, LPCAT1 and LPCAT2 on lipid metabolic diseases

Many diseases are associated with increased levels of plasma lipids like diabetes and atherosclerosis [145, 147]. Medication that targets lipid release into the blood circulation would be beneficial for these diseases. However, the reduction of lipid release leads to accumulation of lipids within cells, which results in obesity, inflammation and interference with cellular function up to cell death [144, 145, 149]. In this context, medications that block one of the processes strongly will also strongly accelerate the pathologic development of the other process. Therefore, the knowledge about the function and regulation of LPCAT1, LPCAT2 and DGAT2 might render them useful as targets for medication. The phenotypes of LPCAT1 and LPCAT2 knock-down are relatively modest. Thus, a light reduction in lipid release might lower the level of plasma lipids below the pathologic threshold, but causes only minor lipid accumulations within cells. Therefore, the use of LPCAT1 and LPCAT2 as targets can elongate the timeframe until insulin resistance develops and for therapies like food restriction and sports. Additionally, targeting the cellular LPCAT activity might improve inflammation

in obesity, as it was reported to regulate the inflammatory response to microbial stimuli and cytokine production in monocytes and epithelial cells [183].

Concerning DGAT2, it is the main DGAT in the liver and it is involved in lipid release [182]. However, mice overexpressing DGAT2 exhibit low plasma lipid level, but lipid accumulation in the liver [184]. Interestingly, DGAT2 overexpression was not associated with insulin resistance, but could result in the development of hepatic steatosis. Therefore, it might be an interesting target to treat hepatic steatosis or to reduce the plasma lipid level. As DGAT2 is crucial for survival, direct medication targeting DGAT2 itself might lead to severe adverse effects. Therefore, understanding the regulation of DGAT2 provides new targets for treatment of metabolic diseases. Targeting for example ACSL1 might influence DGAT2, but could exhibit reduced adverse effects.

Besides metabolic disorders, medication targeting LPCAT1 and DGAT2 could improve the treatment for hepatitis C virus infection. As hepatitis C virus release is strongly linked to lipoprotein particle release [154] and this process is connected to the activity of LPCAT1 and DGAT2, inhibition of their activity could reduce the dispersion of the virus within the body.

In conclusion, detailed knowledge of the function and regulation of single players in lipid metabolism helps to understand regulations and effects on the whole cellular lipid metabolism and allows to explain and manipulate lipid mediated effects on the entire organism.

6. Materials and Methods

6.1. Materials

6.1.1. Cell lines, cell culture media, bacteria strains and *Drosophila melanogaster* strains

The human fibroblast skin cell line A431 and the african green monkey kidney fibroblast cell line COS7 were from ATCC (Virginia, US) with the ID numbers CRL-1555 and CRL-1651, respectively. The human hepatoma cell line HuH7 was from HSRRB (Shinjuku, Japan) with the ID number JCRB0403. Dulbeccos modified Eagles medium with high glucose and sodium pyruvate (DMEM), Dulbeccos modified Eagles medium without pyridoxine hydrochloride, L-glutamine, sodium pyruvate, L-methionine and L-cysteine, Opti-MEM, RPMI 1640, fetal calf serum (FCS) and trypsin were obtained from Gibco (Karlsruhe, Germany). Delipidated FCS was prepared by solvent extraction with diisopropylether and butanol and dialysis against PBS. Non-essential amino acids and L-glutamine were from Invitrogen (Karlsruhe, Germany). For cloning and expression the E.coli strains DH5 α , JM110 (dam-) and ER2566 were used. The following *Drosophila melanogaster* strains were obtained from Bloomington (Indiana, US): wildtype, OregonR (ORK); white-mutant, w1118; strain 13872, y1 P{SUPor-P}CG32699KG05104; strain 19866, y1 w67c23 P{EPgy2}CG32699 EY07993 and strain 10101, w1118 P{EP}EP912EP912 CG32699EP912.

6.1.2. Chemicals

Thin layer chromatography (TLC) silica gel 60 plates were from Merck (Darmstadt, Germany). Human apolipoprotein B ELISA^{PRO} was from Mabtech (Nacka Strand, Sweden). Protein detection assay was from Bio-Rad (Munich, Germany). The transfection reagent Lipofectamine 2000 was from Invitrogen (Karlsruhe, Germany) and Interferin from BIOMOL (Hamburg, Germany). CoenzymeA (CoA) sodium salt hydrate was from Sigma (St. Louis, US). The dye 4',6-Diamidino-2-phenylindol (DAPI) was from Sigma-Aldrich Chemie GmbH

6. Materials and Methods

(Taufkirchen, Germany), 4,4-difluoro-1,3,5,7,8-penta-methyl-4-bora-3a,4a-diaza-s-indacene (BODIPY 493/503) was from MoBiTec and LD540 was provided by Christoph Thiele and Johanna Spandl. Protein A sepharose (CL4B) was from GE Healthcare, streptavidin-sepharose was from Amersham Bioscience (Uppsala, Sweden). Digitonin was from Applichem (Darmstadt, Germany).

6.1.3. Plasmids, ESTs, DNA primer, siRNAs, enzymes

Table 6.1.: Plasmids

	names	expression product	organism	resistance	production	used restriction sites	source
1	pMOHA, pMOHA-A35	triple HA-tag (3HA)	mammal	Ampicillin	from pcDNA3.1 by insertion of 3HA		Monika Suchanek
2	pN3HA	triple HA-tag (3HA) +	mammal	Kanamycin			Christoph Thiele
3	pFastbac1SBPseq, D713		baculovirus	Ampicillin			Konstantinos Anastasiadis
4	pET24D, plk75, p90		bacteria	Kanamycin			Protein Expression Facility
5	pN3HA-hDGAT2	3HA-human DGAT2	mammal	Kanamycin	PCR from plk91 and insertion into pN3HA	BglII, Xba1	
6	pN3HA-hLPCAT1, pCT56	3HA-human LPCAT1	mammal	Kanamycin	PCR from LPCAT1-EST RZPD: IMAGp998F2213627Q, IMAGE ID: 6205077	Xho1, Xba1	Johanna Spandl, Christoph Thiele
7	pN3HA-hLPCAT2, pCT60	3HA-human LPCAT2	mammal	Kanamycin	PCR from LPCAT2-EST RZPD: IRAUp969E0210D6, IMAGE ID: 3347690	HindIII, Xba1	Johanna Spandl, Christoph Thiele
8	pmRFP1-ER, plk14	directs monomeric DsRed to ER	mammal	Kanamycin			Lars Kürschner
9	pMOHA-hCaveolin1, C26	human Caveolin1-3HA	mammal	Ampicillin			Monika Suchanek
10	pMOHA-hACSL1	human ACSL1-3HA	mammal	Ampicillin	PCR from EST , insertion into pMOHA	HindIII, Xba1	
11	pMOHA-hDGAT2, plk24	human DGAT2-3HA	mammal	Ampicillin			Lars Kürschner
12	phDGAT2int3xHA, plk34	human DGAT2 w/ internal 3xHA tag inserted at aa ~19	mammal	Ampicillin			Lars Kürschner
13	pMOHA-hDGAT2wt, plk91	human DGAT2	mammal	Ampicillin			Lars Kürschner
14	pMOHA-hLPCAT1	human LPCAT1-3HA	mammal	Ampicillin	PCR from pCT56, insertion into pMOHA	Xho1, Xba1	
15	pMOHA-hLPCAT1wt	human LPCAT1	mammal	Ampicillin	PCR from pCT56, insertion into pMOHA	Xho1, Xba1	
16	pMOHA-hLPCAT2	human LPCAT2-3HA	mammal	Ampicillin	PCR from pCT60, insertion into pMOHA	HindIII, Xba1	
17	pMOHA-hLPCAT2wt	human LPCAT2	mammal	Ampicillin	PCR from pCT60, insertion into pMOHA	HindIII, Xba1	
18	pcDNA3.1-N(200)hDGAT2-TEV-3HA-P-SBP	N-terminal 66 aa of human DGAT2 followed by TEV cleavage site-3HA-Precision cleavage site-Streptavidin-Binding-Protein (SBP)-tag	mammal	Ampicillin	Tags and N-terminus of human DGAT2 were inserted stepwise into pMOHA, first HA-tag was removed, then PCR from D713, SBP-tag and precision cleavage site were inserted via ApaI and Xba1, then PCR from pMOHA, 3HA and TEV cleavage site were inserted via KpnI and Xba1, then PCR of N(200)hDGAT2 form plk91 and insertion via Nhe1 and KpnI.	ApaI, Xba1, KpnI, Nhe1	
19	pET24D-tags	TEV cleavage site-3HA-Precision cleavage site-Streptavidin-Binding-Protein (SBP)-tag	bacteria	Kanamycin	PCR from pET24D-N(200)hDGAT2-TEV-3HA-P-SBP and insertion into pET24D	Nhe1, HindIII	
20	pET24D-EGFP-tags	EGFP followed by TEV cleavage site-3HA-Precision cleavage site-Streptavidin-Binding-Protein (SBP)-tag	bacteria	Kanamycin	PCR from pcDNA3.1-EGFP-C1 vector and insertion into pET24D-tags	Nhe1, KpnI	
21	pET24D-N(200)hDGAT2-TEV-3HA-P-SBP	N-terminal 66 aa of human DGAT2 followed by TEV cleavage site-3HA-Precision cleavage site-Streptavidin-Binding-Protein (SBP)-tag	bacteria	Kanamycin	PCR from pcDNA3.1-N(200)hDGAT2-TEV-3HA-P-SBP and insertion into pET24D	Nhe1, HindIII	

ESTs were obtained from RZPD (Heidelberg, Germany) with the following ID numbers: LPCAT1-EST IMAGp998F2213627Q, LPCAT2-EST IRAUp969E0210D6 and ACSL1-EST IRAKp961A1191Q. All primers were from Biospring (Frankfurt, Germany). All siRNA sequences were from Ambion (Austin, Texas) with the following order IDs: siRNA1#1: 127470, siRNA1#2: 127471, siRNA1#3: 127469, siRNA2#1: 25681 and siRNA2#2: 140447. Enzymes for cloning and calf intestine alkaline phosphatase (CIAP) were obtained from New England Biolabs (Frankfurt, Germany), Fermentas (Mannheim, Germany) or the MPI-CBG protein expression facility. Proteinase K was obtained from Applichem (Darmstadt, Germany).

6.1.4. Lipids and radioactive substances

16:0-LPC, 16:0-LPA and CDP-choline were from Fluka, oleoyl-CoA, palmitoyl-CoA and dioleoyl-diacylglycerol (DODG) were from Sigma (St. Louis, US). Oleate and palmitate were from Acros (Geel, Belgium). Synthetic lipid standards were from Avanti Polar Lipids Inc. (Alabaster, AL), Larodan Fine Chemicals (Malmö, Sweden) and Sigma-Aldrich Chemie GmbH (Munich, Germany). [14C]CDP-choline was from Biotrend (Cologne, Germany), [3H]oleate was from Hartmann Analytic (Braunschweig, Germany). [3H]acyl-CoAs were synthesized as described [185]. [35S]methionine was from Perkin Elmer Life Science (Rodgau, Germany).

6.1.5. Antibodies

Primary antibodies

Table 6.2.: Primary antibodies

antigen	species	property	source
Acyl-cholesterol acyltransferase 1 (ACAT1)	rabbit	polyclonal	T. Chang, Dartmouth College, Hannover
Acyl-CoA acyltransferase 3 (ACSL3)	rabbit	polyclonal	C. Thiele
Adipophilin (ADRP)	mouse	monoclonal	PROGEN
ApolipoproteinB	goat	polyclonal	Calbiochem
Calnexin	rabbit	polyclonal	Stressgen
Caveolin1 clone N20	rabbit	polyclonal	Santa Cruz Biotechnology
Cytochrome C oxidase subunit 4 (COXIV)	rabbit	monoclonal	Cell Signaling
Diacylglycerol acyltransferase 2 (DGAT2)	rabbit	polyclonal	L. Kuerschner
Hemagglutinin (HA) clone F7	mouse	monoclonal	Santa Cruz Biotechnology
Lyso-phosphatidylcholine acyltransferase 1 (LPCAT1)	rabbit	polyclonal	C. Thiele
Lyso-phosphatidylcholine acyltransferase 2 (LPCAT2)	rabbit	polyclonal	C. Thiele
Sterol dehydrogenase (NSDHL)	rabbit	polyclonal	C. Thiele
Protein-Disulfid-Isomerase (PDI)	mouse	monoclonal	Stressgen
Protein-Disulfid-Isomerase (PDI)	rabbit	polyclonal	Stressgen
Tail interacting protein 47 (TIP47)	rabbit	polyclonal	S. Hoening, Cologne University, Cologne

Secondary antibodies

The goat anti-mouse and the goat anti-rabbit antibodies coupled with the fluorophore Alexa488, Alexa555 or Alexa647 and the rabbit anti-goat antibody coupled with horseradish

peroxidase (HRP) were obtained from Invitrogen (Karlsruhe, Germany). The goat anti-mouse and anti-rabbit antibodies coupled with horseradish peroxidase (HRP) were obtained from Jacksons Immunological (West Grove, PA).

6.2. Methods

6.2.1. Methods of molecular biology

6.2.1.1. Cloning

First, primer for amplification of the desired DNA sequence by PCR were designed and the appropriate restriction enzyme sites were added. The DNA fragment was amplified by PCR either from an EST sequence or from an already existing construct. The PCR product was purified with the Qiaquick PCR purification kit and the chosen vector and the purified product were digested with the appropriate restriction enzymes over-night. The resulting open ends in the vector were dephosphorylated with CIAP. Then, the restricted products were separated according to their size by agarose gel electrophoresis and the DNA fragments of the desired size were cut out and purified with the Qiaquick gel extraction kit from Qiagen (Hilden, Germany). The digested and purified vector and PCR products were fast ligated (10 min at RT) and transfected into E.coli DH5 α . Successfully transfected E.coli were selected on agar-plates supplemented with antibiotics matching the antibiotic resistance gene of the vector. Resistant colonies were raised in small (2 ml) suspension cultures and plasmids were isolated with the QiaPrep[®] Spin MiniPrep kit. All newly constructed plasmids were verified by sequencing. Bacteria colonies with correct plasmids were grown in big cultures (450 ml) and plasmids were isolated with the QiaPrep[®] Spin MaxiPrep or Nucleobond AX kit from Macherey-Nagel (Düren, Germany).

6.2.2. Methods of cell biology

6.2.2.1. Bacteria culture

E.coli strains were grown at 37°C on LB-agar-plates or in LB-medium consisting of 5 g/l yeast extract, 10 g/l NaCl, 10 g/l tryptone and containing ampicillin (100 μ g/ml) or kanamycin (50 μ g/ml).

6.2.2.2. Cell culture

A431 and COS7 cells were maintained in DMEM (Gibco 31966) with 10% FCS, HuH7 cells in RPMI (Gibco 31870) supplemented with 10 mM HEPES, 0.1 mM non-essential amino acids, 2 mM L-glutamine and 10% FCS at 37°C and 5% CO₂. If indicated, normal FCS was replaced by delipidated FCS (DL-FCS).

6.2.2.3. Fly culture

Drosophila melanogaster strains were kept at room temperature in tubes with food. The food source contained 8 g agar, 10 g soybean, 18 g yeast extract, 80 g maize, 22 g glucose sirup, 80 g malt, 1.5 g nipagin in 5 ml ethanol and 6 ml propionic acid in 1 l water. Flies were transferred to new tubes not later than two weeks.

6.2.2.4. Isolation of larval fat bodies from *Drosophila melanogaster*

Four to five L3 larvae of each strain were collected and dissected in PBS on ice. Fat bodies were transferred in PBS onto an object slide on ice and covered with a coverslip. Microscopy was performed with a 100x NA 1.3 oil objective using bright field.

6.2.2.5. Transfection

Bacteria were either transfected by heat shock or by electroporation. For the heat shock, DNA and bacteria were mixed on ice for about 10 min, then exposed to 42°C for 90 sec and spread onto agar-plates for selection. For electroporation, bacteria and DNA were mixed on ice in a cuvette and exposed to an electric pulse. The cuvette was filled with bacteria culture medium and bacteria were spread on agar-plates for selection.

Mammalian cells were transfected with Lipofectamine 2000 for plasmids and with Interferin for siRNAs. For the transfection of plasmids, Lipofectamine 2000 and plasmids were equilibrated in Opti-MEM for 5-10 min in separate tubes. Then, they were mixed in a ratio 1 to 2 up to 1 to 5 DNA to Lipofectamine 2000 and incubated for 20 min. Meanwhile, cell culture medium on about 70-90% confluent cells was exchanged to Opti-MEM and the DNA-Lipofectamine 2000-mixture was added for 4 h. Then, transfection medium was exchanged with cell culture medium or cell culture medium was added to the transfection medium. For the transfection of siRNA, 16 h prior to transfection 5000 cells were plated per well of a 24-well plate. Then 100 µl Opti-MEM were mixed with 7 µl 125 nM siRNA

and 2 μ l Interferin and incubated for 10 min. Meanwhile cell culture medium on cells was set to 500 μ l cell culture medium per well of a 24-well plate and 100 μ l of the transfection mixture was added for 48 h to 72 h.

6.2.2.6. Imaging

Immunofluorescence microscopy For immunofluorescence, cells were grown on glass coverslips to about 80% confluency. Depending on the experiment cells were either transfected with DNA or siRNA (see 6.2.2.5) or were directly fixed with 3% w/v paraformaldehyde in PBS for 30 minutes, washed with PBS, blocked and permeabilized for 30 minutes in PBS containing 0.5% BSA and 0.1% saponin (blocking buffer, BB). Cells were incubated with primary antibodies for 1 h in BB, washed three times with BB, incubated with secondary antibody in BB, washed three times in PBS and counterstained with Bodipy 493/503 or LD540 [186] in PBS, followed by three washes in PBS. After rinsing in water, coverslips were mounted in Mowiol 4-88 containing 2.5% 1,4-diazabicyclo[2.2.2]octane. When antibody incubations were not required, cells were fixed without permeabilization and then stained with DAPI and BODIPY 493/503. Images were acquired with laserpoint scanning confocal microscopes, either a Zeiss LSM 510 or a Zeiss Meta microscope, equipped with a 100x NA 1.3 oil objectives and laser excitation at 351/364 nm, 488 nm, 543 nm and 633 nm. Quantification of fluorescent images was done with Image J particle analysis of the lipid droplet detecting channel. For A431 cells threshold was set to 723-maximum, for HuH7 cells to 100-maximum, circularity 0-1 and particle detection only at a size between 0,02 and 20 μ m².

Electron microscopy Lipid droplets were isolated as described in 6.2.2.7 and bound to electron microscopy grids. These four hundred mesh grids were coated with formvar and/or with a thin carbon coat. The carbon coat was charged with a glow-discharger and exposed to a droplet of lipid droplet containing solution for 2 min. The droplet was exchanged to a droplet of 3% molybdate pH 7.0 or 4% uranylacetate pH 6.0. The droplet was either dried on the grid or removed by washing 2 times with 20 mM Hepes/NaOH, pH 7.4.

6.2.2.7. Lipid droplet isolation and density gradients

Cells were grown in 10 cm dishes in normal medium or medium supplemented with 50-100 μ M oleate for 16 h, washed and scraped in ice-cold disruption buffer (20 mM Hepes/NaOH, pH 7.4, 0.25 M sucrose) followed by homogenization in a cooled EMBL cell-cracker (HGM,

Heidelberg, GER) with five strokes using a maximum clearance of 18 μm . The lysate was centrifuged at 1000 g for 10 min, and the post-nuclear supernatant (PNS) was adjusted to 1.1 M sucrose. Four ml of the PNS were loaded to the bottom of a 13 ml centrifuge tube and overlaid with ice-cold disruption buffer. The gradients were centrifuged in a swing-out rotor at 100.000 g at 4°C for 2.5 h up to over-night. Fractions were taken from the top as follows: top 2 ml - LD fraction, next 3.5 ml - intermediate fraction, next 4 ml including the phase boundary between 0.25 and 1.1 M sucrose - floating membranes, last 3.5 ml - bottom fraction. For lipid mass spectrometry, cells were grown in medium supplemented with 10% FCS and 20% horse serum and a layer of 0.5 M sucrose with 100 mM NaHCO_3 pH 11.5 was included between PNS and ice-cold disruption buffer. For electron microscopy, the top two to three ml were exchanged to 20 mM Hepes/NaOH, pH 7.4 without sucrose. For localization of DGAT2 and ACSL1 in COS7 cells a stepwise sucrose gradient ranging from 15 to 70% sucrose was used. Sample was loaded on a 70% sucrose layer and further sucrose layers were added containing 60%, 58%, 55%, 52%, 50%, 48%, 45%, 40%, 35%, 30%, 25% and 15% sucrose. After centrifugation 500 μl fractions were taken, proteins were separated by SDS-PAGE and analyzed by western blot using anti-DGAT2 and anti-ACSL1-HA as well as organelle specific antibodies.

6.2.2.8. ApolipoproteinB, lipid and hepatitis C virus secretion

HuH7 cells were plated in 24-well plates (5000 cells per well) 16 h prior transfection. Cells were transfected with siRNAs (control siRNA scrambled#5 or #6 and siRNA against LPCAT1 siRNA1#1 and siRNA1#3). Transfection was performed in 100 μl Opti-MEM and 500 μl serum-free supplemented RPMI medium.

In case of apoB determination by apoB ELISA, siRNAs were removed after 24 h and cells were grown further for 48 h in 200 μl serum-free RPMI. Supernatants were collected 72 h after transfection and they were subjected to apoB ELISA. The corresponding cells were scraped into PBS and total protein content was measured with BIORAD protein assay. The amount of apoB released was quantified by ELISA, normalized to the total protein content and compared to control.

In case of apoB determination by western blot, supernatants were collected 72 h after transfection and mixed with 5xLämmli buffer and corresponding cells were scraped in 50 μl Lämmli buffer. Supernatant (40 μl) and cell lysates (15 μl) were subjected to SDS-PAGE and western blot and analyzed for apoB and LPCAT1 and GAPDH, respectively. The amounts of apoB and LPCAT1 were normalized to GAPDH and compared to control.

In case of radioactive quantification of lipid release, 1 μCi [^3H]oleate was added to the

medium to each well of a 24-well plate for 24 h. Then, remaining radioactivity and siRNAs were removed and cells were grown further in 200 μ l serum-free supplemented RPMI medium for 48 h. Supernatants were collected 72 h after transfection and lipids were extracted (see 6.2.3.3). The extracted lipids were separated by thin layer chromatography (see 6.2.3.3) or quantified by scintillation counting.

For density determination of apolipoproteinB containing lipoprotein particles, they were separated by differential centrifugation. Five hundred μ l serum-free supernatant collected from HuH7 cells after three days was laid on top of 500 μ l density medium with a density of 1,006 kg/l (0.19 M NaCl, 0.27 mM EDTA, 1 mM NaOH) and centrifuged for 100 min at 60.000 g at 18°C. The top 450 μ l were removed, the rest mixed and 500 μ l were mixed with 500 μ l of density medium with a density of 1,120 kg/l (0.19 M NaCl, 0.27 mM EDTA, 1 mM NaOH, 0.85 M NaBr). Centrifugation was repeated and the top 450 μ l were collected. The rest was mixed and 500 μ l were mixed with 500 μ l of density medium with a density of 1,340 kg/l (0.19 M NaCl, 0.27 mM EDTA, 1 mM NaOH, 5.25 M NaBr). Centrifugation and collection was repeated and the rest was mixed and 450 μ l were collected. Proteins from all collected samples were precipitated with chloroform/methanol and dissolved in Lämmli buffer. Proteins were separated by SDS-polyacrylamide gel electrophoresis.

For the measurement of hepatitis C virus (HCV) replication and release, HuH7.5 cells, HuH7.5 firefly cells and the recombinant HCV Jc2Ra were used. First, 3×10^4 Huh7.5 firefly cells were seeded and 24 h later transfected with interferin and the indicated siRNAs (1.5 nM) or mock transfected. About 24 h post transfection the mixtures were removed and fresh DMEM was added to the cells. About 40 h after transfection, cells were infected (original infection) with the Jc1 derived Jc2Ra reporter HCV at the indicated MOI. About 24 h post infection the medium was replaced by 500 μ l of fresh DMEM and about 72 h post infection the supernatants were collected and 300 μ l were used to infect Huh7.5 cells (reinfection), seeded the day before in a 24-well plate (2×10^4 cells). The originally infected Huh7.5 cells were then lysed and assayed for Renilla Luciferase and Firefly Luciferase counts, to calculate the levels of HCV replication. The data were then analyzed to calculate the effect of the siRNAs on viral replication by comparing the ratio between the average replication in the two controls and after treatment with the siRNA of interest. After 72 h post reinfection, cells were lysed and assayed for Renilla Luciferase counts, to calculate the levels of HCV assembly/release. The analysis of HCV replication and secretion was performed by Gualtierio Alvisi.

6.2.3. Biochemical methods

6.2.3.1. SDS-polyacrylamide gel electrophoresis, Coomassie staining and western blot

All samples for SDS-polyacrylamide gel electrophoresis (SDS-PAGE) were prepared in Lämmli buffer (1x: 62.5 mM Tris-HCl pH 6.8, 2% SDS, 0.002% Bromophenol blue, 10% (w/v) glycerol, 1% β -mercaptoethanol). The Bio-Rad (Munich, Germany) Mini-protean system and the following solutions were used: 1x running Buffer (25 mM Tris, 192 mM glycine, 0.1% SDS), 4x separating gel buffer (1.5 M Tris-HCl pH 8.8, 0.4% (w/v) SDS), 4x stacking gel buffer (0.5 M Tris-HCl pH 6.8, 0.4% SDS), 30% acrylamide stock (30% (w/v) acrylamide, 0.8% (w/v) bisacrylamide), TEMED and 10% ammonium persulfate stock. The gels are either stained with Coomassie blue solution (0.25% (w/v) Coomassie brilliant blue R250, 40% methanol, 10% acetic acid, 50% water) and destained with destaining solution (40% methanol, 10% acetic acid, 50% water) and dried in a gel dryer or the gels were used for western blot. The proteins in the gels were blotted onto a nitrocellulose membrane from Whatman (Dassel, Germany) by semidry transfer using the semidry blotting buffer (40% 1x running buffer, 20% methanol, 40% water) or by wet blot transfer using the wet blotting buffer (10% running buffer, 20% methanol, 70% water). Successful transfer was validated by PonceauS staining of the membrane followed by blocking with blocking solution (PBSMT: PBS containing 4% (w/v) milk powder and 0.2% Tween-20). The membrane was incubated with the primary antibody in PBSMT for 1 h up to over-night. Unbound antibody was removed by three washes with PBSMT followed by incubation with the secondary antibody for 1 h. Unbound antibody was removed by three washes with PBSMT, two washes with PBST and two washes with PBS. Protein detection was performed with ECL western blot detection reagent from GE Healthcare and Biomax Light films from Kodak or ECL Hyperfilms from GE Healthcare.

6.2.3.2. Protein topology

Selective membrane permeabilisation For analysis of protein membrane topology by immunofluorescence, cells were plated on glass coverslips, transfected with either the N- or C-terminally tagged protein of interest, fixed and permeabilized with 0.1% saponin (permeabilizes all cellular membranes) or with 0.001% digitonin (permeabilizes only the plasma membrane) and stained with antibodies against HA-tag, C-terminus of LPCAT1 or LPCAT2 and the luminal ER protein PDI. For further detail on staining procedure see 6.2.2.6.

Digestion protection A 10 cm dish of COS7 or A431 cells was transfected with the N- and C-terminally tagged protein of interest. The cells were scraped into ice-cold PBS and squeezed through a 0.7x40 mm needle. Cell lysates were centrifuged at 600 g for 5 min and supernatant was divided into three tubes and centrifuged at 100.000 g for 30 min. The supernatant was removed and replaced by 100 μ l PBS, 100 μ l PBS with 1% TritonX-100 and 100 μ g Proteinase K or 100 μ l PBS with 100 μ g Proteinase K for 1 h at room temperature. The reaction was stopped by the addition of 1 mM PMSF and 25 μ l 5xLämmli buffer. Proteins were separated by SDS-PAGE and analyzed by western blot for the N- and C-terminal tags and the luminal ER protein PDI.

Membrane association A 10 cm dish of COS7 cells was transfected with a vector for expression of the DGAT2 wildtype protein. Membranes were collected as described above in 6.2.3.2 except that supernatant was divided into six instead of three tubes. Membranes were then incubated for 30 min with 100 μ l PBS, 100 μ l PBS with 1 M NaCl, 100 μ l PBS with 6 M urea, 100 μ l PBS with 0.1 M NaCO₃, 100 μ l PBS with 1% TritonX-100 or 100 μ l PBS with 1% dodecylmaltoside. Then, samples were centrifuged again at 100.000 g for 30 min and supernatant and pellet were mixed with Lämmli buffer. Proteins were separated by SDS-PAGE and analyzed by western blot for the abundance of DGAT2 and the single-span membrane protein calnexin.

6.2.3.3. Radioactive labeling, extraction and identification of cellular lipids

Metabolic labeling with radioactive precursors Cells were either labeled with [3H]oleate for 6 h up to 24 h by adding 1 μ Ci per well of a 24-well plate or with [14C]acetate for 6 h by adding 0.5 μ Ci per well of a 24-well plate to the cell culture medium. The lipids are extracted from cells, separated by TLC or quantified as described in the following paragraphs. For labeling of proteins with [35S]methionine cells were transfected 20 h prior to labeling and kept in Dulbeccos modified Eagles medium without pyridoxine hydrochloride, L-glutamine, sodium pyruvate, L-methionine and L-cysteine for 1 h before the addition of 0.2 mCi [35S]methionine and 10% FCS for 4 h. Proteins were isolated from cells by immunoprecipitation as described in section 6.2.3.6.

Lipid extraction For extraction of cellular lipids directly from a 24-well cell culture dish, cells were washed 1x with ice-cold PBS with 1% BSA and 2x with ice-cold PBS. Then, 30-50 μ l methanol/chloroform (5:1) was added to the cells and the liquid was transferred directly to a thin layer chromatography plate. For lipid extraction from cell supernatants

or activity assays, liquids were mixed with 750 μ l methanol/chloroform (3:1) and 400 μ l water. The mixture was centrifuged at 13.000 rpm for 5 min and the lower lipid containing chloroform phase was transferred to a new tube. Chloroform was removed in vacuo and the lipid pellet was dissolved in 30 μ l methanol/chloroform (1:2). Lipids were separated by thin layer chromatography.

Separation of lipids by thin layer chromatography Thin layer chromatography plates (TLC) plates were loaded with lipid containing solutions with a capillary. Plates were run in solvent 1 (35 ml triethylamine, 50 ml ethanol, 10 ml water, 35 ml chloroform) for 1 h and in solvent 2 (100 ml iso-hexane and 20 ml ethylacetate or 95 ml iso-hexane, 23.8 ml diethylether and 1.2 ml acetate) for 30 min. Dried plates were either sprayed with sulfuric acid to stain the lipids or in case of radioactive labeled lipids exposed on phosphoimager plates (for [14 C]) or dipped into Lumasafe scintillation liquid and exposed to Hyperfilm MP at -80°C (for [3 H]).

Quantification of lipids Lipids were either quantified from autoradiography films or phosphoimager plates with the software IMAGEGAUGE and compared to controls or standards or were quantified directly from the TLC plate on a Biospace Beta-Imager 2000 or in the scintillation counter. For scintillation counting, lipidspots were scraped from the TLC plate and homogenized 30 min by ultrasonification in 1 ml chloroform/ethanol/water (49.5:49.5:1). Then, they were centrifuged for 10 min at 13.000 rpm and supernatant was transferred into scintillation tubes. The liquid was evaporated and the pellet was dissolved in 2 ml ethanol. Then, 15 ml Lumasafe scintillation liquid was added and measured in the scintillation counter with the appropriate program. Lipids in solution were measured directly by mixing with Lumasafe scintillation liquid and measuring in the scintillation counter.

6.2.3.4. Protein and lipid mass spectrometry

For the analysis of the lipid droplet proteome, A431 cells (8 x 10 cm dishes) were grown as described in section 6.2.2.2 and supplemented with 100 μ M oleate for the final 16 h. Cells were lysed and LDs were purified exactly as described in section 6.2.2.7 with the exception of the addition of Roche Complete protease inhibitor tablets to all buffers. Proteins from pooled LD fractions were precipitated using chloroform/methanol, subjected to one-dimensional SDS-PAGE (10% acrylamide gel) and visualized by Coomassie brilliant blue (CBB) staining. The lane was cut into 34 bands that were separately digested with trypsin [187] and recovered peptides were analyzed by LC-MS/MS on LTQ linear ion trap mass

spectrometer. This experiment was performed by Christoph Thiele and Anna Shevchenko. For the analysis of the proteins interacting with the N-terminus of DGAT2, eluates from the streptavidin-sepharose-SBP-tag-column (see 6.2.3.6) were separated by SDS-PAGE and stained with Coomassie. Visible bands were cut out, staining and salts were removed and proteins were digested with trypsin. Protein fragments were crystalized and analyzed by MALDI-TOF mass spectrometry. This analysis was performed by Cornelia Czupalla.

For lipid mass spectrometry, cell lysates, floating membranes or LDs (in 200 μ l 155 mM NH_4HCO_3) were mixed with 20 μ l internal lipid standard mixture providing a spike of 57 pmol PE 17:0/17:0, 47 pmol PC 18:3/18:3, 47 pmol SM 17:0, 37 pmol DAG 17:0/17:0, 37 pmol TAG 17:1/17:1/17:1 and 57 pmol CE 17:0. Samples were extracted with 990 μ l chloroform/methanol (15:1) for 120 min at 4°C [188]. The apolar organic phase was isolated and evaporated. Lipid extracts were dissolved in 200 μ l of 7.5 mM ammonium acetate in chloroform/methanol/2-propanol (1:2:4) and subjected to quantitative lipid analysis in positive ion mode on a QSTAR Pulsar-i instrument (MDS Analytical Technologies) or a LTQ Orbitrap mass spectrometer (Thermo Fisher Scientific) equipped with a TriVersa NanoMate nanoflow ion source (Advion Biosciences, Inc., Ithaca, NJ) [188–191]. This analysis was performed by Christer Ejlsing.

6.2.3.5. Enzyme activity assays

LPCAT and LPAAT activity assay Whole cell lysates (15 μ l or 50 μ l for HuH7 cell lysates upon LPCAT1 knock-down) or LD fractions from sucrose gradient centrifugation (200 μ l) were mixed with 100 μ l of assay buffer (200 mM Tris/HCl pH 7.5, 10 mM MgCl_2 , 2 mg/ml fatty acid free BSA, 10 μ M oleoyl-CoA, 10 μ M palmitoyl-CoA, 1 μ Ci/ml each of [3H]oleoyl-CoA, [3H]palmitoyl-CoA and [3H]myristoyl-CoA). For the LPAAT assay, 100 μ M sn-1-palmitoyl-sn2-lyso-PA, for the LPCAT assay 100 μ M sn-1-palmitoyl-sn2-lyso-PC were added and incubated for 30 min at 30°C or 15 min at 37°C for HuH7 cell lysates upon LPCAT1 knock-down. Reactions were stopped by lipid extraction. Lipids were separated by TLC and plates were either analyzed on a Biospace Beta-Imager 2000 or were sprayed with scintillant and exposed to a X-ray film at -80°C.

Diacylglycerol cholinephosphotransferase assay Whole A431 cell lysates (50 μ l) or a mixture of bottom (50 μ l) and membrane fraction (50 μ l) or LD fractions from sucrose gradient centrifugation (200 μ l) were mixed with 100 μ l of assay buffer (50 mM Tris-HCl pH

8.0, 10 mM MgCl₂, 100 μ M DODG, 0.5 μ Ci [14C]CDP-choline, 200 μ M CDP-choline) and incubated for 30 min at 37°C. The same procedure as described for LPCAT assay followed.

DGAT2 activity assay Aliquots of the LD fraction (200 μ l) or bottom fraction (120 μ l) were mixed with 100 or 180 μ l, respectively, of assay buffer (200 mM Tris, pH 7.4, 10 mM MgCl₂, 2 mg/ml delipidated BSA, 20 μ M oleoyl-CoA, 20 μ M palmitoyl-CoA, 0 or 200 μ M dioleoylglycerol, 0.35 μ Ci each of [9,10-3H]-oleoyl-CoA, [9,10-3H]-palmitoyl-CoA, and [9,10-3H]-myristoyl-CoA) and incubated at 30°C for 1 h. A control sample replacing the LD fraction with homogenization buffer was carried along. Lipids were extracted, separated by TLC in iso-hexane/diethylether/acetic acid 80:20:1, and visualized by autoradiography.

ACSL1 activity assay Proteins were coimmunoprecipitated as described in 6.2.3.6. The beads with the precipitate (100 μ l) were incubated with 100 μ l assay buffer (200 mM Tris-HCl pH 7.4, 20 mM MgCl₂, 0.01 M DTT, 20 mM ATP, 0.6 mM CoA, 0.05 mM oleate, 0.05 mM palmitate, 1 μ Ci [3H]oleate, 1 μ Ci [3H]palmitate) for 1.5 h at 37°C. The reaction was stopped by the addition of 400 μ l isopropanol/iso-hexane/1M HCl (79:19:2). The mixture was centrifuged for 3 min at 13.000 rpm and the supernatant was transferred to a new tube. Beads were pelleted and supernatants were collected. FFAs were extracted from supernatants by the addition of 140 μ l water and 250 μ l iso-hexane. The mixture was centrifuged for 3 min at 13.000 rpm, the upper hexane layer was removed and the rest was mixed with 300 μ l iso-hexane. The upper hexane layer was removed and the procedure was repeated two to three times. Then, 350 μ l of the lower layer were transferred to a scintillation tube and mixed with the same amount of methanol and with 15 ml Lumasafe scintillation liquid. Then, the activity of the remaining product [3H]acyl-CoA in the lower layer was measured in the scintillation counter.

6.2.3.6. Identification of protein-protein interaction

Protein expression and purification The empty pET24D vector, the pET24D-EGFP-tags vector and the pET24D-N(200)hDGAT2-TEV-3HA-P-SBP vector were transfected into the expression bacteria strain ER2566. The transfected strains were grown at 18°C from OD 0.1 till OD 0.5, then protein expression was induced with 0.1 mM isopropyl-beta-D-thiogalactopyranoside at 18°C over-night. Bacteria were collected by centrifugation, the pellet was homogenized in 10 ml lysis buffer (40 mM HEPES pH 7.2, 150 mM NaCl, 2 mM EDTA, 50 mM NaF, 0.2 mM NaOrthovanadate, Roche proteinase inhibitor) and frozen at -20°C. After thawing, bacteria were lysed with an emulsiflex and lysates were centrifuged for

1 h at 23.000 g to remove membrane debris. An aliquot of each bacteria strain lysate was tested by SDS-PAGE and western blot for the expression of the appropriate protein. Meanwhile, streptavidin-sepharose was equilibrated at 4°C, ethanol was removed and the column was washed with bacterial lysis buffer. Then, lysates were incubated with streptavidin-sepharose for 4 h at 4°C to specifically bind the desired proteins via their SBP-tag. The lysates were removed and the column was washed 2x with three volumes bacteria lysis buffer and equilibrated with 2x three volumes recruitment buffer (25 mM HEPES pH 7.2, 125 mM potassium acetate, 2.5 mM magnesium acetate, 1 mM DTT, 5 mM potassiumdihydrogenphosphate, 5 mM glycerol-3-phosphate, Roche proteinase inhibitor).

Liver cytosol preparation Pig (*Sus scrofa*) liver was cut into small pieces, which were further homogenized in recruitment buffer by douncing. Then, the homogenate was centrifuged for 10 min at 10.000 g and the supernatant was centrifuged again for 1 h at 100.000 g. The supernatant was collected as cytosol and the pellet was resuspended in recruitment buffer and collected as membranes. Protein amount was measured and aliquots were frozen at -80°C.

Streptavidin-sepharose-SBP-tag-column Liver cytosol, membrane and a mixture of both (membranes + cytosol) were diluted with recruitment buffer. The membrane and membrane + cytosol samples contained additionally 1% dodecylmaltosid. Samples were incubated with empty streptavidin-sepharose beads. The samples were then added to the SBP-tagged protein loaded streptavidin-sepharose columns (see 6.2.3.6) and incubated over-night. The supernatant was removed and the column was washed with recruitment buffer and buffers with increasing salt concentration (40 mM HEPES pH 7.2 with 10 mM, 30 mM, 50 mM, 100 mM, 150 mM, 200 mM, 300 mM NaCl). The SBP-tagged proteins were eluted from the column together with its binding partners by the addition of elution buffer (lysis buffer with 2.5 mM desthiobiotin). Eluates were separated by SDS-PAGE and gels were stained with Coomassie. Specific bands were cut out and analyzed by protein mass spectrometry (see 6.2.3.4).

Immunoprecipitation Protein A-coupled sepharose beads (60 µl 50% slurry per tube) were washed with PBS and blocked with PBS-1% BSA, washed with PBS and IP lysis buffer (20 mM HEPES pH 7.4, 100 mM NaCl, 5 mM EDTA, 1% TritonX-100, 0.5% NaDesoxycholate, 0.2 mM NaOrthovanadate, 75 mM NaF, Roche proteinase inhibitor). Antibodies (DGAT2 1:2, HA (F7) 1:6) were added with IP lysis buffer for 3 h and washed with PBS-1%

BSA, PBS and IP lysis buffer. Either wildtype or transfected COS7 cells were grown in 6-well plates or 10 cm dishes and were scraped into IP lysis buffer. Lysates were rotated for 10 min at 4°C and centrifuged at 13.000 rpm. The supernatant was incubated with blocked protein A-coupled sepharose beads for 3 h. Then, the supernatant was incubated with the antibody protein A-coupled sepharose beads over-night. The supernatant was removed and beads were washed 3x with 400 μ l light wash buffer (20 mM HEPES pH 7.4, 0.5% CHAPS, 0.2 mM NaOrthovanadate, 75 mM NaF, Roche proteinase inhibitor) and 1x with 400 μ l hard wash buffer (150 mM NaCl, 2 mM EDTA, 100 mM Tris-HCl pH 8.3, 0.1% SDS, 0.5% Nonidet P40, 0.5% NaDesoxycholate, 0.2 mM NaOrthovanadate, 75 mM NaF, Roche proteinase inhibitor). Beads were mixed with Lämmli buffer, proteins were separated by SDS-PAGE and analyzed by western blot. All washing and incubation steps were performed on a rotating wheel at 4°C and beads were pelleted by centrifugation. In case of the IP followed by the ACSL1 assay (6.2.3.5), beads were sedimented by gravitation and modified IP lysis buffer (20 mM HEPES pH 7.4, 100 mM NaCl, 5 mM EDTA, 0.8% digitonin, 0.2 mM NaOrthovanadate, 75 mM NaF, Roche proteinase inhibitor) and wash buffer (20 mM HEPES pH 7.4, 0.2% digitonin , Roche proteinase inhibitor) were used.

A. Supplementary figures

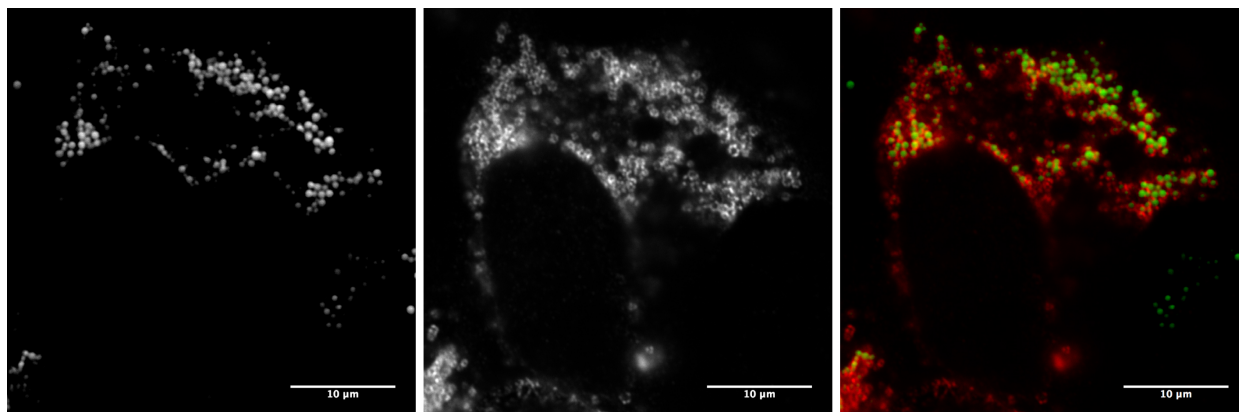


Figure A.1.: DGAT2 localization under oleate-fed conditions

The immunofluorescence image of DGAT2 and LDs under oleate-fed conditions show in figure 4.1 is split into single channels: first image, LDs; second image, DGAT2; third image, merged. Scalebar = 10 μm

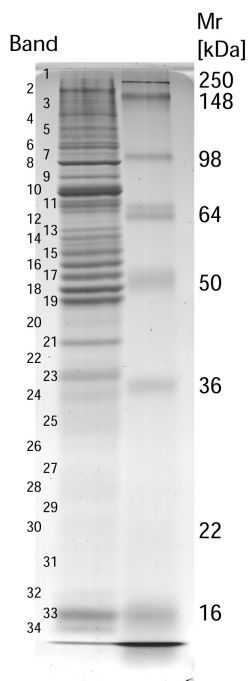


Figure A.2.: Coomassie gel for LD protein mass spectrometric analysis

Proteins were isolated from purified lipid droplets of oleate-fed A431 cells and were subjected to SDS-PAGE followed by Coomassie brilliant blue staining. The lane was cut into 34 slices, each of which was separately digested with trypsin and analyzed by LC-MS/MS. This figure is provided by Christoph Thiele.

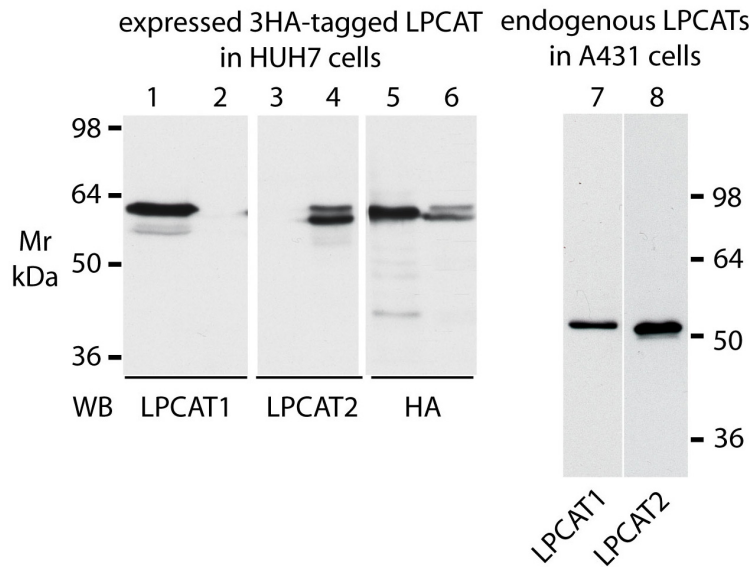


Figure A.3.: Characterization of antibodies against LPCAT1 and LPCAT2

Left panel: HuH7 cells were transfected with vectors for LPCAT1 (lanes 1, 3, 5) or LPCAT2 (lanes 2, 4, 6), both bearing an N-terminal 3HA-tag. Total cell lysates were subjected to SDS-PAGE followed by western blotting. Three identical blots were probed with anti-LPCAT1 (lanes 1+2), anti-LPCAT2 (lanes 3+4), and anti-HA (lanes 5+6). Right panel: Total lysates of non-transfected A431 cells were subjected to SDS-PAGE/western blotting and probed with anti-LPCAT1 and anti-LPCAT2.

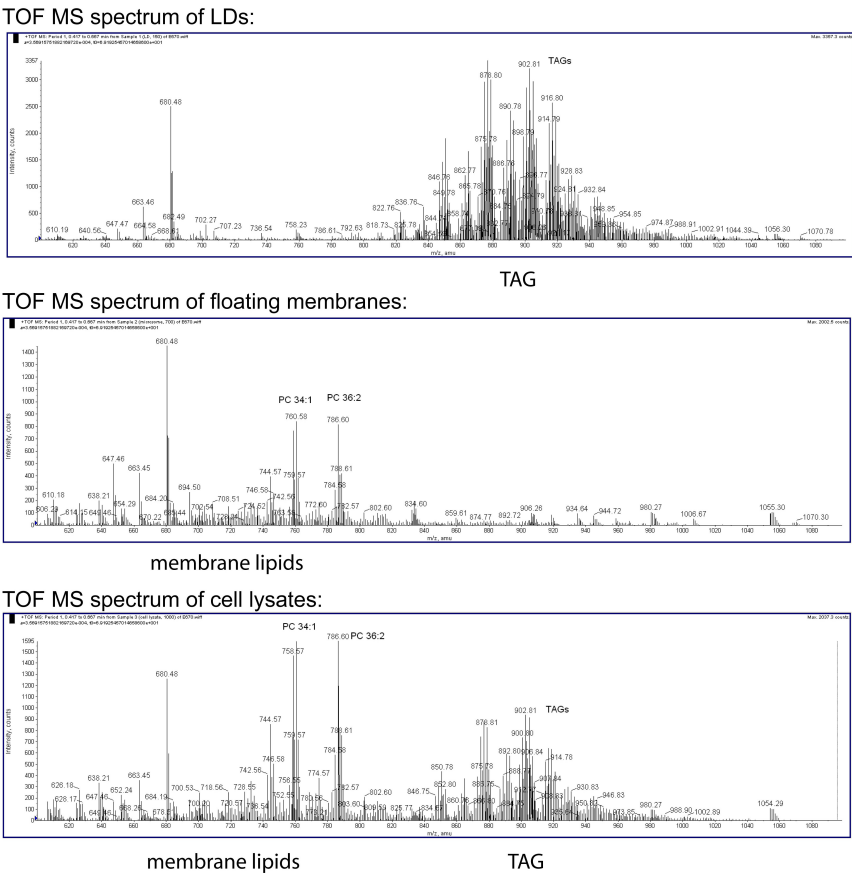


Figure A.4.: Purity of LD fractions used for lipid mass spectrometry

The figure shows ESI Time-of-Flight mass spectra of isolated LDs of A431 cells (upper panel), floating membranes of A431 cells (middle panel) or whole cell lysates of A431 cells (lower panel). Note that lysates contain a mixture of phospholipids and TAG, while floating membranes contain mostly phospholipids, and LDs mostly TAG. This diagram and lipid mass spectrometry is provided by Christer Ejising.

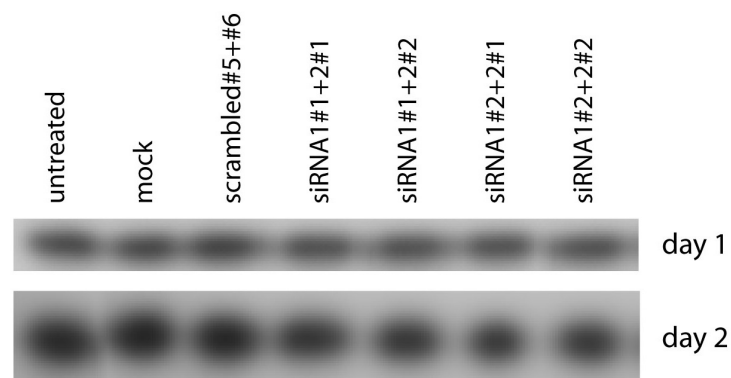


Figure A.5.: Silencing of LPCAT1 and LPCAT2 in A431 cells does not influence TAG synthesis

A431 cells were grown and transfected with siRNA as described in figure 4.12. [3H]oleate was added for further 24 h to the cells either directly (day 1) or 24 h (day 2) after transfection. Lipids were extracted, separated by TLC and visualized by autoradiography. Only the region of newly synthesized [3H]TAG is shown.

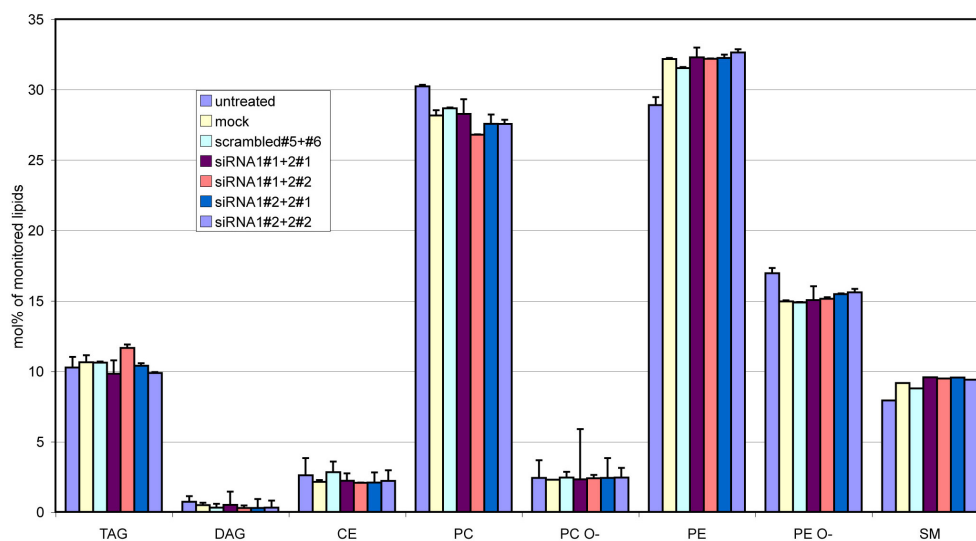


Figure A.6.: Silencing of LPCAT1 and LPCAT2 in A431 cells does not influence the amount of stored TAG

A431 cells were transfected as described in figure 4.12. After 48 h, total lipid extracts were analyzed by mass spectrometry. Each sample was measured in duplicate, and species abundances were normalized to the corresponding internal standard. The molar contents of each species of the same class were summed up and normalized to the total content of all detectable lipids. This diagram and lipid mass spectrometry is provided by Christer Ejlsing.

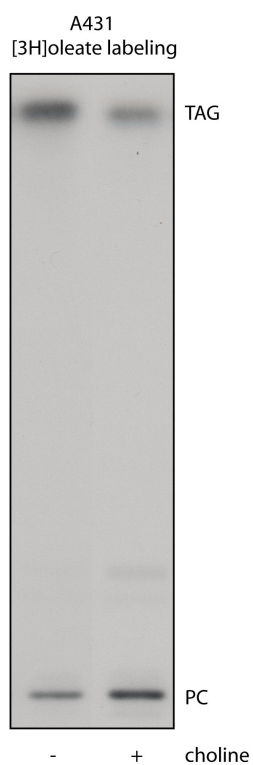


Figure A.7.: Inhibition of PC de novo synthesis channels fatty acids towards TAG synthesis

A431 cells were grown in DMEM medium with 10% FCS or in DMEM without choline with 10% FCS. [3H]oleate was added for 24 h to the cells. Lipids were extracted, separated by TLC and visualized by autoradiography. The panel shows the changes in the ratio of PC and TAG labeled by incorporation of [3H]oleate upon choline deficiency.

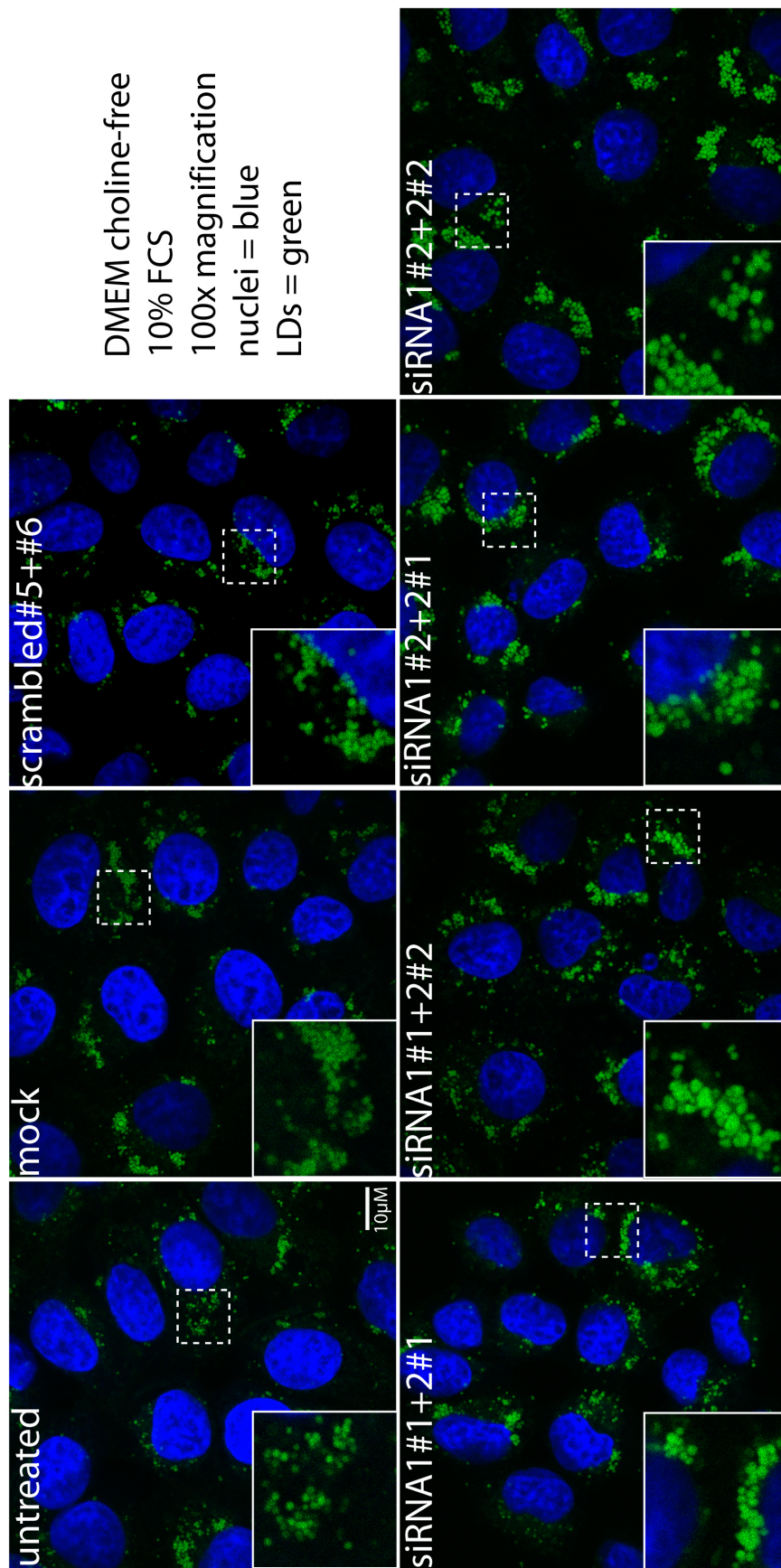


Figure A.8.: Silencing of LPCAT1 and LPCAT2 in choline-depleted A431 cells increases LD size
Confocal images as in figure 4.13 but A431 cells were grown in choline-free medium after the siRNA transfection. Inserts are the regions marked by dashed white squares in higher magnification. Note that LDs are larger as compared to cells grown with choline. Nuclei (blue), LDs (green), scalebar = 10 μ m

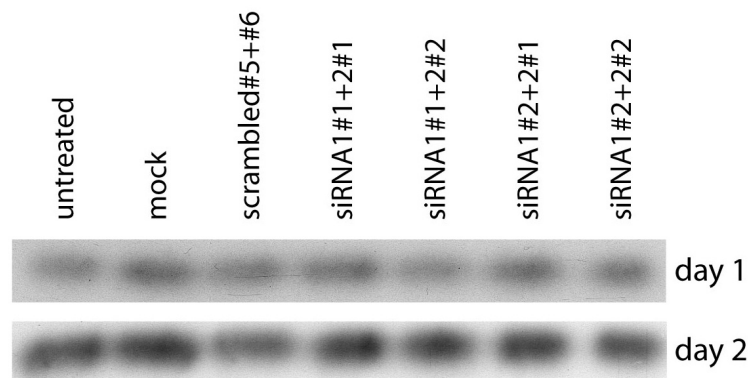


Figure A.9.: Silencing of LPCAT1 and LPCAT2 in choline-depleted A431 cells does not influence TAG synthesis
Same experiment as in supplementary figure A.5, but cells were grown in choline-free medium after the siRNA transfection

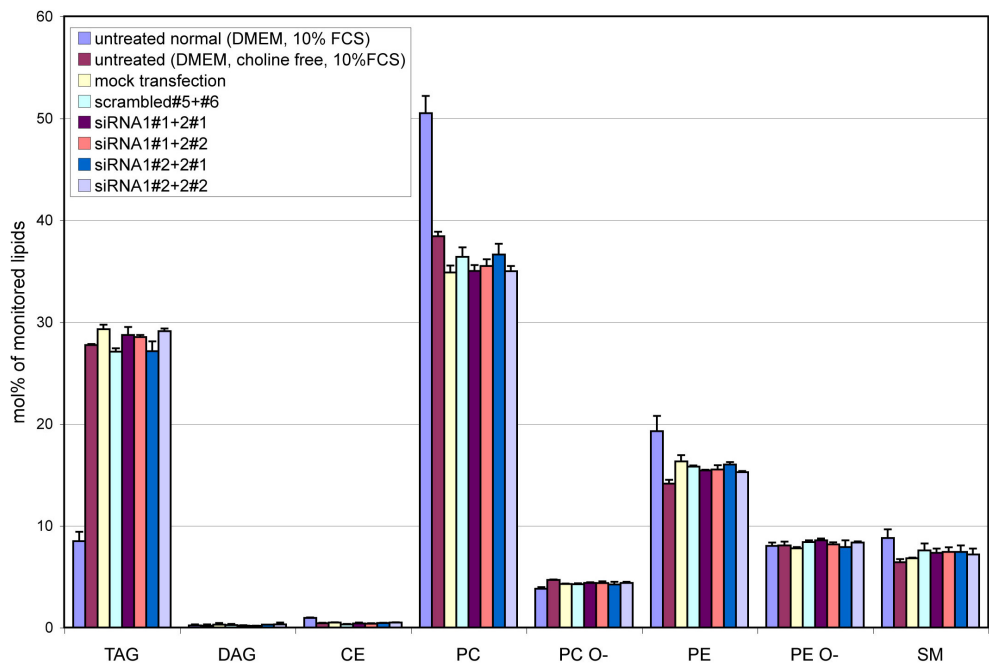


Figure A.10.: Silencing of LPCAT1 and LPCAT2 in choline-depleted A431 cells does not influence the amount of stored TAG
Same experiment as in supplementary figure A.6, but cells were grown in choline-free medium after the siRNA transfection. Additionally, this panel contains data of control cells grown in normal medium to demonstrate the influence of choline depletion. This diagram and lipid mass spectrometry is provided by Christer Ejlsing.

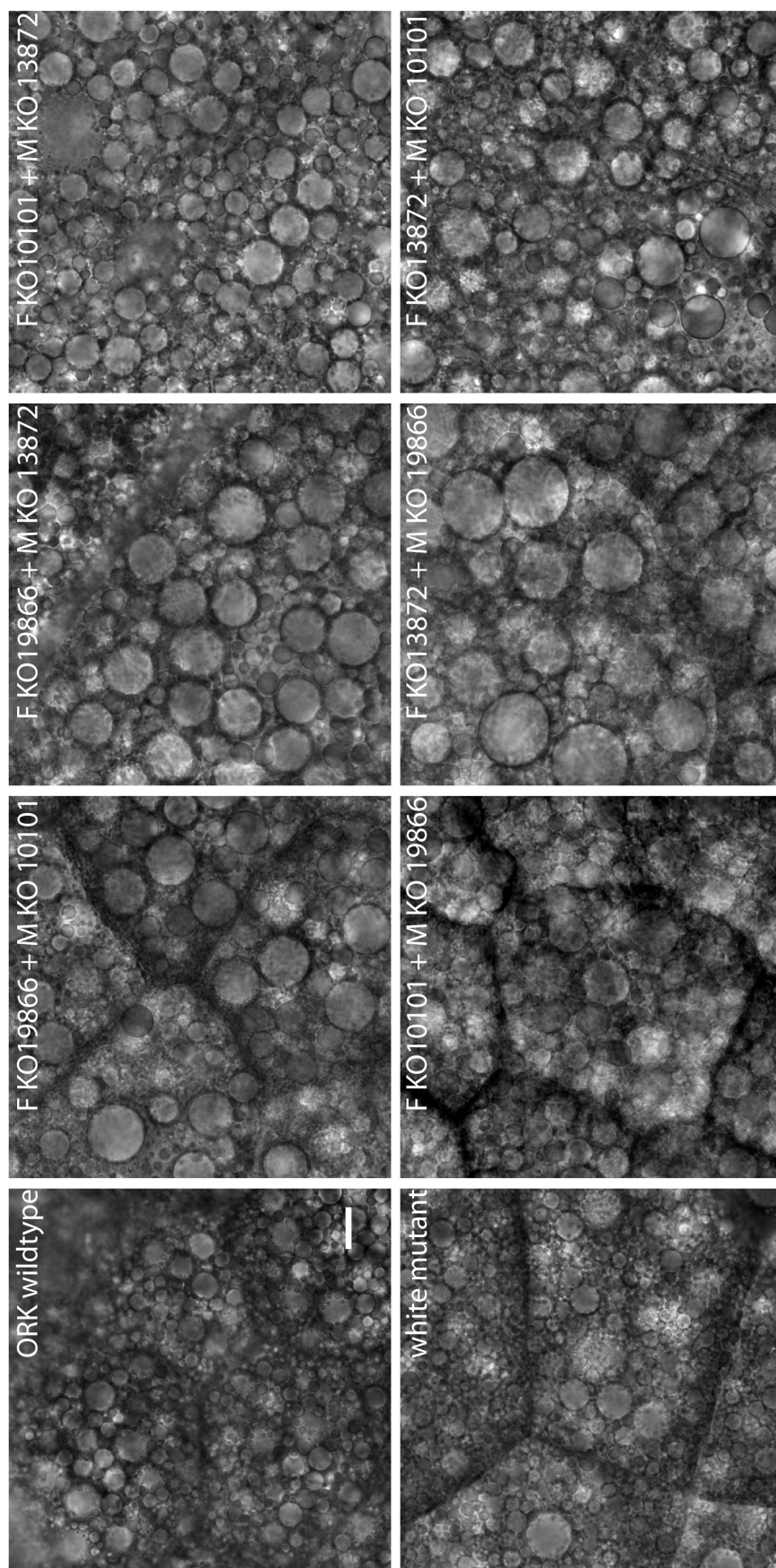


Figure A.11.: L3 larvae of crosses between the three different CG32699 *Drosophila melanogaster* knockout strains show enlarged LDs in the fat body
Female virgins (F) of each CG32699 knockout strain were crossed with males (M) of each of the other CG32699 knockout strains and vice versa. Fat bodies were isolated and imaged as described in figure 4.21. Representative bright field images of fat bodies of wildtype, white mutant and the crosses between the knockout strains 10101, 13872 and 19866 are shown. Scalebar = 10 μ m

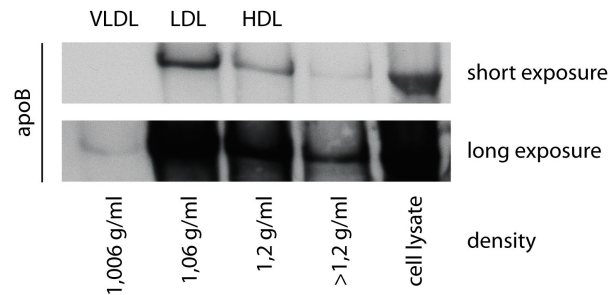


Figure A.12.: ApoB secreted by HuH7 cells is associated with lipoprotein particles
HuH7 cells were grown in serum-free supplemented RPMI medium for three days. Supernatant was collected and sequentially centrifugated with different density buffers. Density fractions and cell lysates as indicated were collected, proteins precipitated and analyzed by SDS-PAGE and western blot for apoB. Note that 8-times more cell lysate than density fractions was loaded.

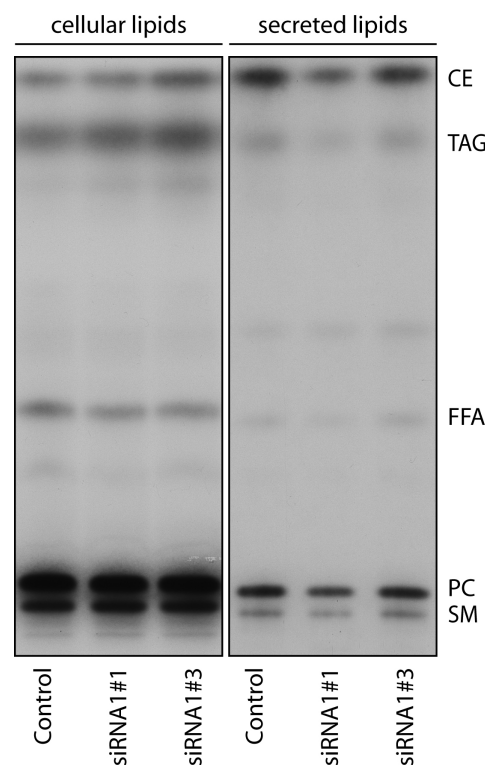


Figure A.13.: Secreted radioactively labeled lipids from HuH7 cells
HuH7 cells were grown in serum-free supplemented RPMI medium and transfected with scrambled siRNA (Control) or siRNA targeting LPCAT1 were grown for 24 h in the presence of [3H]oleate. The siRNAs and radioactivity were removed and cells were grown further for 48 h in serum-free supplemented RPMI medium. Lipids were extracted from supernatant and cells and separated by TLC.

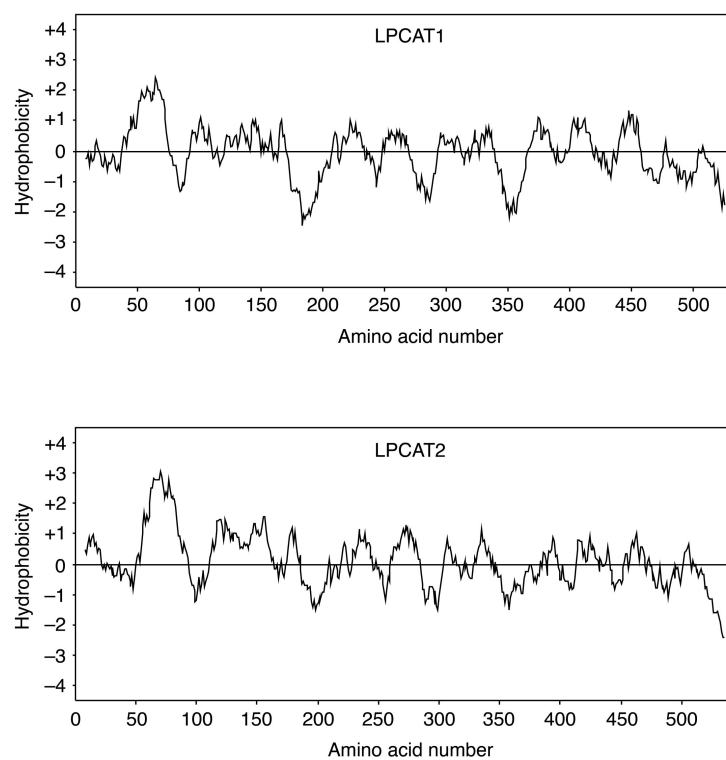


Figure A.14.: Hydrophobicity plots of human LPCAT1 and LPCAT2

Hydrophobicity profiles of human LPCAT1 and LPCAT2 were calculated using the Kyte-Doolittle algorithm with a window of 17 amino acids. Note the single long hydrophobic stretch close to the N-terminus of the proteins. This figure is provided by Christoph Thiele.

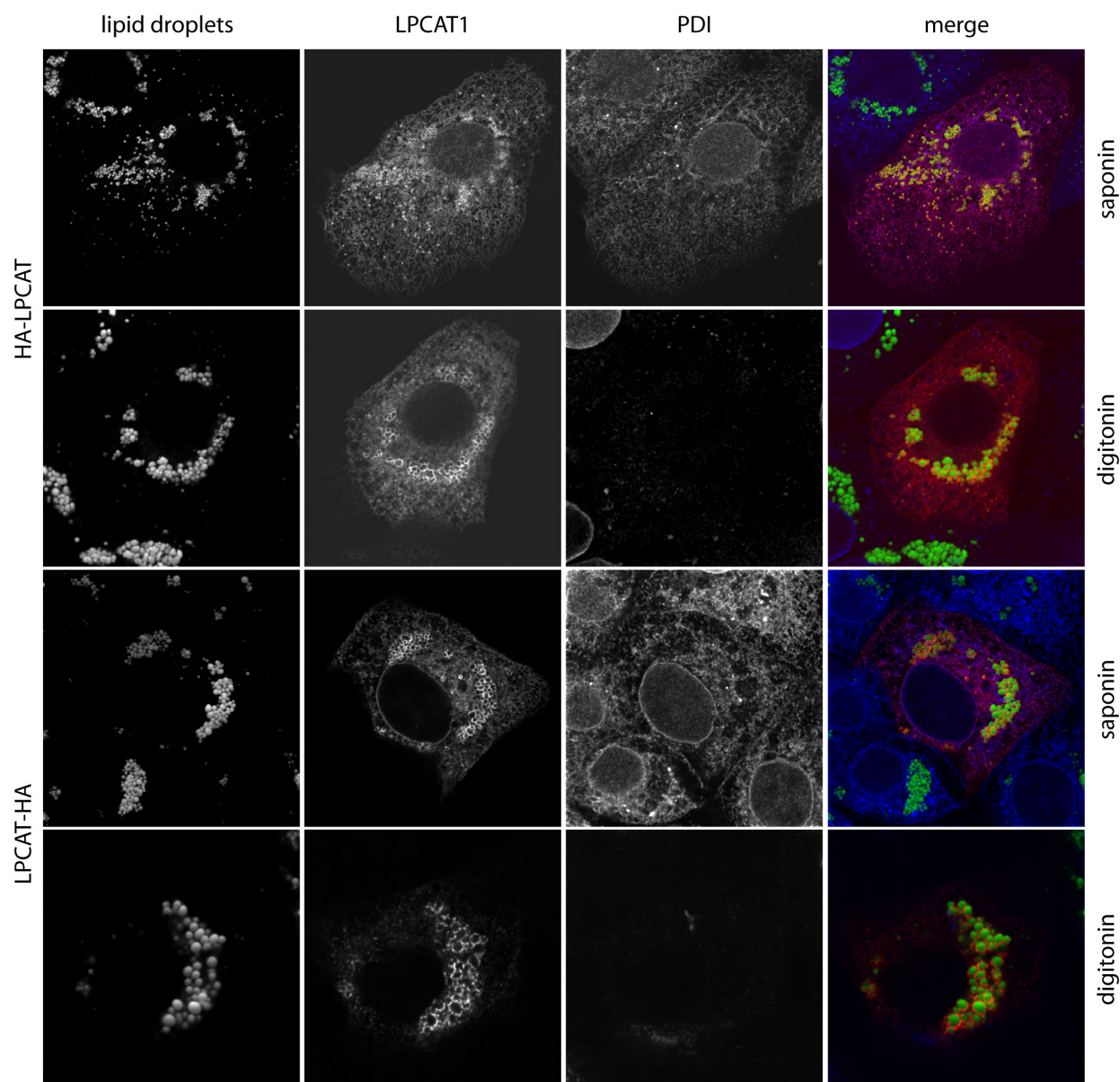


Figure A.15.: Topology of LPCAT1

A431 cells were transfected with vectors coding for LPCAT1 with either N-terminal 3HA-tag (HA-LPCAT) or C-terminal 3HA-tag (LPCAT-HA) and were cultivated for 16 hours in the presence of 100 μ M oleate. Cells were fixed and processed for immunofluorescence microscopy using either saponin (permeabilizes all membranes) or digitonin (permeabilizes plasma membrane, but not the ER membrane) for permeabilization. Cells were stained with BODIPY 493/503 to stain LDs (lipid droplets, green in the merged picture), anti-HA to detect transfected LPCAT proteins (LPCAT1, red) and anti-PDI (PDI, blue) as a luminal ER marker.

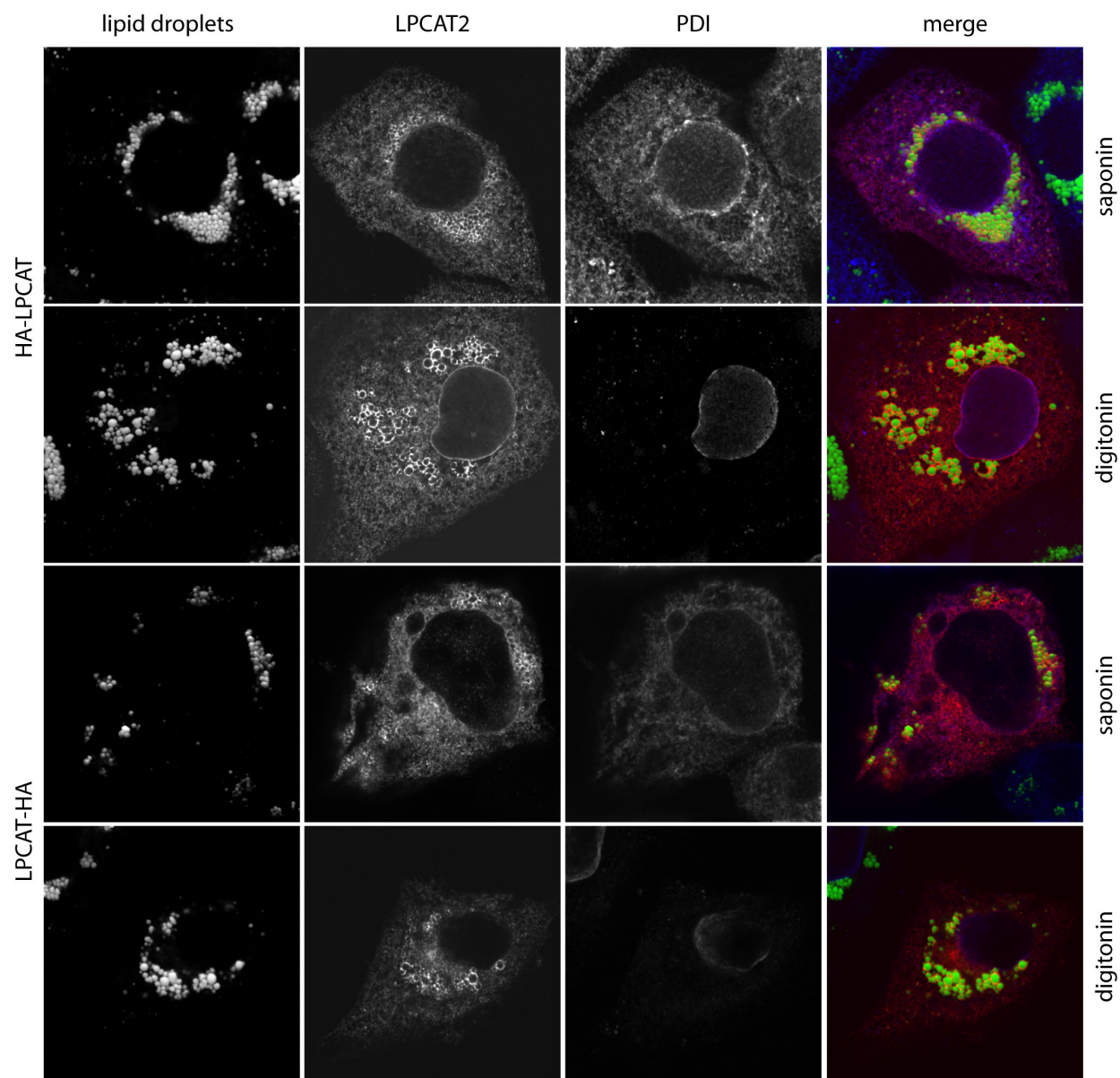


Figure A.16.: Topology of LPCAT2

As described in supplementary figure A.15, but A431 cells were transfected with vectors coding for LPCAT2. Lipid droplets are green, anti-HA to detect transfected LPCAT2 proteins is red and PDI as a luminal ER marker is blue in the merged pictures.

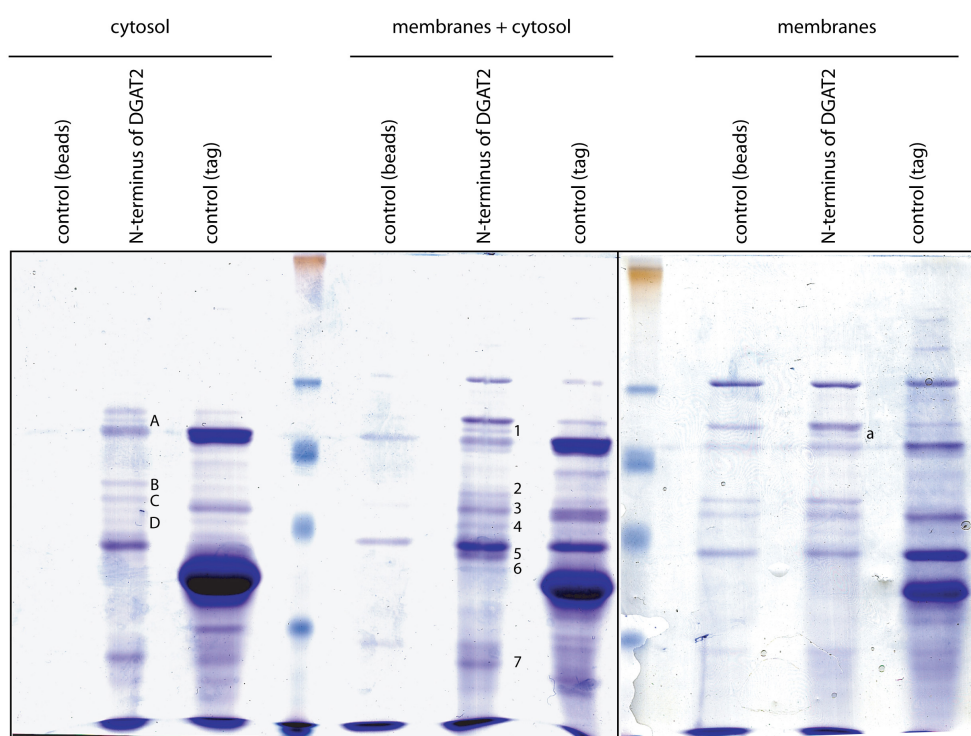


Figure A.17.: Coomassie gels for identification of DGAT2 interaction partner

The coomassie gels show the proteins accumulated in the eluates of the columns used to isolate specific interaction partner of DGAT2. In lane 1 (control (beads)) the proteins in the eluate of the column loaded with empty vector expressing bacteria lysates, in lane 2 (N-terminus of DGAT2) the eluate of the column loaded with the bacterial expressed construct described in figure 4.30a and in lane 3 (control (tag)) the eluate of the column loaded with a EGFP control construct (EGFP cloned in front of the tag described in figure 4.30) are shown. The left gel represents the proteins bound from pig liver cytosol, the middle gel represents proteins bound from pig liver membranes + cytosol and the right gel represents proteins bound from pig liver membranes. Bands labeled with letters (A-D, a) or numbers (1-7) only appeared in lane 2 and were cut out and analyzed by mass spectrometry (see table B.4).

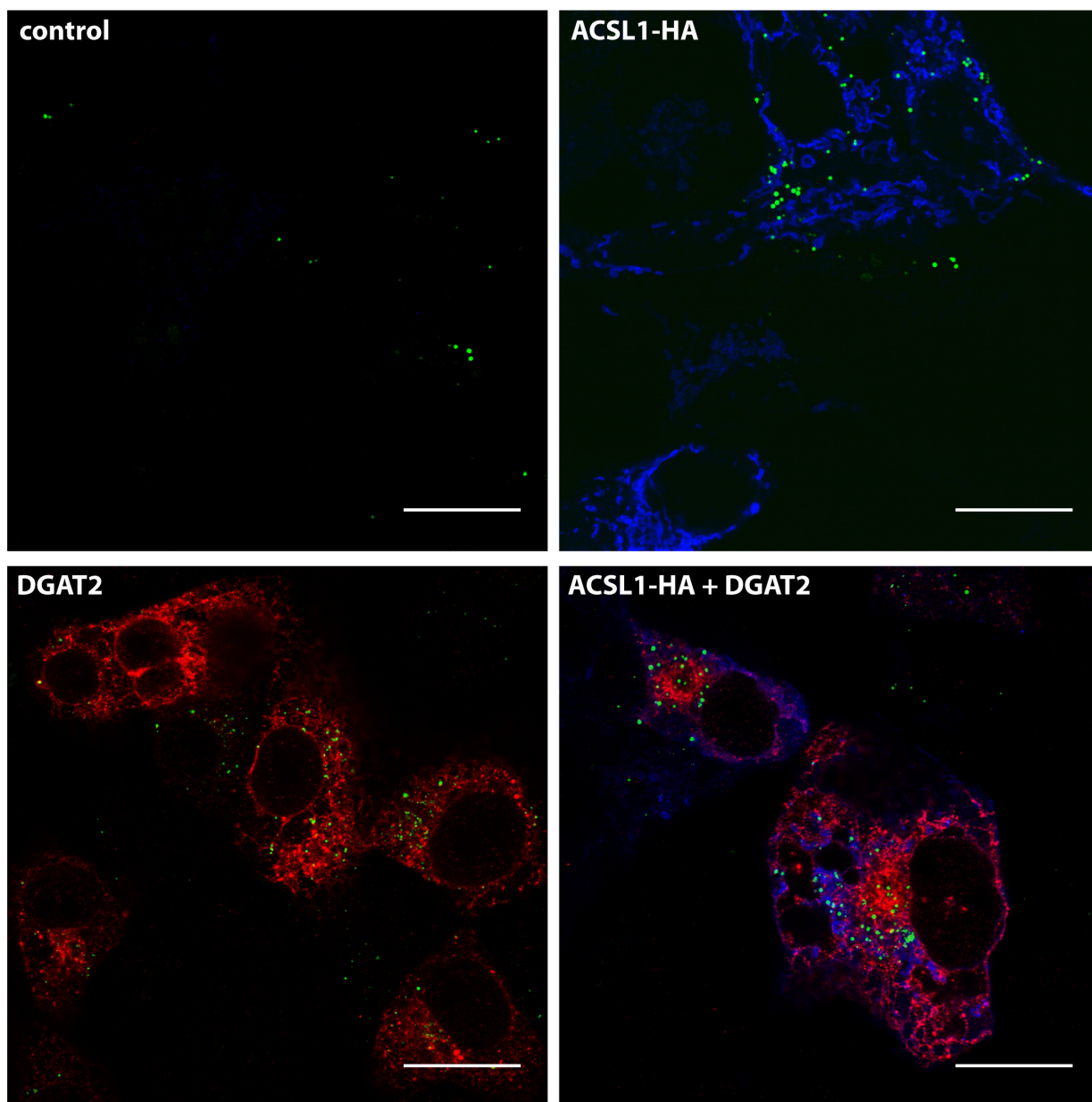


Figure A.18.: Cellular localization of DGAT2 and ACSL1 under delipidated conditions
 COS7 cells were transfected with empty vector (control), human C-terminal HA-tagged ACSL1 (ACSL1-HA), wild-type human DGAT2 (DGAT2) or wildtype human DGAT2 and human C-terminal HA-tagged ACSL1 (ACSL1-HA + DGAT2) for 24 h. Cells were grown in DMEM medium supplemented with delipidated FCS. Cells were analyzed by immunofluorescence for lipid droplets (green), ACSL1 (blue) and DGAT2 (red). Scalebar = 10 μ m.

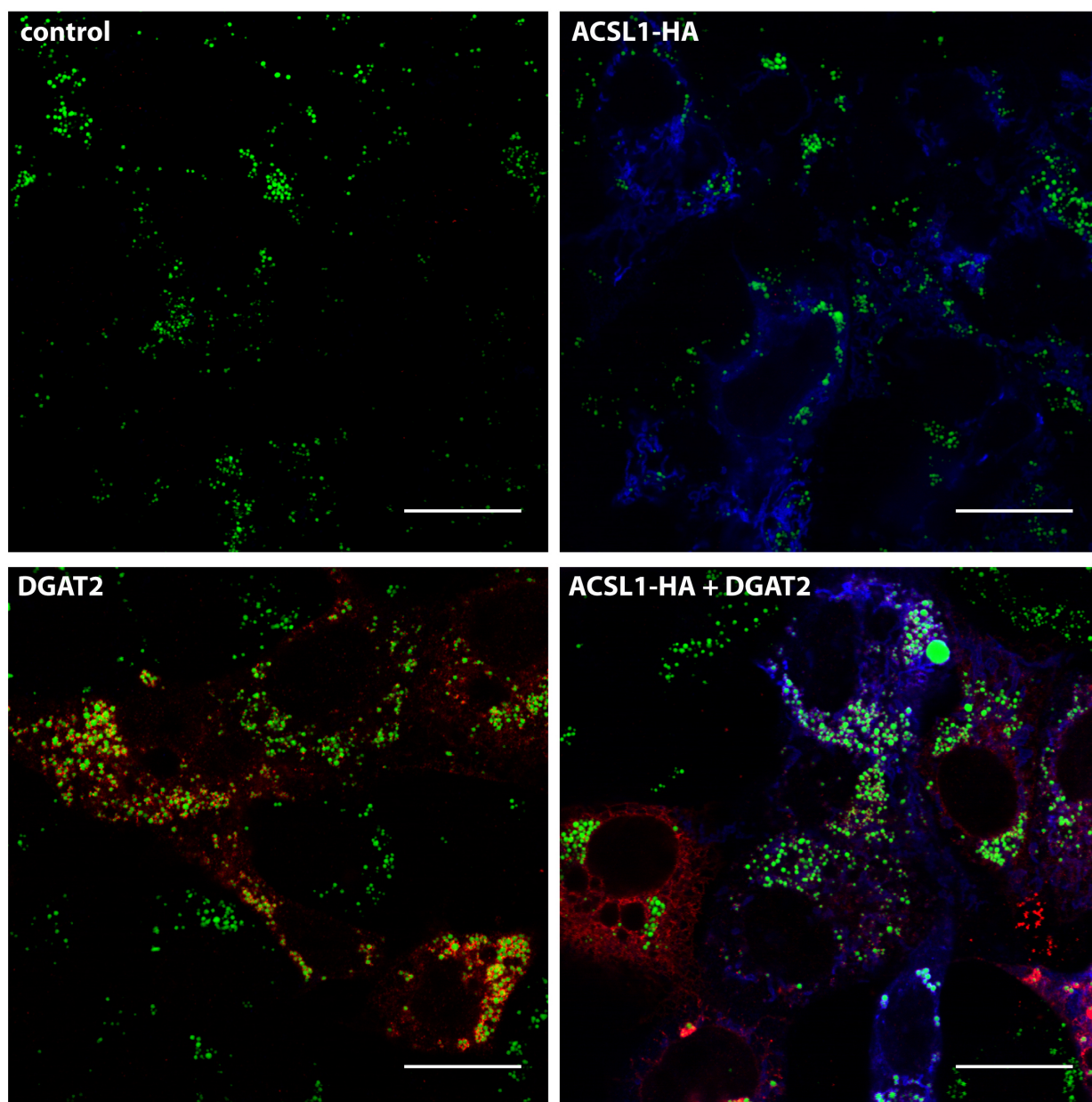


Figure A.19.: Cellular localization of DGAT2 and ACSL1 under oleate conditions

COS7 cells were transfected with empty vector (control), human C-terminal HA-tagged ACSL1 (ACSL1-HA), wild-type human DGAT2 (DGAT2) or wildtype human DGAT2 and human C-terminal HA-tagged ACSL1 (ACSL1-HA + DGAT2) for 24 h. Cells were grown in DMEM medium supplemented with FCS and 100 μ M oleate. Cells were analyzed by immunofluorescence for lipid droplets (green), ACSL1 (blue) and DGAT2 (red). Scalebar = 10 μ m.

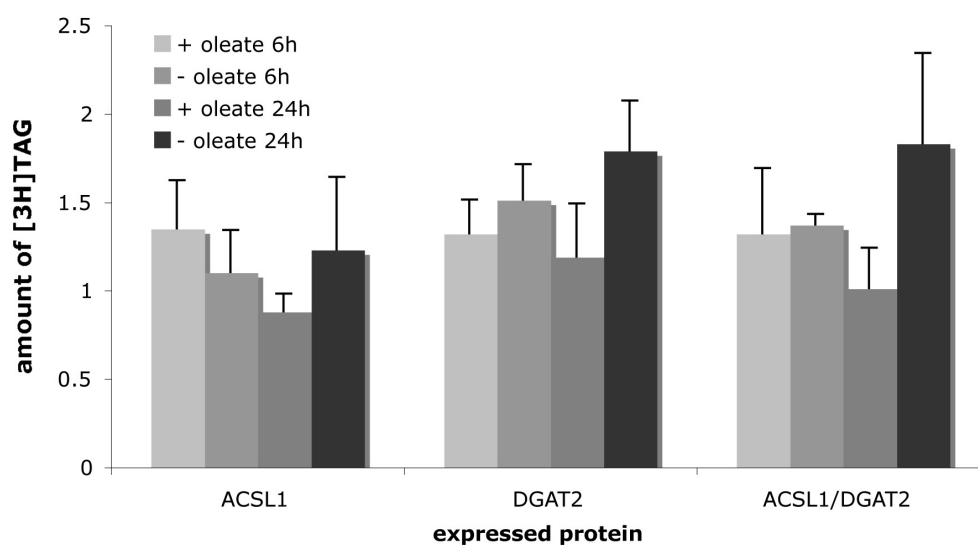


Figure A.20.: Interaction with ACSL1 does not increase DGAT2 activity in COS7 cells

COS7 cells were transfected with empty vector (control), human C-terminal HA-tagged ACSL1 (ACSL1), wildtype human DGAT2 (DGAT2) or transfected with wildtype human DGAT2 and human C-terminal HA-tagged ACSL1 (ACSL1/DGAT2) for 24 h. Cells were grown further in DMEM/FCS medium supplemented with [3H]labeled oleate for 6 h or 24 h either with (+) or without (-) additional 100 μ M non-radioactively labeled oleate. Lipids were extracted, separated by TLC and detected by autoradiography. The TAG signal obtained from control cells was normalized to 1.

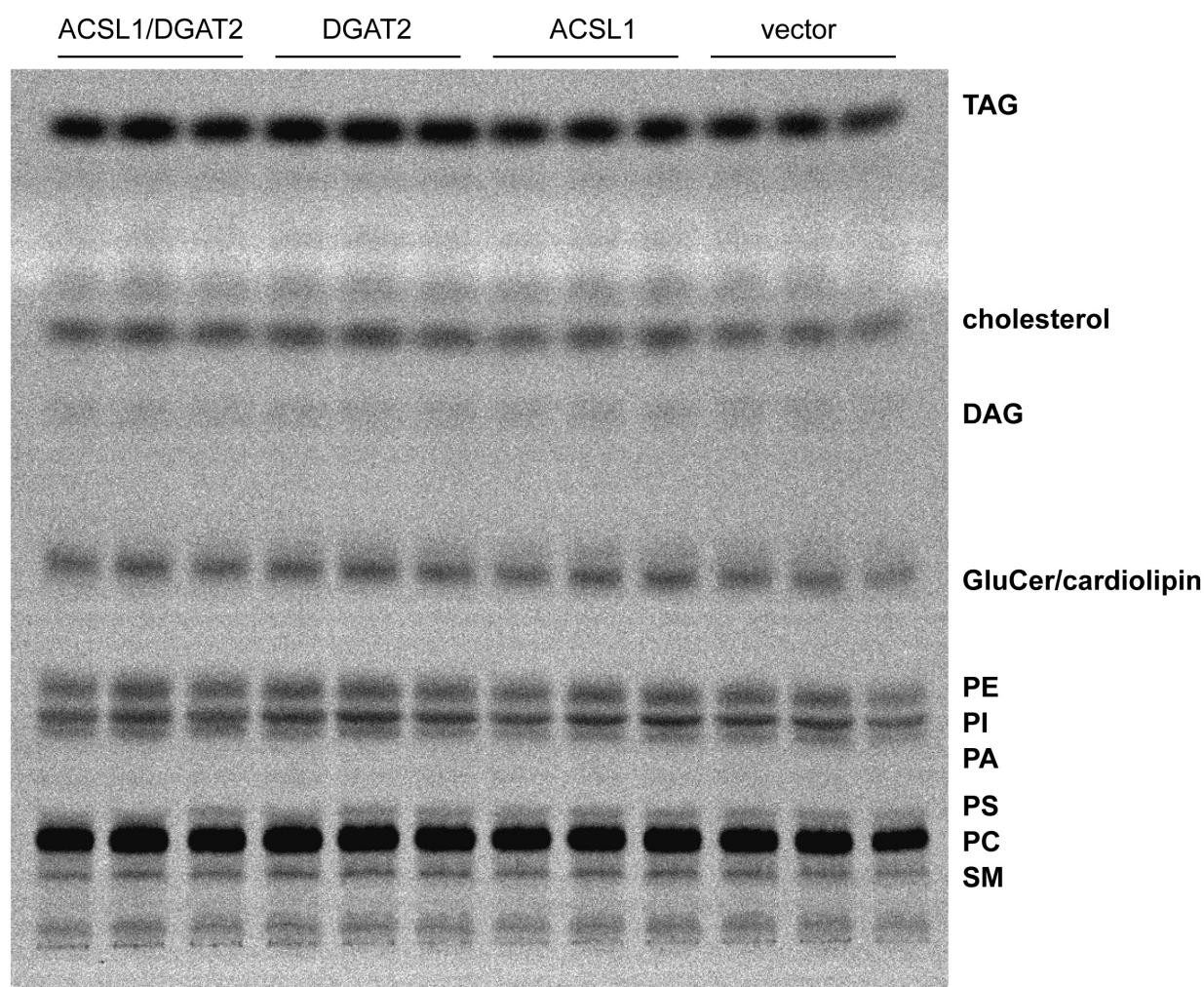


Figure A.21.: Interaction of ACSL1 and DGAT2 does not change fatty acid flux in COS7 cells
 COS7 cells were transfected with empty vector (vector), human C-terminal HA-tagged ACSL1 (ACSL1), wild-type human DGAT2 (DGAT2) or with wildtype human DGAT2 and human C-terminal HA-tagged ACSL1 (ACSL1/DGAT2) for 24 h. Cells were further grown in DMEM/FCS medium supplemented with [^{14}C]labeled acetate for 6 h. Lipids were extracted, separated by TLC and detected by autoradiography.

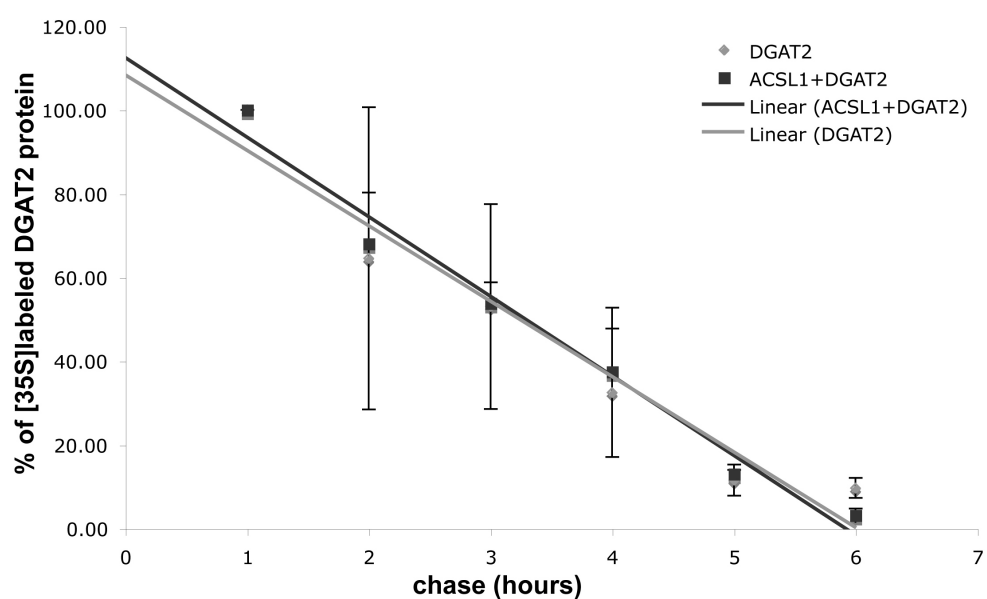


Figure A.22.: Interaction with ACSL1 does not influence stability of DGAT2 in COS7 cells

COS7 cells were transfected with wildtype human DGAT2 (DGAT2) or with wildtype human DGAT2 and human C-terminal HA-tagged ACSL1 (ACSL1 + DGAT2) for 24 h. Proteins were labeled with [35S]methionine and labeled DGAT2 protein was immunoprecipitated with the DGAT2 antibody after different chase times. Proteins in the immunoprecipitate were separated by SDS-PAGE and analyzed by autoradiography. The acquired specific DGAT2 bands were quantified with IMAGEGAUGE and compared to the maximum signal obtained after [35S] labeling.

B. Supplementary tables

Band	Identification	Name	Function	Swiss-Prot	Mass	Uniq. Pep.	Seq-Cov	A-index
18	Tail interacting protein of 47kDa	TIP47	PAT	O60664	47131	28	67%	11,71
10	Long-chain acyl-CoA synthetase 3	ACSL3	Lip. Met.	O95573	80368	34	51%	6,09
21	NAD(P)H steroid dehydrogenase-like protein	NSDHL	Lip. Met.	Q15738	41874	22	63%	5,73
33	Calcyclin	S100A6	unknown	Q5RHS4	10173	3	24%	4,00
29	Ubiquitin	UBIQ	Ubiqu-PD	P62988	8535	6	69%	3,67
20	Ancient ubiquitous protein 1	AUP1	Ubiqu-PD	Q9Y679	52995	20	37%	3,30
4	KIAA1881 protein	S3-12	PAT	Q96Q06	132978	56	50%	3,27
32	Ubiquitin-conjugating enzyme E2G 2	Ube2g2	Ubiqu-PD	P60604	18667	4	28%	3,00
10	Lanosterol synthase	ERG7	Lip. Met.	P48449	83241	35	50%	2,91
14	Adipose triglyceride lipase	ATGL	Lip. Met.	Q96AD5	58166	20	42%	2,75
30	RAB18	RAB18	Memb. Traf.	Q9NP72	22963	12	60%	2,58
23	Annexin II	ANXA2	Memb. Traf.	Q567R4	38580	28	65%	2,43
29	RAB7	RAB7	Memb. Traf.	P51149	23475	14	65%	2,36
11	UBX domain containing 2	Ubx2	Ubiqu-PD	Q92575	56743	7	17%	2,29
15	UBX domain containing 8	Ubx8	Ubiqu-PD	Q96CS3	52591	16	43%	2,25
33	Calgizzarin	S100A11	unknown	Q5VTK0	11733	4	41%	2,25
14	LPCAT2	LPCAT1	Lip. Met.	Q8NF37	59113	19	33%	2,21
16	LPCAT1	LPCAT2	Lip. Met.	Q7L5N7	60169	26	43%	2,19
19	Probable saccharopine dehydrogenase	CGI-49	unknown	Q8NBX0	47121	19	65%	2,05
19	Abhydrolase domain containing 5	CGI-58	Lip. Met.	Q8WTS1	39071	10	38%	2,00

Table B.1.: Mass spectrometric analysis of LD proteins from A431 cells

The numbers indicate protein bands of the coomassie gel shown in supplementary figure A.2, which were analyzed by mass spectrometry. The resulting list of more than 700 identified proteins was sorted according to the abundance index (A-index, [192]) with a cut-off of 2, which provided 40 abundant proteins. Out of this list, we further removed 20 typical protein contaminants, commonly encountered in biochemical purifications, such as histones, ribosomal proteins, cytoskeletal proteins, heat shock proteins and metabolic enzymes. Note that no membrane proteins were removed. The remaining 20 proteins were annotated according to putative functions: perilipin-adipophilin-TIP47 family members (PAT); enzymes or regulators of lipid metabolism (Lip. Met.); proteins related to ubiquitination and ubiquitin-dependent protein degradation (Ubiqu-PD); and membrane traffic (Memb. Traf.). The number of unique peptides matched to the corresponding sequences and achieved sequence coverage are presented in the table; LPCAT1 and LPCAT2 are in bold. This table is provided by Ana Shevchenko and Christoph Thiele.

treatment/siRNA	number of LDs	total fluorescent area in μm^2	mean LD size in μm^2	significance of mean LD size
wt	117	45199.799	0.363	0.0763473
mock	132	38921.481	0.277	0.7538167
scrambled#5+#6	150	47231.75	0.288	
siRNA1#1+2#1	132	53809.29	0.391	0.0129434
siRNA1#1+2#2	150	66317.235	0.432	0.0004995
siRNA1#2+2#1	135	49902.5	0.373	0.0293086
siRNA1#2+2#2	166	68644.258	0.383	0.0130029
StDev				
wt	48	30.532	0.169	
mock	54	23.414	0.114	
scrambled#5+#6	71	30.075	0.122	
siRNA1#1+2#1	64	34.127	0.161	
siRNA1#1+2#2	54	34.455	0.158	
siRNA1#2+2#1	43	23.543	0.147	
siRNA1#2+2#2	68	44.962	0.136	

Table B.2.: Quantification of LD size changes upon silencing of LPCAT1 and LPCAT2 by siRNA in A431 cells

Confocal images as described in figure 4.13 from three different experiments were quantified with Image J and mean numbers are displayed for the number of LDs, total fluorescent area measured, LD size per image and the corresponding significances of the differences in LD size calculated by unpaired two-sided t-test analysis relative to scrambled#5+#6.

treatment/siRNA	number of LDs	total fluorescent area in μm^2	mean LD size in μm^2	significance of mean LD size
wt	447	147.580	0.292	
mock	354	88.260	0.234	0.0569339
scrambled#5	400	117.972	0.264	0.3867085
scrambled#6	403	131.495	0.267	0.4740958
siRNA1#1	315	168.513	0.497	0.0000002
siRNA1#3	408	190.260	0.437	0.0000153
StDev				
wt	242	117.797	0.128	
mock	201	68.993	0.087	
scrambled#5	195	91.319	0.109	
scrambled#6	270	122.117	0.123	
siRNA1#1	282	174.110	0.135	
siRNA1#3	216	128.350	0.108	

Table B.3.: Quantification of LD size changes upon silencing of LPCAT1 by siRNA in HuH7 cells

Confocal images as described in figure 4.16 from three different experiments were quantified with Image J and mean numbers are displayed for the number of LDs, total fluorescent area measured, LD size per image and the corresponding significances of the differences in LD size calculated by unpaired two-sided t-test analysis relative to wt.

Spot No.	SwissProt entry	Protein	Predicted MW (kDa)	MS/MS (Score)	PMF Score	Matched Peptides	Sequence Coverage
1	ACSL1_CAVPO (Guinea pig)	Long-chain-fatty-acid-CoA ligase 1	77.65	2 (25,47)	-	4/30	5%
2		Keratin					
3	ATPB_BOVIN	ATP synthase subunit beta, mitochondrial	56.25	-	70	9/41	26%
	ATPB1_BOVIN	ATP synthase subunit alpha heart isoform, mitochondrial	59.68	-	63	10/41	21%
4	HYEP_PIG	Epoxide hydrolase 1	52.36	-	129	13/40	27%
5	ACTB_BOVIN	Actin, cytoplasmic 1	41.71	-	108	11/36	31%
6	ACTB_XENLA (Xenopus laevis)	Actin, cytoplasmic 1	41.74	2 (31,15)	-	4/12	14%
7	ADH1_MOUSE	Alcohol dehydrogenase 1	39.62	1 (49)	-		
A	HXK3_RAT	Hexokinase-3	100.19	-	56	7/17	10%
B	DLDH_ECO57	Dihydrolipoyl dehydrogenase	50.53	-	87	9/28	26%
C	AL1A1_SHEEP	Retinal dehydrogenase 1	54.66	1 (24)	-	7/25	14%
	HA19_MOUSE	H-2 class I histocompatibility antigen, Q9 alpha chain	23.01	-	67	6/23	32%
D	CAS1_BOVIN	Alpha-S1-casein precursor	24.51	-	66	6/23	25%
	PYGL_SHEEP	Glycogen phosphorylase, liver form	97.28		66	9/23	12%
a	ACSL1_CAVPO (Guinea pig)	Long-chain-fatty-acid-CoA ligase 1	77.65	1 (32)	-		

Table B.4.: Potential interaction partner of DGAT2

In the table the proteins identified by mass spectrometry in the bands cut from the coomassie gels shown in supplementary figure A.17 are listed. The numbering of the hits corresponds the numbering of the bands in supplementary figure A.17. The grey shaded protein was identified under two different conditions. The mass spectrometric analysis and the table is provided by Cornelia Czupalla.

C. Abbreviations

3T3-L1	mouse fibroblast cell line able to differentiate into adipocytes
A431	human epithelial fibroblast cell line
ACAT1	acylcholesterol acyltransferase 1
ACSL	acyl-CoA synthetase ligase
ADRP	adipophilin
ATGL	adipose triacylglyceride lipase
CE	cholesterol ester
CHO-K2	chinese hamster ovary cell line
COS7	african green monkey kidney fibroblast cell line
CPT	CDP-choline 1,2-diacylglycerol cholinephosphotransferase
DAG/DG	diacylglycerol, diacylglycerides
DGAT	diacylglycerol acyltransferase
ER	endoplasmic reticulum
FA	fatty acid
FFA	free fatty acid
FCS	fetal calf serum
GAPDH	glycerol-3-phosphate dehydrogenase
HA	hemagglutinin
HCV	hepatitis C virus
HepG2	human hepatocellular carcinoma cell line
HSL	hormone sensitive lipase
HuH7	human hepatoma cell line
LD	lipid droplet
LPA	lyso-phosphatidic acid
LPAAT	lyso-phosphatidic acid acyltransferase
LPC	lyso-phosphatidylcholine
LPCAT	lyso-phosphatidylcholine acyltransferase
LPE	lyso-phosphatidylethanolamine

MAM	mitochondria-associated membrane
NSDHL	NAD(P)H steroid dehydrogenase-like protein
PA	phosphatidic acid
PAT	protein domain named after perilipin, adipophilin and tail-interacting protein 47
PC	phosphatidylcholine
PDI	protein disulfide isomerase
PE	phosphatidylethanolamine
PLA ₂	phospholipase A ₂
PM	plasma membrane
PP	pyrophosphate
SM	sphingomyelin
TAG/TG	triacylglycerol, triacylglycerides
TIP47	tail-interacting protein 47
TLC	thin layer chromatography
PI	phosphatidylinositol
PS	phosphatidylserine

D. Bibliography

- [1] G. F. Gibbons, K. Islam, and R. J. Pease. Mobilisation of triacylglycerol stores. *Biochim Biophys Acta*, 1483(1):37–57, 2000.
- [2] S. Martin and R. G. Parton. Lipid droplets: a unified view of a dynamic organelle. *Nat Rev Mol Cell Biol*, 7(5):373–8, 2006.
- [3] A. Marcinkiewicz, D. Gauthier, A. Garcia, and D. L. Brasaemle. The phosphorylation of serine 492 of perilipin directs lipid droplet fragmentation and dispersion. *J Biol Chem*, 281(17):11901–9, 2006.
- [4] M. Nagayama, T. Uchida, and K. Gohara. Temporal and spatial variations of lipid droplets during adipocyte division and differentiation. *J Lipid Res*, 48(1):9–18, 2007.
- [5] L. Kuerschner, C. S. Ejsing, K. Ekroos, A. Shevchenko, K. I. Anderson, and C. Thiele. Polyene-lipids: a new tool to image lipids. *Nat Methods*, 2(1):39–45, 2005.
- [6] C. S. Shaw, M. Sherlock, P. M. Stewart, and A. J. Wagenmakers. Adipophilin distribution and colocalization with lipid droplets in skeletal muscle. *Histochem Cell Biol*, 131(5):575–81, 2009.
- [7] D. J. Murphy and J. Vance. Mechanisms of lipid-body formation. *Trends Biochem Sci*, 24(3):109–15, 1999.
- [8] K. Tauchi-Sato, S. Ozeki, T. Houjou, R. Taguchi, and T. Fujimoto. The surface of lipid droplets is a phospholipid monolayer with a unique fatty acid composition. *J Biol Chem*, 277(46):44507–12, 2002.
- [9] D. L. Brasaemle, G. Dolios, L. Shapiro, and R. Wang. Proteomic analysis of proteins associated with lipid droplets of basal and lipolytically stimulated 3t3-l1 adipocytes. *J Biol Chem*, 279(45):46835–42, 2004.
- [10] Y. Fujimoto, H. Itabe, J. Sakai, M. Makita, J. Noda, M. Mori, Y. Higashi, S. Kojima, and T. Takano. Identification of major proteins in the lipid droplet-enriched fraction isolated from the human hepatocyte cell line huh7. *Biochim Biophys Acta*, 1644(1):47–59, 2004.
- [11] P. Liu, Y. Ying, Y. Zhao, D. I. Mundy, M. Zhu, and R. G. Anderson. Chinese hamster ovary k2 cell lipid droplets appear to be metabolic organelles involved in membrane traffic. *J Biol Chem*, 279(5):3787–92, 2004.
- [12] E. Umlauf, E. Csaszar, M. Moertelmaier, G. J. Schuetz, R. G. Parton, and R. Prohaska. Association of stomatin with lipid bodies. *J Biol Chem*, 279(22):23699–709, 2004.
- [13] S. Ozeki, J. Cheng, K. Tauchi-Sato, N. Hatano, H. Taniguchi, and T. Fujimoto. Rab18 localizes to lipid droplets and induces their close apposition to the endoplasmic reticulum-derived membrane. *J Cell Sci*, 118(Pt 12):2601–11, 2005.
- [14] S. Sato, M. Fukasawa, Y. Yamakawa, T. Natsume, T. Suzuki, I. Shoji, H. Aizaki, T. Miyamura, and M. Nishijima. Proteomic profiling of lipid droplet proteins in hepatoma cell lines expressing hepatitis c virus core protein. *J Biochem*, 139(5):921–30, 2006.
- [15] S. Turro, M. Ingelmo-Torres, J. M. Estanyol, F. Tebar, M. A. Fernandez, C. V. Albor, K. Gaus, T. Grewal, C. Enrich, and A. Pol. Identification and characterization of associated with lipid droplet protein 1: A novel membrane-associated protein that resides on hepatic lipid droplets. *Traffic*, 7(9):1254–69, 2006.
- [16] R. Bartz, J. K. Zehmer, M. Zhu, Y. Chen, G. Serrero, Y. Zhao, and P. Liu. Dynamic activity of lipid droplets: protein phosphorylation and gtp-mediated protein translocation. *J Proteome Res*, 6(8):3256–65, 2007.
- [17] A. S. Greenberg, J. J. Egan, S. A. Wek, N. B. Garty, E. J. Blanchette-Mackie, and C. Londos. Perilipin, a major hormonally regulated adipocyte-specific phosphoprotein associated with the periphery of lipid storage droplets. *J Biol Chem*, 266(17):11341–6, 1991.
- [18] D. L. Brasaemle, T. Barber, N. E. Wolins, G. Serrero, E. J. Blanchette-Mackie, and C. Londos. Adipose differentiation-related protein is an ubiquitously expressed lipid storage droplet-associated protein. *J Lipid Res*, 38(11):2249–63, 1997.
- [19] H. W. Heid, R. Moll, I. Schwetlick, H. R. Rackwitz, and T. W. Keenan. Adipophilin is a specific marker of lipid accumulation in diverse cell types and diseases. *Cell Tissue Res*, 294(2):309–21, 1998.

- [20] E. Diaz and S. R. Pfeffer. Tip47: a cargo selection device for mannose 6-phosphate receptor trafficking. *Cell*, 93(3):433–43, 1998.
- [21] S. Miura, J. W. Gan, J. Brzostowski, M. J. Parisi, C. J. Schultz, C. Londos, B. Oliver, and A. R. Kimmel. Functional conservation for lipid storage droplet association among perilipin, adrp, and tip47 (pat)-related proteins in mammals, drosophila, and dictyostelium. *J Biol Chem*, 277(35):32253–7, 2002.
- [22] A. V. Bulankina, A. Deggerich, D. Wenzel, K. Mutenda, J. G. Wittmann, M. G. Rudolph, K. N. Burger, and S. Honing. Tip47 functions in the biogenesis of lipid droplets. *J Cell Biol*, 185(4):641–55, 2009.
- [23] N. E. Wolins, B. K. Quaynor, J. R. Skinner, A. Tzekov, M. A. Croce, M. C. Gropler, V. Varma, A. Yao-Borengasser, N. Rasouli, P. A. Kern, B. N. Finck, and P. E. Bickel. Oxpat/pat-1 is a ppar-induced lipid droplet protein that promotes fatty acid utilization. *Diabetes*, 55(12):3418–28, 2006.
- [24] N. E. Wolins, J. R. Skinner, M. J. Schoenfish, A. Tzekov, K. G. Bensch, and P. E. Bickel. Adipocyte protein s3-12 coats nascent lipid droplets. *J Biol Chem*, 278(39):37713–21, 2003.
- [25] N. E. Wolins, B. K. Quaynor, J. R. Skinner, M. J. Schoenfish, A. Tzekov, and P. E. Bickel. S3-12, adipophilin, and tip47 package lipid in adipocytes. *J Biol Chem*, 280(19):19146–55, 2005.
- [26] D. Zwytick, K. Athenstaedt, and G. Daum. Intracellular lipid particles of eukaryotic cells. *Biochim Biophys Acta*, 1469(2):101–20, 2000.
- [27] D. J. Murphy. The biogenesis and functions of lipid bodies in animals, plants and microorganisms. *Prog Lipid Res*, 40(5):325–438, 2001.
- [28] L. Kuerschner, C. Moessinger, and C. Thiele. Imaging of lipid biosynthesis: how a neutral lipid enters lipid droplets. *Traffic*, 9(3):338–52, 2008.
- [29] R. Bartz, W. H. Li, B. Venables, J. K. Zehmer, M. R. Roth, R. Welti, R. G. Anderson, P. Liu, and K. D. Chapman. Lipidomics reveals that adiposomes store ether lipids and mediate phospholipid traffic. *J Lipid Res*, 48(4):837–47, 2007.
- [30] J. E. Schaffer. Lipotoxicity: when tissues overeat. *Curr Opin Lipidol*, 14(3):281–7, 2003.
- [31] M. A. Welte. Proteins under new management: lipid droplets deliver. *Trends Cell Biol*, 17(8):363–9, 2007.
- [32] S. Cermelli, Y. Guo, S. P. Gross, and M. A. Welte. The lipid-droplet proteome reveals that droplets are a protein-storage depot. *Curr Biol*, 16(18):1783–95, 2006.
- [33] P. Pacheco, F. A. Bozza, R. N. Gomes, M. Bozza, P. F. Weller, H. C. Castro-Faria-Neto, and P. T. Bozza. Lipopolysaccharide-induced leukocyte lipid body formation in vivo: innate immunity elicited intracellular loci involved in eicosanoid metabolism. *J Immunol*, 169(11):6498–506, 2002.
- [34] H. D’Avila, R. C. Melo, G. G. Parreira, E. Werneck-Barroso, H. C. Castro-Faria-Neto, and P. T. Bozza. Mycobacterium bovis bacillus calmette-guerin induces tlr2-mediated formation of lipid bodies: intracellular domains for eicosanoid synthesis in vivo. *J Immunol*, 176(5):3087–97, 2006.
- [35] R. G. Hope and J. McLauchlan. Sequence motifs required for lipid droplet association and protein stability are unique to the hepatitis c virus core protein. *J Gen Virol*, 81(Pt 8):1913–25, 2000.
- [36] Y. Miyanari, K. Atsuzawa, N. Usuda, K. Watashi, T. Hishiki, M. Zayas, R. Bartenschlager, T. Wakita, M. Hijikata, and K. Shimotohno. The lipid droplet is an important organelle for hepatitis c virus production. *Nat Cell Biol*, 9(9):1089–97, 2007.
- [37] A. Shavinskaya, S. Boulant, F. Penin, J. McLauchlan, and R. Bartenschlager. The lipid droplet binding domain of hepatitis c virus core protein is a major determinant for efficient virus assembly. *J Biol Chem*, 282(51):37158–69, 2007.
- [38] Y. Kumar, J. Cocchiario, and R. H. Valdivia. The obligate intracellular pathogen chlamydia trachomatis targets host lipid droplets. *Curr Biol*, 16(16):1646–51, 2006.
- [39] H. Robenek, O. Hofnagel, I. Buers, M. J. Robenek, D. Troyer, and N. J. Severs. Adipophilin-enriched domains in the er membrane are sites of lipid droplet biogenesis. *J Cell Sci*, 119(Pt 20):4215–24, 2006.
- [40] T. C. Walther and Jr. Farese, R. V. The life of lipid droplets. *Biochim Biophys Acta*, 1791(6):459–66, 2009.
- [41] S. Collins and R. S. Surwit. The beta-adrenergic receptors and the control of adipose tissue metabolism and thermogenesis. *Recent Prog Horm Res*, 56:309–28, 2001.
- [42] G. Fredrikson, P. Stralfors, N. O. Nilsson, and P. Belfrage. Hormone-sensitive lipase of rat adipose tissue. purification and some properties. *J Biol Chem*, 256(12):6311–20, 1981.

-
- [43] N. O. Nilsson, P. Stralfors, G. Fredrikson, and P. Belfrage. Regulation of adipose tissue lipolysis: effects of noradrenaline and insulin on phosphorylation of hormone-sensitive lipase and on lipolysis in intact rat adipocytes. *FEBS Lett*, 111(1):125–30, 1980.
- [44] J. G. Granneman, H. P. Moore, R. L. Granneman, A. S. Greenberg, M. S. Obin, and Z. Zhu. Analysis of lipolytic protein trafficking and interactions in adipocytes. *J Biol Chem*, 282(8):5726–35, 2007.
- [45] A. Lass, R. Zimmermann, G. Haemmerle, M. Riederer, G. Schoiswohl, M. Schweiger, P. Kienesberger, J. G. Strauss, G. Gorkiewicz, and R. Zechner. Adipose triglyceride lipase-mediated lipolysis of cellular fat stores is activated by cgi-58 and defective in chanarin-dorfman syndrome. *Cell Metab*, 3(5):309–19, 2006.
- [46] R. Zimmermann, J. G. Strauss, G. Haemmerle, G. Schoiswohl, R. Birner-Gruenberger, M. Riederer, A. Lass, G. Neuberger, F. Eisenhaber, A. Hermetter, and R. Zechner. Fat mobilization in adipose tissue is promoted by adipose triglyceride lipase. *Science*, 306(5700):1383–6, 2004.
- [47] G. M. Clifford, C. Londos, F. B. Kraemer, R. G. Vernon, and S. J. Yeaman. Translocation of hormone-sensitive lipase and perilipin upon lipolytic stimulation of rat adipocytes. *J Biol Chem*, 275(7):5011–5, 2000.
- [48] C. L. Su, C. Sztalryd, J. A. Contreras, C. Holm, A. R. Kimmel, and C. Londos. Mutational analysis of the hormone-sensitive lipase translocation reaction in adipocytes. *J Biol Chem*, 278(44):43615–9, 2003.
- [49] G. Fredrikson, H. Tornqvist, and P. Belfrage. Hormone-sensitive lipase and monoacylglycerol lipase are both required for complete degradation of adipocyte triacylglycerol. *Biochim Biophys Acta*, 876(2):288–93, 1986.
- [50] R. Zimmermann, A. Lass, G. Haemmerle, and R. Zechner. Fate of fat: the role of adipose triglyceride lipase in lipolysis. *Biochim Biophys Acta*, 1791(6):494–500, 2009.
- [51] D. L. Brasaemle, B. Rubin, I. A. Harten, J. Gruia-Gray, A. R. Kimmel, and C. Londos. Perilipin a increases triacylglycerol storage by decreasing the rate of triacylglycerol hydrolysis. *J Biol Chem*, 275(49):38486–93, 2000.
- [52] M. Imamura, T. Inoguchi, S. Ikuyama, S. Taniguchi, K. Kobayashi, N. Nakashima, and H. Nawata. Adrp stimulates lipid accumulation and lipid droplet formation in murine fibroblasts. *Am J Physiol Endocrinol Metab*, 283(4):E775–83, 2002.
- [53] K. T. Dalen, T. Dahl, E. Holter, B. Arntsen, C. Londos, C. Sztalryd, and H. I. Nebb. Lsd5 is a pat protein specifically expressed in fatty acid oxidizing tissues. *Biochim Biophys Acta*, 1771(2):210–27, 2007.
- [54] H. Miyoshi, 2nd Perfield, J. W., S. C. Souza, W. J. Shen, H. H. Zhang, Z. S. Stancheva, F. B. Kraemer, M. S. Obin, and A. S. Greenberg. Control of adipose triglyceride lipase action by serine 517 of perilipin a globally regulates protein kinase a-stimulated lipolysis in adipocytes. *J Biol Chem*, 282(2):996–1002, 2007.
- [55] S. Y. Toh, J. Gong, G. Du, J. Z. Li, S. Yang, J. Ye, H. Yao, Y. Zhang, B. Xue, Q. Li, H. Yang, Z. Wen, and P. Li. Up-regulation of mitochondrial activity and acquirement of brown adipose tissue-like property in the white adipose tissue of fsp27 deficient mice. *PLoS One*, 3(8):e2890, 2008.
- [56] N. Nishino, Y. Tamori, S. Tateya, T. Kawaguchi, T. Shibakusa, W. Mizunoya, K. Inoue, R. Kitazawa, S. Kitazawa, Y. Matsuki, R. Hiramatsu, S. Masubuchi, A. Omachi, K. Kimura, M. Saito, T. Amo, S. Ohta, T. Yamaguchi, T. Osumi, J. Cheng, T. Fujimoto, H. Nakao, K. Nakao, A. Aiba, H. Okamura, T. Fushiki, and M. Kasuga. Fsp27 contributes to efficient energy storage in murine white adipocytes by promoting the formation of unilocular lipid droplets. *J Clin Invest*, 118(8):2808–21, 2008.
- [57] Vance DE and Vance JE. *Biochemistry of Lipids, Lipoproteins and Membranes*. Elsevier, 5th edition, 2008.
- [58] J. A. Hamilton. Fast flip-flop of cholesterol and fatty acids in membranes: implications for membrane transport proteins. *Curr Opin Lipidol*, 14(3):263–71, 2003.
- [59] J. C. Holthuis and T. P. Levine. Lipid traffic: floppy drives and a superhighway. *Nat Rev Mol Cell Biol*, 6(3):209–20, 2005.
- [60] J. F. Glatz, J. J. Luiken, and A. Bonen. Involvement of membrane-associated proteins in the acute regulation of cellular fatty acid uptake. *J Mol Neurosci*, 16(2-3):123–32; discussion 151–7, 2001.
- [61] C. T. Coburn, Jr. Knapp, F. F., M. Febbraio, A. L. Beets, R. L. Silverstein, and N. A. Abumrad. Defective uptake and utilization of long chain fatty acids in muscle and adipose tissues of cd36 knockout mice. *J Biol Chem*, 275(42):32523–9, 2000.
- [62] A. Ibrahimi, A. Bonen, W. D. Blinn, T. Hajri, X. Li, K. Zhong, R. Cameron, and N. A. Abumrad. Muscle-specific overexpression of fat/cd36 enhances fatty acid oxidation by contracting muscle, reduces plasma triglycerides and fatty acids, and increases plasma glucose and insulin. *J Biol Chem*, 274(38):26761–6, 1999.
-

- [63] D. G. Mashek and R. A. Coleman. Cellular fatty acid uptake: the contribution of metabolism. *Curr Opin Lipidol*, 17(3):274–8, 2006.
- [64] M. Digel, R. Ehehalt, W. Stremmel, and J. Fullekrug. Acyl-coa synthetases: fatty acid uptake and metabolic channeling. *Mol Cell Biochem*, 326(1-2):23–8, 2009.
- [65] A. E. Thumser, J. E. Voysey, and D. C. Wilton. The binding of lysophospholipids to rat liver fatty acid-binding protein and albumin. *Biochem J*, 301 (Pt 3):801–6, 1994.
- [66] D. R. Prows, E. J. Murphy, and F. Schroeder. Intestinal and liver fatty acid binding proteins differentially affect fatty acid uptake and esterification in l-cells. *Lipids*, 30(10):907–10, 1995.
- [67] E. P. Newberry, Y. Xie, S. Kennedy, X. Han, K. K. Buhman, J. Luo, R. W. Gross, and N. O. Davidson. Decreased hepatic triglyceride accumulation and altered fatty acid uptake in mice with deletion of the liver fatty acid-binding protein gene. *J Biol Chem*, 278(51):51664–72, 2003.
- [68] R. Ehehalt, J. Fullekrug, J. Pohl, A. Ring, T. Herrmann, and W. Stremmel. Translocation of long chain fatty acids across the plasma membrane–lipid rafts and fatty acid transport proteins. *Mol Cell Biochem*, 284(1-2): 135–40, 2006.
- [69] Y. Yang, P. H. Pritchard, J. Bhuiyan, D. W. Secombe, and M. H. Moghadasian. Overexpression of acyl-coa binding protein and its effects on the flux of free fatty acids in mca-rh 7777 cells. *Lipids*, 36(6):595–600, 2001.
- [70] P. A. Watkins. Very-long-chain acyl-coa synthetases. *J Biol Chem*, 283(4):1773–7, 2008.
- [71] T. M. Lewin, J. H. Kim, D. A. Granger, J. E. Vance, and R. A. Coleman. Acyl-coa synthetase isoforms 1, 4, and 5 are present in different subcellular membranes in rat liver and can be inhibited independently. *J Biol Chem*, 276(27):24674–9, 2001.
- [72] D. G. Mashek, L. O. Li, and R. A. Coleman. Rat long-chain acyl-coa synthetase mrna, protein, and activity vary in tissue distribution and in response to diet. *J Lipid Res*, 47(9):2004–10, 2006.
- [73] E. Soupene and F. A. Kuypers. Mammalian long-chain acyl-coa synthetases. *Exp Biol Med (Maywood)*, 233 (5):507–21, 2008.
- [74] C. G. Van Horn, J. M. Caviglia, L. O. Li, S. Wang, D. A. Granger, and R. A. Coleman. Characterization of recombinant long-chain rat acyl-coa synthetase isoforms 3 and 6: identification of a novel variant of isoform 6. *Biochemistry*, 44(5):1635–42, 2005.
- [75] Y. Fujimoto, J. Onoduka, K. J. Homma, S. Yamaguchi, M. Mori, Y. Higashi, M. Makita, T. Kinoshita, J. Noda, H. Itabe, and T. Takano. Long-chain fatty acids induce lipid droplet formation in a cultured human hepatocyte in a manner dependent of acyl-coa synthetase. *Biol Pharm Bull*, 29(11):2174–80, 2006.
- [76] Y. Fujimoto, H. Itabe, T. Kinoshita, K. J. Homma, J. Onoduka, M. Mori, S. Yamaguchi, M. Makita, Y. Higashi, A. Yamashita, and T. Takano. Involvement of acsl in local synthesis of neutral lipids in cytoplasmic lipid droplets in human hepatocyte huh7. *J Lipid Res*, 48(6):1280–92, 2007.
- [77] H. Yao and J. Ye. Long chain acyl-coa synthetase 3-mediated phosphatidylcholine synthesis is required for assembly of very low density lipoproteins in human hepatoma huh7 cells. *J Biol Chem*, 283(2):849–54, 2008.
- [78] S. Y. Bu, M. T. Mashek, and D. G. Mashek. Suppression of long chain acyl-coa synthetase 3 (acsl3) decreases hepatic de novo fatty acid synthesis through decreased transcriptional activity. *J Biol Chem*, 2009.
- [79] Y. C. Liang, C. H. Wu, J. S. Chu, C. K. Wang, L. F. Hung, Y. J. Wang, Y. S. Ho, J. G. Chang, and S. Y. Lin. Involvement of fatty acid-coa ligase 4 in hepatocellular carcinoma growth: roles of cyclic amp and p38 mitogen-activated protein kinase. *World J Gastroenterol*, 11(17):2557–63, 2005.
- [80] Y. K. Sung, S. Y. Hwang, M. K. Park, H. I. Bae, W. H. Kim, J. C. Kim, and M. Kim. Fatty acid-coa ligase 4 is overexpressed in human hepatocellular carcinoma. *Cancer Sci*, 94(5):421–4, 2003.
- [81] L. O. Li, D. G. Mashek, J. An, S. D. Doughman, C. B. Newgard, and R. A. Coleman. Overexpression of rat long chain acyl-coa synthetase 1 alters fatty acid metabolism in rat primary hepatocytes. *J Biol Chem*, 281 (48):37246–55, 2006.
- [82] C. E. Gargiulo, S. M. Stuhlsatz-Krouper, and J. E. Schaffer. Localization of adipocyte long-chain fatty acyl-coa synthetase at the plasma membrane. *J Lipid Res*, 40(5):881–92, 1999.
- [83] M. R. Richards, J. D. Harp, D. S. Ory, and J. E. Schaffer. Fatty acid transport protein 1 and long-chain acyl coenzyme a synthetase 1 interact in adipocytes. *J Lipid Res*, 47(3):665–72, 2006.

-
- [84] R. A. Coleman, T. M. Lewin, C. G. Van Horn, and M. R. Gonzalez-Baro. Do long-chain acyl-coa synthetases regulate fatty acid entry into synthetic versus degradative pathways? *J Nutr*, 132(8):2123–6, 2002.
- [85] L. O. Li, J. M. Ellis, H. A. Paich, S. Wang, N. Gong, G. N. Altshuller, R. J. Thresher, T. R. Koves, S. M. Watkins, D. M. Muoio, G. W. Cline, G. I. Shulman, and R. A. Coleman. Liver-specific loss of long-chain acyl-coa synthetase-1 decreases triacylglycerol synthesis and beta-oxidation, and alters phospholipid fatty acid composition. *J Biol Chem*, 2009.
- [86] H. A. Parkes, E. Preston, D. Wilks, M. Ballesteros, L. Carpenter, L. Wood, E. W. Kraegen, S. M. Furler, and G. J. Cooney. Overexpression of acyl-coa synthetase-1 increases lipid deposition in hepatic (hepg2) cells and rodent liver in vivo. *Am J Physiol Endocrinol Metab*, 291(4):E737–44, 2006.
- [87] F. Tong, P. N. Black, R. A. Coleman, and C. C. DiRusso. Fatty acid transport by vectorial acylation in mammals: roles played by different isoforms of rat long-chain acyl-coa synthetases. *Arch Biochem Biophys*, 447(1):46–52, 2006.
- [88] S. Lobo, B. M. Wiczer, and D. A. Bernlohr. Functional analysis of long-chain acyl-coa synthetase 1 in 3t3-l1 adipocytes. *J Biol Chem*, 284(27):18347–56, 2009.
- [89] R. A. Coleman and D. P. Lee. Enzymes of triacylglycerol synthesis and their regulation. *Prog Lipid Res*, 43(2):134–76, 2004.
- [90] S. Cases, S. J. Stone, P. Zhou, E. Yen, B. Tow, K. D. Lardizabal, T. Voelker, and Jr. Farese, R. V. Cloning of dgat2, a second mammalian diacylglycerol acyltransferase, and related family members. *J Biol Chem*, 276(42):38870–6, 2001.
- [91] S. Cases, S. J. Smith, Y. W. Zheng, H. M. Myers, S. R. Lear, E. Sande, S. Novak, C. Collins, C. B. Welch, A. J. Lusis, S. K. Erickson, and Jr. Farese, R. V. Identification of a gene encoding an acyl coa:diacylglycerol acyltransferase, a key enzyme in triacylglycerol synthesis. *Proc Natl Acad Sci U S A*, 95(22):13018–23, 1998.
- [92] S. J. Stone, M. C. Levin, and Jr. Farese, R. V. Membrane topology and identification of key functional amino acid residues of murine acyl-coa:diacylglycerol acyltransferase-2. *J Biol Chem*, 281(52):40273–82, 2006.
- [93] S. J. Smith, S. Cases, D. R. Jensen, H. C. Chen, E. Sande, B. Tow, D. A. Sanan, J. Raber, R. H. Eckel, and Jr. Farese, R. V. Obesity resistance and multiple mechanisms of triglyceride synthesis in mice lacking dgat. *Nat Genet*, 25(1):87–90, 2000.
- [94] H. C. Chen, S. J. Smith, Z. Ladha, D. R. Jensen, L. D. Ferreira, L. K. Pulawa, J. G. McGuire, R. E. Pitas, R. H. Eckel, and Jr. Farese, R. V. Increased insulin and leptin sensitivity in mice lacking acyl coa:diacylglycerol acyltransferase 1. *J Clin Invest*, 109(8):1049–55, 2002.
- [95] S. J. Stone, H. M. Myers, S. M. Watkins, B. E. Brown, K. R. Feingold, P. M. Elias, and Jr. Farese, R. V. Lipopenia and skin barrier abnormalities in dgat2-deficient mice. *J Biol Chem*, 279(12):11767–76, 2004.
- [96] C. L. Yen, M. Monetti, B. J. Burri, and Jr. Farese, R. V. The triacylglycerol synthesis enzyme dgat1 also catalyzes the synthesis of diacylglycerols, waxes, and retinyl esters. *J Lipid Res*, 46(7):1502–11, 2005.
- [97] D. Cheng, J. Iqbal, J. Devenny, C. H. Chu, L. Chen, J. Dong, R. Seethala, W. J. Keim, A. V. Azzara, R. M. Lawrence, M. A. Pelleymounter, and M. M. Hussain. Acylation of acylglycerols by acyl coenzyme a:diacylglycerol acyltransferase 1 (dgat1). functional importance of dgat1 in the intestinal fat absorption. *J Biol Chem*, 283(44):29802–11, 2008.
- [98] V. A. Payne, W. S. Au, S. L. Gray, E. D. Nora, S. M. Rahman, R. Sanders, D. Hadaschik, J. E. Friedman, S. O’Rahilly, and J. J. Rochford. Sequential regulation of diacylglycerol acyltransferase 2 expression by caat/enhancer-binding protein beta (c/ebp β) and c/ebp α during adipogenesis. *J Biol Chem*, 282(29):21005–14, 2007.
- [99] R. Suzuki, K. Tobe, M. Aoyama, K. Sakamoto, M. Ohsugi, N. Kamei, S. Nemoto, A. Inoue, Y. Ito, S. Uchida, K. Hara, T. Yamauchi, N. Kubota, Y. Terauchi, and T. Kadowaki. Expression of dgat2 in white adipose tissue is regulated by central leptin action. *J Biol Chem*, 280(5):3331–7, 2005.
- [100] C. S. Choi, D. B. Savage, A. Kulkarni, X. X. Yu, Z. X. Liu, K. Morino, S. Kim, A. Distefano, V. T. Samuel, S. Neschen, D. Zhang, A. Wang, X. M. Zhang, M. Kahn, G. W. Cline, S. K. Pandey, J. G. Geisler, S. Bhanot, B. P. Monia, and G. I. Shulman. Suppression of diacylglycerol acyltransferase-2 (dgat2), but not dgat1, with antisense oligonucleotides reverses diet-induced hepatic steatosis and insulin resistance. *J Biol Chem*, 282(31):22678–88, 2007.
- [101] S. J. Stone, M. C. Levin, P. Zhou, J. Han, T. C. Walther, and Jr. Farese, R. V. The endoplasmic reticulum enzyme dgat2 is found in mitochondria-associated membranes and has a mitochondrial targeting signal that promotes its association with mitochondria. *J Biol Chem*, 284(8):5352–61, 2009.
-

- [102] W. C. Man, M. Miyazaki, K. Chu, and J. Ntambi. Colocalization of *scd1* and *dgat2*: implying preference for endogenous monounsaturated fatty acids in triglyceride synthesis. *J Lipid Res*, 47(9):1928–39, 2006.
- [103] J. M. Ntambi, M. Miyazaki, J. P. Stoeckl, H. Lan, C. M. Kendziora, B. S. Yandell, Y. Song, P. Cohen, J. M. Friedman, and A. D. Attie. Loss of stearoyl-coa desaturase-1 function protects mice against adiposity. *Proc Natl Acad Sci U S A*, 99(17):11482–6, 2002.
- [104] E. P. Kennedy and S. B. Weiss. The function of cytidine coenzymes in the biosynthesis of phospholipides. *J Biol Chem*, 222(1):193–214, 1956.
- [105] W. E. Lands. Metabolism of glycerolipides; a comparison of lecithin and triglyceride synthesis. *J Biol Chem*, 231(2):883–8, 1958.
- [106] X. Chen, B. A. Hyatt, M. L. Mucenski, R. J. Mason, and J. M. Shannon. Identification and characterization of a lysophosphatidylcholine acyltransferase in alveolar type ii cells. *Proc Natl Acad Sci U S A*, 103(31):11724–9, 2006.
- [107] H. Nakanishi, H. Shindou, D. Hishikawa, T. Harayama, R. Ogasawara, A. Suwabe, R. Taguchi, and T. Shimizu. Cloning and characterization of mouse lung-type acyl-coa:lysophosphatidylcholine acyltransferase 1 (*lpcat1*). expression in alveolar type ii cells and possible involvement in surfactant production. *J Biol Chem*, 281(29):20140–7, 2006.
- [108] H. Shindou, D. Hishikawa, H. Nakanishi, T. Harayama, S. Ishii, R. Taguchi, and T. Shimizu. A single enzyme catalyzes both platelet-activating factor production and membrane biogenesis of inflammatory cells. cloning and characterization of acetyl-coa:lyso-paf acetyltransferase. *J Biol Chem*, 282(9):6532–9, 2007.
- [109] E. Soupene, H. Fyrist, and F. A. Kuypers. Mammalian acyl-coa:lysophosphatidylcholine acyltransferase enzymes. *Proc Natl Acad Sci U S A*, 105(1):88–93, 2008.
- [110] Y. Zhao, Y. Q. Chen, T. M. Bonacci, D. S. Bredt, S. Li, W. R. Bensch, D. E. Moller, M. Kowala, R. J. Konrad, and G. Cao. Identification and characterization of a major liver lysophosphatidylcholine acyltransferase. *J Biol Chem*, 283(13):8258–65, 2008.
- [111] D. Hishikawa, H. Shindou, S. Kobayashi, H. Nakanishi, R. Taguchi, and T. Shimizu. Discovery of a lysophospholipid acyltransferase family essential for membrane asymmetry and diversity. *Proc Natl Acad Sci U S A*, 105(8):2830–5, 2008.
- [112] T. M. Lewin, P. Wang, and R. A. Coleman. Analysis of amino acid motifs diagnostic for the sn-glycerol-3-phosphate acyltransferase reaction. *Biochemistry*, 38(18):5764–71, 1999.
- [113] K. Hofmann. A superfamily of membrane-bound o-acyltransferases with implications for wnt signaling. *Trends Biochem Sci*, 25(3):111–2, 2000.
- [114] T. Harayama, H. Shindou, R. Ogasawara, A. Suwabe, and T. Shimizu. Identification of a novel noninflammatory biosynthetic pathway of platelet-activating factor. *J Biol Chem*, 283(17):11097–106, 2008.
- [115] T. Harayama, H. Shindou, and T. Shimizu. Biosynthesis of phosphatidylcholine by human lysophosphatidylcholine acyltransferase 1. *J Lipid Res*, 2009.
- [116] H. Shindou and T. Shimizu. Acyl-coa:lysophospholipid acyltransferases. *J Biol Chem*, 284(1):1–5, 2009.
- [117] M. Kazachkov, Q. Chen, L. Wang, and J. Zou. Substrate preferences of a lysophosphatidylcholine acyltransferase highlight its role in phospholipid remodeling. *Lipids*, 43(10):895–902, 2008.
- [118] S. Jain, X. Zhang, P. J. Khandelwal, A. J. Saunders, B. S. Cummings, and P. Oelkers. Characterization of human lysophospholipid acyltransferase 3. *J Lipid Res*, 50(8):1563–70, 2009.
- [119] K. W. Wirtz. Phospholipid transfer proteins in perspective. *FEBS Lett*, 580(23):5436–41, 2006.
- [120] E. J. Blanchette-Mackie, N. K. Dwyer, T. Barber, R. A. Coxey, T. Takeda, C. M. Rondinone, J. L. Theodorakis, A. S. Greenberg, and C. Londos. Perilipin is located on the surface layer of intracellular lipid droplets in adipocytes. *J Lipid Res*, 36(6):1211–26, 1995.
- [121] Y. Ohsaki, J. Cheng, M. Suzuki, A. Fujita, and T. Fujimoto. Lipid droplets are arrested in the er membrane by tight binding of lipidated apolipoprotein b-100. *J Cell Sci*, 121(Pt 14):2415–22, 2008.
- [122] P. Liu, R. Bartz, J. K. Zehmer, Y. S. Ying, M. Zhu, G. Serrero, and R. G. Anderson. Rab-regulated interaction of early endosomes with lipid droplets. *Biochim Biophys Acta*, 1773(6):784–93, 2007.

-
- [123] D. Binns, T. Januszewski, Y. Chen, J. Hill, V. S. Markin, Y. Zhao, C. Gilpin, K. D. Chapman, R. G. Anderson, and J. M. Goodman. An intimate collaboration between peroxisomes and lipid bodies. *J Cell Biol*, 173(5):719–31, 2006.
- [124] Y. Ohsaki, J. Cheng, A. Fujita, T. Tokumoto, and T. Fujimoto. Cytoplasmic lipid droplets are sites of convergence of proteasomal and autophagic degradation of apolipoprotein b. *Mol Biol Cell*, 17(6):2674–83, 2006.
- [125] R. Singh, S. Kaushik, Y. Wang, Y. Xiang, I. Novak, M. Komatsu, K. Tanaka, A. M. Cuervo, and M. J. Czaja. Autophagy regulates lipid metabolism. *Nature*, 458(7242):1131–5, 2009.
- [126] R. G. Sturmey, P. J. O’Toole, and H. J. Leese. Fluorescence resonance energy transfer analysis of mitochondrial:lipid association in the porcine oocyte. *Reproduction*, 132(6):829–37, 2006.
- [127] S. Jagerstrom, S. Polesie, Y. Wickstrom, B. R. Johansson, H. D. Schroder, K. Hojlund, and P. Bostrom. Lipid droplets interact with mitochondria using snap23. *Cell Biol Int*, 33(9):934–40, 2009.
- [128] M. J. Savage, D. J. Goldberg, and S. Schacher. Absolute specificity for retrograde fast axonal transport displayed by lipid droplets originating in the axon of an identified aplysia neuron in vitro. *Brain Res*, 406(1-2):215–23, 1987.
- [129] M. A. Welte, S. Cermelli, J. Griner, A. Viera, Y. Guo, D. H. Kim, J. G. Gindhart, and S. P. Gross. Regulation of lipid-droplet transport by the perilipin homolog lsd2. *Curr Biol*, 15(14):1266–75, 2005.
- [130] P. Bostrom, M. Rutberg, J. Ericsson, P. Holmdahl, L. Andersson, M. A. Frohman, J. Boren, and S. O. Olofsson. Cytosolic lipid droplets increase in size by microtubule-dependent complex formation. *Arterioscler Thromb Vasc Biol*, 25(9):1945–51, 2005.
- [131] P. Bostrom, L. Andersson, M. Rutberg, J. Perman, U. Lidberg, B. R. Johansson, J. Fernandez-Rodriguez, J. Ericson, T. Nilsson, J. Boren, and S. O. Olofsson. Snare proteins mediate fusion between cytosolic lipid droplets and are implicated in insulin sensitivity. *Nat Cell Biol*, 9(11):1286–93, 2007.
- [132] Y. Guo, K. R. Cordes, Jr. Farese, R. V., and T. C. Walther. Lipid droplets at a glance. *J Cell Sci*, 122(Pt 6):749–52, 2009.
- [133] M. M. Hussain, J. Shi, and P. Dreizen. Microsomal triglyceride transfer protein and its role in apob-lipoprotein assembly. *J Lipid Res*, 44(1):22–32, 2003.
- [134] M. Wettsten, K. Bostrom, G. Bondjers, M. Jarfeldt, P. I. Norfeldt, M. Carrella, O. Wiklund, J. Boren, and S. O. Olofsson. Pulse-chase studies of the synthesis of apolipoprotein b in a human hepatoma cell line, hep g2. *Eur J Biochem*, 149(3):461–6, 1985.
- [135] J. L. Dixon, S. Furukawa, and H. N. Ginsberg. Oleate stimulates secretion of apolipoprotein b-containing lipoproteins from hep g2 cells by inhibiting early intracellular degradation of apolipoprotein b. *J Biol Chem*, 266(8):5080–6, 1991.
- [136] D. Wiggins and G. F. Gibbons. The lipolysis/esterification cycle of hepatic triacylglycerol. its role in the secretion of very-low-density lipoprotein and its response to hormones and sulphonylureas. *Biochem J*, 284 (Pt 2):457–62, 1992.
- [137] C. Lefevre, F. Jobard, F. Caux, B. Bouadjar, A. Karaduman, R. Heilig, H. Lakhdar, A. Wollenberg, J. L. Verret, J. Weissenbach, M. Ozguc, M. Lathrop, J. F. Prud’homme, and J. Fischer. Mutations in cgi-58, the gene encoding a new protein of the esterase/lipase/thioesterase subfamily, in chnarin-dorfman syndrome. *Am J Hum Genet*, 69(5):1002–12, 2001.
- [138] J. Fischer, C. Lefevre, E. Morava, J. M. Mussini, P. Laforet, A. Negre-Salvayre, M. Lathrop, and R. Salvayre. The gene encoding adipose triglyceride lipase (pnpla2) is mutated in neutral lipid storage disease with myopathy. *Nat Genet*, 39(1):28–30, 2007.
- [139] S. L. Sturley, M. C. Patterson, W. Balch, and L. Liscum. The pathophysiology and mechanisms of npc disease. *Biochim Biophys Acta*, 1685(1-3):83–7, 2004.
- [140] J. Magre, M. Delepine, E. Khallouf, Jr. Gedde-Dahl, T., L. Van Maldergem, E. Sobel, J. Papp, M. Meier, A. Megarbane, A. Bachy, A. Verloes, F. H. d’Abronzio, E. Seemanova, R. Assan, N. Baudic, C. Bourut, P. Czernichow, F. Huet, F. Grigorescu, M. de Kerdanet, D. Lacombe, P. Labrune, M. Lanza, H. Loret, F. Matsuda, J. Navarro, A. Nivelon-Chevalier, M. Polak, J. J. Robert, P. Tric, N. Tubiana-Rufi, C. Vigouroux, J. Weissenbach, S. Savasta, J. A. Maassen, O. Trygstad, P. Bogalho, P. Freitas, J. L. Medina, F. Bonnici, B. I. Joffe, G. Loyson, V. R. Panz, F. J. Raal, S. O’Rahilly, T. Stephenson, C. R. Kahn, M. Lathrop, and J. Capeau. Identification of the gene altered in berardinelli-seip congenital lipodystrophy on chromosome 11q13. *Nat Genet*, 28(4):365–70, 2001.
-

- [141] C. A. Kim, M. Delepine, E. Boutet, H. El Mourabit, S. Le Lay, M. Meier, M. Nemani, E. Bridel, C. C. Leite, D. R. Bertola, R. K. Semple, S. O’Rahilly, I. Dugail, J. Capeau, M. Lathrop, and J. Magre. Association of a homozygous nonsense caveolin-1 mutation with berardinelli-seip congenital lipodystrophy. *J Clin Endocrinol Metab*, 93(4):1129–34, 2008.
- [142] R. Jeffcoat. Obesity - a perspective based on the biochemical interrelationship of lipids and carbohydrates. *Med Hypotheses*, 68(5):1159–71, 2007.
- [143] S. Gesta, Y. H. Tseng, and C. R. Kahn. Developmental origin of fat: tracking obesity to its source. *Cell*, 131(2):242–56, 2007.
- [144] G. H. Goossens. The role of adipose tissue dysfunction in the pathogenesis of obesity-related insulin resistance. *Physiol Behav*, 94(2):206–18, 2008.
- [145] A. Guilherme, J. V. Virbasius, V. Puri, and M. P. Czech. Adipocyte dysfunctions linking obesity to insulin resistance and type 2 diabetes. *Nat Rev Mol Cell Biol*, 9(5):367–77, 2008.
- [146] J. M. Lavoie and M. S. Gauthier. Regulation of fat metabolism in the liver: link to non-alcoholic hepatic steatosis and impact of physical exercise. *Cell Mol Life Sci*, 63(12):1393–409, 2006.
- [147] S. O. Olofsson, O. Wiklund, and J. Boren. Apolipoproteins a-i and b: biosynthesis, role in the development of atherosclerosis and targets for intervention against cardiovascular disease. *Vasc Health Risk Manag*, 3(4):491–502, 2007.
- [148] L. Puglielli, R. E. Tanzi, and D. M. Kovacs. Alzheimer’s disease: the cholesterol connection. *Nat Neurosci*, 6(4):345–51, 2003.
- [149] A. Fernandez, L. Llacuna, J. C. Fernandez-Checa, and A. Colell. Mitochondrial cholesterol loading exacerbates amyloid beta peptide-induced inflammation and neurotoxicity. *J Neurosci*, 29(20):6394–405, 2009.
- [150] B. Aguado and R. D. Campbell. Characterization of a human lysophosphatidic acid acyltransferase that is encoded by a gene located in the class iii region of the human major histocompatibility complex. *J Biol Chem*, 273(7):4096–105, 1998.
- [151] S. Jackowski, J. Wang, and I. Baburina. Activity of the phosphatidylcholine biosynthetic pathway modulates the distribution of fatty acids into glycerolipids in proliferating cells. *Biochim Biophys Acta*, 1483(3):301–15, 2000.
- [152] E. L. Arrese and J. L. Soulages. Insect fat body: Energy, metabolism, and regulation. *Annu Rev Entomol*, 2009.
- [153] F. Lallanne, G. Lambert, M. J. Amar, M. Chetiveaux, Y. Zair, A. L. Jarnoux, K. Ouguerram, J. Friburg, N. G. Seidah, Jr. Brewer, H. B., M. Krempf, and P. Costet. Wild-type pcsk9 inhibits ldl clearance but does not affect apob-containing lipoprotein production in mouse and cultured cells. *J Lipid Res*, 46(6):1312–9, 2005.
- [154] H. Huang, F. Sun, D. M. Owen, W. Li, Y. Chen, Jr. Gale, M., and J. Ye. Hepatitis c virus production by human hepatocytes dependent on assembly and secretion of very low-density lipoproteins. *Proc Natl Acad Sci U S A*, 104(14):5848–53, 2007.
- [155] T. Fujimoto, H. Kogo, K. Ishiguro, K. Tauchi, and R. Nomura. Caveolin-2 is targeted to lipid droplets, a new “membrane domain” in the cell. *J Cell Biol*, 152(5):1079–85, 2001.
- [156] M. Ohashi, N. Mizushima, Y. Kabeya, and T. Yoshimori. Localization of mammalian nad(p)h steroid dehydrogenase-like protein on lipid droplets. *J Biol Chem*, 278(38):36819–29, 2003.
- [157] A. G. Ostermeyer, J. M. Paci, Y. Zeng, D. M. Lublin, S. Munro, and D. A. Brown. Accumulation of caveolin in the endoplasmic reticulum redirects the protein to lipid storage droplets. *J Cell Biol*, 152(5):1071–8, 2001.
- [158] A. Pol, R. Luetterforst, M. Lindsay, S. Heino, E. Ikonen, and R. G. Parton. A caveolin dominant negative mutant associates with lipid bodies and induces intracellular cholesterol imbalance. *J Cell Biol*, 152(5):1057–70, 2001.
- [159] H. Caldas and G. E. Herman. Nsdhl, an enzyme involved in cholesterol biosynthesis, traffics through the golgi and accumulates on er membranes and on the surface of lipid droplets. *Hum Mol Genet*, 12(22):2981–91, 2003.
- [160] P. Dupree, R. G. Parton, G. Raposo, T. V. Kurzchalia, and K. Simons. Caveolae and sorting in the trans-golgi network of epithelial cells. *Embo J*, 12(4):1597–605, 1993.
- [161] A. G. Ostermeyer, L. T. Ramcharan, Y. Zeng, D. M. Lublin, and D. A. Brown. Role of the hydrophobic domain in targeting caveolin-1 to lipid droplets. *J Cell Biol*, 164(1):69–78, 2004.

-
- [162] V. Litvak, Y. D. Shaul, M. Shulewitz, R. Amarilio, S. Carmon, and S. Lev. Targeting of nir2 to lipid droplets is regulated by a specific threonine residue within its pi-transfer domain. *Curr Biol*, 12(17):1513–8, 2002.
- [163] J. K. Zehmer, R. Bartz, P. Liu, and R. G. Anderson. Identification of a novel n-terminal hydrophobic sequence that targets proteins to lipid droplets. *J Cell Sci*, 121(Pt 11):1852–60, 2008.
- [164] V. Subramanian, A. Garcia, A. Sekowski, and D. L. Brasaemle. Hydrophobic sequences target and anchor perilipin a to lipid droplets. *J Lipid Res*, 45(11):1983–91, 2004.
- [165] Y. Ohsaki, T. Maeda, M. Maeda, K. Tauchi-Sato, and T. Fujimoto. Recruitment of tip47 to lipid droplets is controlled by the putative hydrophobic cleft. *Biochem Biophys Res Commun*, 347(1):279–87, 2006.
- [166] H. Plutner, H. W. Davidson, J. Saraste, and W. E. Balch. Morphological analysis of protein transport from the er to golgi membranes in digitonin-permeabilized cells: role of the p58 containing compartment. *J Cell Biol*, 119(5):1097–116, 1992.
- [167] S. Martin and R. G. Parton. Caveolin, cholesterol, and lipid bodies. *Semin Cell Dev Biol*, 16(2):163–74, 2005.
- [168] J. M. Shockey, S. K. Gidda, D. C. Chapital, J. C. Kuan, P. K. Dhanoa, J. M. Bland, S. J. Rothstein, R. T. Mullen, and J. M. Dyer. Tung tree dgat1 and dgat2 have nonredundant functions in triacylglycerol biosynthesis and are localized to different subdomains of the endoplasmic reticulum. *Plant Cell*, 18(9):2294–313, 2006.
- [169] M. M. Kater, G. M. Koningstein, H. J. Nijkamp, and A. R. Stuitje. The use of a hybrid genetic system to study the functional relationship between prokaryotic and plant multi-enzyme fatty acid synthetase complexes. *Plant Mol Biol*, 25(5):771–90, 1994.
- [170] A. R. Hawkins and H. K. Lamb. The molecular biology of multidomain proteins. selected examples. *Eur J Biochem*, 232(1):7–18, 1995.
- [171] J. Cheng, A. Fujita, Y. Ohsaki, M. Suzuki, Y. Shinohara, and T. Fujimoto. Quantitative electron microscopy shows uniform incorporation of triglycerides into existing lipid droplets. *Histochem Cell Biol*, 132(3):281–91, 2009.
- [172] A. Gubern, M. Barcelo-Torns, J. Casas, D. Barneda, R. Masgrau, F. Picatoste, J. Balsinde, M. A. Balboa, and E. Claro. Lipid droplet biogenesis induced by stress involves triacylglycerol synthesis that depends on group via phospholipase a2. *J Biol Chem*, 284(9):5697–708, 2009.
- [173] A. Gubern, J. Casas, M. Barcelo-Torns, D. Barneda, X. de la Rosa, R. Masgrau, F. Picatoste, J. Balsinde, M. A. Balboa, and E. Claro. Group i va phospholipase a2 is necessary for the biogenesis of lipid droplets. *J Biol Chem*, 283(41):27369–82, 2008.
- [174] R. E. Duncan, E. Sarkadi-Nagy, K. Jaworski, M. Ahmadian, and H. S. Sul. Identification and functional characterization of adipose-specific phospholipase a2 (adpla). *J Biol Chem*, 283(37):25428–36, 2008.
- [175] K. Jaworski, M. Ahmadian, R. E. Duncan, E. Sarkadi-Nagy, K. A. Varady, M. K. Hellerstein, H. Y. Lee, V. T. Samuel, G. I. Shulman, K. H. Kim, S. de Val, C. Kang, and H. S. Sul. Adpla ablation increases lipolysis and prevents obesity induced by high-fat feeding or leptin deficiency. *Nat Med*, 15(2):159–68, 2009.
- [176] J. B. Massey, D. H. Bick, and H. J. Pownall. Spontaneous transfer of monoacyl amphiphiles between lipid and protein surfaces. *Biophys J*, 72(4):1732–43, 1997.
- [177] A. Vancura and D. Haldar. Regulation of mitochondrial and microsomal phospholipid synthesis by liver fatty acid-binding protein. *J Biol Chem*, 267(20):14353–9, 1992.
- [178] J. Zimmerberg and M. M. Kozlov. How proteins produce cellular membrane curvature. *Nat Rev Mol Cell Biol*, 7(1):9–19, 2006.
- [179] L. V. Chernomordik and M. M. Kozlov. Protein-lipid interplay in fusion and fission of biological membranes. *Annu Rev Biochem*, 72:175–207, 2003.
- [180] M. S. Han, S. Y. Park, K. Shinzawa, S. Kim, K. W. Chung, J. H. Lee, C. H. Kwon, K. W. Lee, C. K. Park, W. J. Chung, J. S. Hwang, J. J. Yan, D. K. Song, Y. Tsujimoto, and M. S. Lee. Lysophosphatidylcholine as a death effector in the lipoapoptosis of hepatocytes. *J Lipid Res*, 49(1):84–97, 2008.
- [181] J. R. Skinner, T. M. Shew, D. M. Schwartz, A. Tzekov, C. M. Lepus, N. A. Abumrad, and N. E. Wolins. Diacylglycerol-enrichment of endoplasmic reticulum or lipid droplets recruits perilipin3/tip47 during lipid storage and mobilization. *J Biol Chem*, 2009.
- [182] Y. Liu, J. S. Millar, D. A. Cromley, M. Graham, R. Crooke, J. T. Billheimer, and D. J. Rader. Knockdown of acyl-coa:diacylglycerol acyltransferase 2 with antisense oligonucleotide reduces vldl tg and apob secretion in mice. *Biochim Biophys Acta*, 1781(3):97–104, 2008.
-

- [183] S. K. Jackson, W. Abate, J. Parton, S. Jones, and J. L. Harwood. Lysophospholipid metabolism facilitates toll-like receptor 4 membrane translocation to regulate the inflammatory response. *J Leukoc Biol*, 84(1):86–92, 2008.
- [184] M. Monetti, M. C. Levin, M. J. Watt, M. P. Sajjan, S. Marmor, B. K. Hubbard, R. D. Stevens, J. R. Bain, C. B. Newgard, Sr. Farese, R. V., A. L. Hevener, and Jr. Farese, R. V. Dissociation of hepatic steatosis and insulin resistance in mice overexpressing dgat in the liver. *Cell Metab*, 6(1):69–78, 2007.
- [185] D. C. Taylor, N. Weber, L. R. Hogge, and E. W. Underhill. A simple enzymatic method for the preparation of radiolabeled erucoyl-coa and other long-chain fatty acyl-coas and their characterization by mass spectrometry. *Anal Biochem*, 184(2):311–6, 1990.
- [186] J. Spandl, D. J. White, J. Peychl, and C. Thiele. Live cell multicolor imaging of lipid droplets with a new dye, Id540. *Traffic*, 2009.
- [187] A. Shevchenko, H. Tomas, J. Havlis, J. V. Olsen, and M. Mann. In-gel digestion for mass spectrometric characterization of proteins and proteomes. *Nat Protoc*, 1(6):2856–60, 2006.
- [188] C. S. Ejsing, J. L. Sampaio, V. Surendranath, E. Duchoslav, K. Ekroos, R. W. Klemm, K. Simons, and A. Shevchenko. Global analysis of the yeast lipidome by quantitative shotgun mass spectrometry. *Proc Natl Acad Sci U S A*, 106(7):2136–41, 2009.
- [189] C. S. Ejsing, E. Duchoslav, J. Sampaio, K. Simons, R. Bonner, C. Thiele, K. Ekroos, and A. Shevchenko. Automated identification and quantification of glycerophospholipid molecular species by multiple precursor ion scanning. *Anal Chem*, 78(17):6202–14, 2006.
- [190] D. Schwudke, J. T. Hannich, V. Surendranath, V. Grimard, T. Moehring, L. Burton, T. Kurzchalia, and A. Shevchenko. Top-down lipidomic screens by multivariate analysis of high-resolution survey mass spectra. *Anal Chem*, 79(11):4083–93, 2007.
- [191] K. Ekroos, I. V. Chernushevich, K. Simons, and A. Shevchenko. Quantitative profiling of phospholipids by multiple precursor ion scanning on a hybrid quadrupole time-of-flight mass spectrometer. *Anal Chem*, 74(5):941–9, 2002.
- [192] A. Shevchenko, A. Roguev, D. Schaft, L. Buchanan, B. Habermann, C. Sakalar, H. Thomas, N. J. Krogan, and A. F. Stewart. Chromatin central: towards the comparative proteome by accurate mapping of the yeast proteomic environment. *Genome Biol*, 9(11):R167, 2008.

E. Publications and Awards

Publications

Imaging of lipid biosynthesis: how a neutral lipid enters lipid droplets.

Kuerschner L, Moessinger C, Thiele C.

Traffic. 2008 Mar;9(3):338-52. Epub 2007 Dec 11.

Lipid droplets expand their surface layer by local synthesis of phosphatidylcholine

Christine Moessinger, Julia Massier, Johanna Spandl and Christoph Thiele

Chemistry and Physics of Lipids, Volume 154, Supplement 1, August 2008, Pages S6-S7

LPCAT1 and LPCAT2 synthesize phosphatidylcholine on the surface of lipid droplets and influence lipid droplet morphology and lipoprotein secretion.

Christine Moessinger, Gualtiero Alvisi, Christer S. Ejsing, Julia Massier, Johanna Spandl, Andrej Shevchenko, Ralf Bartenschlager and Christoph Thiele

(was submitted to Cell Metabolism, currently reformatted for submission to JCB)

Parts of this thesis were already orally presented at the 49th ICBL (International Conference on the Bioscience of Lipids) conference 2008 in Maastricht, The Netherlands and the Frontier Lipidology: Lipidomics in Health and Disease conference 2009 in Gothenburg, Sweden.

Awards

Oral communication award

49th Annual Conference, Maastricht 2008

Theme: Lipidology: Bridge between Basic Science and Clinical Pathology

Topic of presentation: Lipid droplets expand their surface layer by local synthesis of phosphatidylcholine

DIGS-BB Travel Award

49th Annual Meeting of the American Society of Cell Biology, San Diego 2009

Title of the poster: Lipid droplets expand their surface layer by local synthesis of phosphatidylcholine

F. Acknowledgments

First of all I want to thank my supervisor Prof. Dr. Christoph Thiele for the chance to work in his lab on these interesting and challenging projects. Thank you for all your support, for bringing out the best in me and for teaching me some secrets of biochemistry. I also want to thank Prof. Dr. Bernard Hoflack for taking me as his PhD student and for his permanent support and advices as a member in my thesis advisory committee. Another special thank goes to my thesis advisory committee member Prof. Dr. Michele Solimena for his permanent support and his extremely motivating and helpful critiques on my projects.

A special and big thank to the current and former members of the Thiele lab namely Julia Massier, Johanna Spandl, Doris Richter, Mario Schöne, Ana Stevanovic, Daniel Lohmann, Vinciane Grimard, Lars Kürschner and Monika Suchanek for the fantastic atmosphere, for sharing ideas, reagents, protocols and for your open ears and help in all my good and bad moods.

I was especially happy to work together with several people, who strongly participated in bringing forward my projects. Therefore I want to thank Cornelia Czupalla (Hoflack lab) for protein mass spectrometry as well as Ana Shevchenko (protein mass spectrometry facility). Furthermore, I thank Christer Ejlsing (former member of the Shevchenko lab, now group leader in Odense, Denmark) for lipid mass spectrometry. Special thanks to Gualtiero Alvisi (Bartenschlager lab at the University of Heidelberg) for all experiments concerning hepatitis C virus and Xabier Contreras (Wieland and Brügger lab at the University of Heidelberg) for quantifying our radioactive TLC plates. Many thanks to the Eaton lab especially Wilhelm Palm, Falko Riedel and Marco Brankatsch for introducing me into and fascinating me for the work with flies and Manuela Völkner (trainee in our lab) for her help in studying DGAT2-ACSL1 interaction. Last but not least I want to thank Anne Tuukkanen (Schröder lab) for the bioinformatic data in the DGAT2 project.

A big thank goes to the MPI-CBG facilities in particular the Light microscopy facility, the EM facility especially Kevin Manygoats and Daniela Vorkel, the Protein Expression facility especially Mike Tipswood, the flykitchen and the media kitchen. I want to thank all

the people of homebase 2 South (Simons lab, Lammert lab, Neugebauer lab, Solveig Otto and Susann Babucke) for the wonderful atmosphere and for sharing all kinds of ideas and reagents and a thank also to the whole institute for the supportive atmosphere.

Many thanks for proofreading my thesis to Vinciane Grimard, Johanna Spandl, Doris Richter, Ana Stevanovic and Wilhelm Palm.

The biggest thank goes to my parents for their unquestioning support during my whole life, to my brother Alexander for his support in all kinds of technical and thesis related problems that can occur and to my partner André Brödner. Dear André, thank you for sharing all the good and the bad times with me, for your support and your believe in everything I decided, for helping me with all kinds of computer problems, which would have otherwise prevented the existence of this thesis and for all the wonderful moments there are no words to describe.